Detection of aeolian sand strips and their characteristics using terrestrial laser scanning

The dependency between aeolian sand strip development and the environmental conditions occurring at the Noordwijk beach

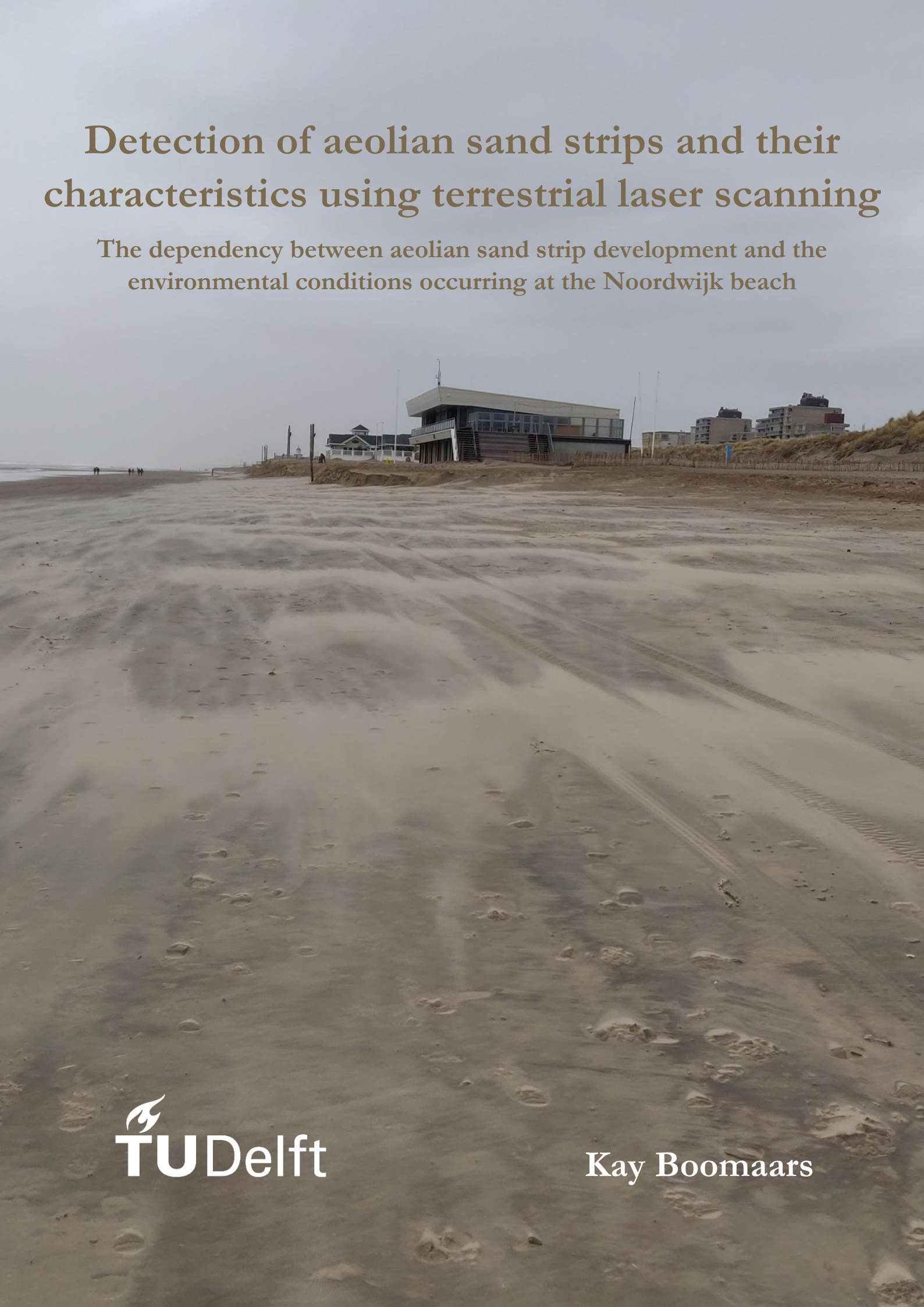

TU Delft

Kay Boomaars

MSc. Thesis

Detection of aeolian sand strips and their characteristics using terrestrial laser scanning

The dependency between aeolian sand strip development and the environmental conditions occurring at the Noordwijk beach

MSc. Thesis

by

Kay Boomaars

In partial fulfilment of the requirements for the degree of
Master of Science
in Civil Engineering: Hydraulic Engineering

At the Delft University of Technology

Student number: 4705092

Committee:	Dr.ir.	A.J.H.M. Reniers	TU Delft	(chair)
	Dr.	R.C. Lindenbergh	TU Delft	
	Dr.	S.E. Vos	TU Delft	
	M.Sc.	C.O. van IJzendoorn	TU Delft	
	M.Sc.	M. Kuschnerus	TU Delft	

TU Delft
Delft University of Technology

Abstract

Sea level rise causes more difficulties for coastal maintenance. In the past hard structures were built to prevent for flooding, which need to be maintained more often due to the rising sea level. More recently nature based solutions are therefore preferred over these hard structures. For the application of nature based solutions, a better understanding of the coastal processes and variability is desired. Sand is deposited on the beach with hydrodynamic forces. Subsequently, the sand dries and is transported towards the dunes as a form of aeolian transport. Multiple processes are included in aeolian transport, whose bedform development is understudied while knowledge on this is important for a better understanding of the coastal processes. One of the most visually clear bedforms is organised dry sand over a moist beach, referred to as sand strips. In order to improve the knowledge on sand strips, this study focusses on sand strip properties and environmental conditions that occurred during their presence at the Noordwijk beach, using data acquired by a terrestrial laser scanning (TLS) device.

Sand strips are detected with the Fourier transform. Since surface moisture can be derived from the reflectance intensity of the TLS-data, and due to the different moisture content of the sand strips compared to the surrounding beach, the Fourier transform is applied on the reflectance intensity. Sand strips are detected based on the spectral energy in the variance density spectrum for a wavenumber-range corresponding to sand strips. Due to the dataset-dependent derivation of surface moisture from the reflectance intensity, calibration of the detection threshold is necessary before applying the threshold on other datasets. For the detected sand strips the wavelength, orientation, and height are determined and these shape properties are analysed based on the average values for each scan. The detected sand strips were oriented alongshore to oblique-alongshore with a mean wavelength and height of 13.2 *m* and 4.0 *cm* respectively, which is in correspondence with similar sand strip-related studies.

According to sand samples of the beach the grain size varies in transverse direction of the sand strips. This variation is comparable with the grain size variation of aeolian sand ripples, with the coarser grains located at the crest and the finer grains at the lee-side. Additionally, the samples also showed a significant difference in gravimetric moisture content between the sand strips and surrounding beach, as expected due to the reflectance-based detection. At the sand strips, the maximum moisture content was 5.3%, while the minimum determined moisture content at the surrounding beach was 6.0%. The mean values were equal to 2.6% and 9.4% for the sand strips and surrounding beach respectively.

In addition, sand strips mainly occurred during (almost) alongshore wind events with a wind velocity in excess of 8 *m/s*. However, the threshold wind velocity for sand strip formation is determined at 10 *m/s*. Due to the significant height difference that can remain present during precipitation events, these events are not necessarily restrictive factors for sand strip development, although the reflectance intensity suggests different. Furthermore, sand strips mostly formed during falling tide and they were mostly destroyed by the increasing water level during rising tide.

The one life cycle of the sand strips that is analysed showed dynamic sand strip behaviour. The migration rate of the sand strips varied over the width of the beach, causing more inland oriented sand strips. This dynamic behaviour cannot be related to weather conditions since they remained constant, however it could be related to topographic steering caused by the dune. Nevertheless, the results of the dynamic properties are only indicative and encourage further study of dynamic sand strip properties.

Keywords: aeolian transport, sand strips, terrestrial laser scanning, point cloud, Noordwijk, coastal processes, Fourier transform, reflectance intensity, environmental conditions

Acknowledgements

When I started my bachelor's degree in Civil Engineering back in 2017 I did not have a specific idea where I would stand five years later. Or at least, I did not know that five years later my master's degree in Hydraulic Engineering would be within grasp. Looking back on my student time now, five years later, I can say that I really enjoyed it. The last two years I gained a lot of knowledge that I combined in this thesis, which marks the end of my study time at Delft University of Technology. Throughout my master's degree, I followed several courses with great interest. However, after following the Coastal Dynamics II course, aeolian transport had my interest almost immediately since a lot was still unknown in this field. The decision for a thesis topic related to aeolian transport was therefore obvious for me. When working on this topic, my interest in remote sensing techniques increased as well and the possibilities with the different techniques still fascinate me. Therefore I am glad that I studied this topic where information on aeolian transport is obtained by a spectral analysis on data that is acquired by a remote sensing technique.

I would like to thank all committee members, Sander Vos, Christa van IJzendoorn, Mieke Kuschnerus, Ad Reniers, and Roderik Lindenbergh for their supervision, guidance, and providing of feedback during all meetings. In particular, I would like to thank Sander and Christa for their supervision throughout the entire thesis duration. I recognize that all the weekly meetings we had, where we discussed our ideas and findings, took a lot of time. Besides these weekly meetings, you took the time for other things as well, for instance the fieldwork trips to the Noordwijk beach for collecting the sand samples. You also helped me a lot with 'zooming-out', since I can get stuck in small details sometimes which are not really worth the time. Thank you Mieke and Roderik for mentioning the 3D surveying course where both of you are involved in and the guidance through this course where we started with the first steps of this research, besides the thesis related guidance. Thank you Ad, particularly for your ideas and help related to the spectral analysis which was fundamental for this thesis. I really appreciate your time.

Second, I would like to thank some fellow students. In particular Maikel and Maarten, my housemates who supported me throughout my full student time and with whom I lived for the last four and a half years. Furthermore I want to thank Zelin, Emily, and Fanhao. Together, we started working on the very first steps of the method during the 3D surveying course. The programming tips really increased my programming skills and helped me with developing a proper method. Lastly, thanks to all other people I have met during my study time. Without you, my study time in Delft would be very different.

Besides my fellow students, a word of gratitude goes out to my family and friends in Zundert as well for their support, interest and advice. Their interest in my study helped me with explaining hydraulic engineering related topics to people of other disciplines. Not only their interest, but also their support and advice helped me when I wanted to discuss my thesis. With these messages said, there is only one last thing to say: enjoy the read.

Delft, November 2022

Kay Boomaars

Table of contents

List of figures

List of tables

List of symbols

k	(Resultant) wavenumber
k_x	Wavenumber in x-direction
k_y	Wavenumber in y-direction
L	Wavelength
θ	Angle of orientation of the sand strips
$E(k)$	Variance density spectrum in the space domain
Δk	Wavenumber bandwidth
a_m	Mean amplitude
m_0	Zeroth order spectral moment
H_{m_0}	Significant wave height
Γ	Full width at half maximum
D_{50}	Median grain size
w	Gravimetric moisture content
m_{wet}	Original mass of the sediment sample
m_{dry}	Dried mass of the sediment sample
r	Pearson correlation coefficient
u_*	Shear velocity
u_{*t}	Threshold shear velocity for dry surfaces
u_{*tw}	Threshold shear velocity for wet surfaces
μ	Mean value
σ	Standard deviation
$M; Q2$	Median value
$Q1$	First quartile; 25th percentile
$Q3$	Third quartile; 75th percentile
$E\text{-}FN$	Epoch-based false negatives
$E\text{-}FP$	Epoch-based false positives
$A\text{-}FN$	Area-based false negatives
$A\text{-}FP$	Area-based false positives
N_{FN}	Number of scans where present sand strips are not detected
$N_{sand\ strips}$	Number of scans where sand strips are present
N_{FP}	Number of scans where sand strips are detected while not present

$N_{no\ sand\ strips}$	Number of scans where sand strips are detected while not present
$A_{sand\ strips}$	Area where sand strips are present
$A_{detected}$	Area where sand strips are detected according to the detection method
$A_{no\ sand\ strips}$	Area where no sand strips are detected
$A_{false\ detected}$	Area where sand strips are detected while sand strips are not present

List of abbreviations

ABSL	**A**ctive **b**ed **s**urface **l**ayer
FFT	**F**ast **F**ourier **t**ransform
FN	**F**alse **n**egative
FP	**F**alse **p**ositive
FWHM	**F**ull **w**idth at **h**alf **m**aximum
IFFT	**I**nverse **f**ast **F**ourier **t**ransform
IQR	**I**nter**q**uartile **r**ange
KNMI	**K**oninklijk **N**ederlands **M**eteorologisch **I**nstituut / **R**oyal **N**etherlands **M**eteorological **I**nstitute
LiDAR	**Li**ght **D**etection **A**nd **R**anging
MSL	**M**ean **S**ea **L**evel
pdf	**p**robability **d**ensity **f**unction
PLS	**P**ermanent **L**aser **S**canning
RD	**R**ijks**d**riehoek
RMSE	**R**oot **m**ean **s**quare **e**rror
TLS	**T**errestrial **L**aser **S**canning
TOF	**T**ime **o**f **F**light

1. Introduction

Sea level rise causes more difficulties for coastline maintenance. In the past coastlines were stabilized to prevent for flooding by building hard structures (Stive et al., 2013). The rising sea level causes a more frequently heightening and widening of these structures, subsequently causing less sustainable structures. Besides, they also hinder natural accumulation of sediments (Temmerman et al., 2013), which is especially important for sandy beaches. More recently nature based solutions are therefore preferred over hard structures, which allow for a larger degree of natural dynamics. Furthermore, the attractiveness of coastal areas for people to live increase (Small & Nicholls, 2003), causing changes in the coastal ecosystems (Temmerman et al., 2013). Due to the highly dynamic behaviour of sandy coasts (Vos et al., 2022) in combination with the preference for nature based solution over hard structures, a better understanding in the coastal processes and variability is important. Especially for sandy beaches since they cover around one third of the total coastal area around the word (Luijendijk et al., 2018).

However, not all transport processes on sandy beaches are fully understood, especially sand transport towards the dunes and the restoration of the coast after a storm (Anders et al., 2019). Coastal resilience and its behaviour after such a storm event depends on many mechanisms (Figure 1.1). With hydrodynamic forces the sand in the water column is transported and deposited on the beach. On the beach this sand can dry and subsequently it can be transported towards the dunes as a form of aeolian transport. Aeolian sediment transport dynamics on beaches are not fully understood yet due to their complex non-linearity and variability (Baas & Sherman, 2006). It becomes even more difficult to understand with the knowledge that aeolian sand transport towards the dunes can occur in several forms, while some terms of forms are used interchangeably (Sherman et al., 2019).

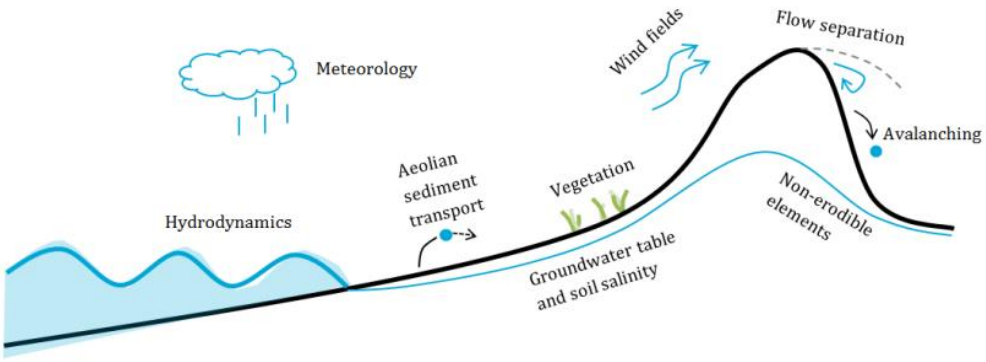

Figure 1.1. Representation of relevant processes related to dune recovery (van Westen, 2018)

In order to increase the fundamental scientific understanding of aeolian sediment transport, and therefore to eventually increase the application of nature based solutions, it is important to identify conditions that cause aeolian transport to occur. One of the most visually clear signs of aeolian transport is when an organised low, slipfaceless bedform with dry sand moves over a wet beach (Figure 1.2), known as sand strips (Hage et al., 2018b). Sand strip behaviour and development is largely unknown under a wide range of environmental conditions and bed properties. Close monitoring of the coast can help to obtain a better understanding of the processes that cause aeolian transport and more specifically aeolian transport in the form of sand strips.

Figure 1.2. Sand strips present on the Noordwijk beach (6 April 2022)

Several projects are executed where sandy coasts are closely monitored, i.e., the CoastScan-project that uses a terrestrial laser scanning (TLS) technique to analyse natural variations at short time scales for a longer time period (Vos et al., 2020). The obtained TLS data is displayed with point clouds of the beach surface, and enables analysing sand transport at high temporal and spatial detail (Anders et al., 2019). The (x, y, z)-coordinates as well as the reflectance intensity are considered the most important output parameters of the point clouds for the study of sand strips since surface properties, such as moisture content, can be derived from the reflectance intensity (Nield et al., 2011). Figure 1.2 indicates a different moisture content between the sand strips and the surrounding beach due to the colour differences, suggesting the visualization of sand strips in the point clouds based on the reflectance intensity.

1.1 Research goal

This thesis has the aim to provide a better understanding on the behaviour of the sand strips found at the beach of Noordwijk aan Zee, the Netherlands, using data of the TLS device. The focus is therefore on the properties of the sand strips and the environmental conditions that occur during sand strip development. The corresponding research question that is studied in this master thesis is therefore:

Which factors determine the properties of the aeolian sand strips on a sandy beach, and to what extent?

To answer this research question, multiple sub-questions should be answered. Point clouds of an approximately three-year time period are available, and a method should be found to detect the sand strips in these point clouds. The applicability of the detection method on other point clouds can be analysed as well. After the detection the shape properties, such as wavelength, orientation, and height, will be determined and analysed as well. Furthermore, the environmental conditions during each scan can be compared to each other to obtain the required conditions for sand strip development. Dynamic properties are analysed, which eventually can be extended to the computation of transported sand. However, this study does not discuss the amount of sand transported due to the focus on the properties only. Besides this sand strip-scale, the grain-scale of the sand strips will be studied as well to a certain extent since the sand properties of the sand strips are not known. Therefore, the following sub-questions will be answered in this master thesis:

1. *How should the data obtained with the permanent laser scanner be processed to detect sand strips?*
2. *Is the derived method for the Noordwijk beach applicable on other sandy beaches?*
3. *What are the shape properties of the formed aeolian sand strips (e.g. wavelength, orientation)?*
4. *How do the grain size and surface moisture vary over the aeolian sand strips?*
5. *What are the environmental conditions for aeolian sand strip development?*
6. *What are the dynamic properties of the formed aeolian sand strips (e.g. migration rate, changes over time)?*

Since not every question can be answered immediately without answering the previous sub-question, a workflow is visualized in appendix A. This workflow shows the order to answer the sub-questions.

1.2 Research scope

Like any other study has this study its limits which define the scope. First, only one area along the Dutch coast is examined. The studied area is part of the Noordwijk beach, The Netherlands. Noordwijk is a small coastal village at the centre of the Dutch coastline. The laser scanner is located on top of Grand Hotel Huis ter Duin and scans the dunes, beach and tidal area in front of the hotel. The exact study area is therefore bordered by the limited view of the laser scanner over the beach. For more information regarding the study area, a reference is made to section 3.1.

The TLS is scanning the beach on an hourly interval and is therefore considered continuous. The time period of the studied data ranges from January 30th until February 28th 2022 and the data is obtained during the CoastScan project. During this time period, four storms passed over the Netherlands. The first storm passed over at January 31st (storm Corrie), the other three later in February for six consecutive days. Storm Dudley during February 16th and 17th, storm Eunice during February 18th and 19th and finally storm Franklin during the 20th and 21st. Besides these four storms, fieldwork is also executed in the form of sand sample acquisition in this time period.

These sand samples are also taken at the study area bordered by the limited view of the TLS in order to determine possible grain size variation and moisture content differences over the sand strips as well as compared to the surrounding beach. These samples are taken when sand strips were present during stormy weather conditions on the 4th of February, February 17th (during storm Dudley), February 18th (during storm Eunice) and April 6th. Due to the difference in summer and winter profile of the beach, differences in grain size between these two periods are possible (Medina et al., 1994) and therefore the results of the fieldwork could differ from comparable fieldwork executed during summer months.

The temporal scale at which the sand strips will be studied is in the order of hours to days. It is expected that sand strips will not be present for more than a few consecutive days on the beach due to the changing environmental conditions. In this way, short-term changes in morphology can be visualized and long-term morphological changes of the coast are not considered.

Environmental data will be requested to correlate the occurrence of sand strips to environmental conditions. The requested data will be regional data, which can differ from local (near-surface) data occurring at the beach. One example is the possibility for wind deflection on the beach as a result of the presence of the dunes. This can cause different behaviour of the sand strips than expected, but since all of the already executed sand strip-related studies use regional data it will most likely not cause problems. Nevertheless, local weather data can differ slightly compared to regional weather data and it is worth mentioning.

1.3 Thesis outline

The main outline of the thesis consists of mainly six parts. In the first part, a short introduction is given from which the research questions are derived. In the second part a theoretical background is given with information that is already known with respect to aeolian sand strips. In the third part the study area and the obtained data from the TLS are described as well as the data acquisition for the grain size analysis. In part four a description is given regarding the processing of the TLS data as well as the processing steps required for the detection method and the detection method itself. The detected sand strips are analysed in part five, which is divided in the analysis of the shape properties, the occurred environmental conditions and the dynamic behaviour of sand strips. Lastly, a discussion as well as a conclusion is drawn in combination with recommendations for further research.

2. Theoretical background

Aeolian transport includes processes as creep, saltation, reptation and the migration of bedforms. Most aeolian transport studies are related to saltation, leaving the other aeolian processes understudied (Pye & Tsoar, 2008). Saltation is caused by wind eddies travelling down towards the surface through the boundary layer and scraping across the bed resulting in streamers (Baas et al., 2005; Hage et al., 2018a). In Figure 2.1 it can be observed that there is a clear difference between saltation streamers and sand strips. Sand strips are more organised bedforms (right figure), while streamers are saltating features (left figure). Local bed properties are not a necessary condition for the formation of streamers, while they are important for the formation of sand strips (Baas, 2007). It is reasonable to divide sand strips in aeolian transport processes related to bedform migration. However, complexity arises when focussing on the definitions of creep and reptation. Creep is defined as the movement of grains in continuous or near-continuous contact with a sand bed (Walker, 1981) and reptation as the movement of low-energy hopping particles without the ability to rebound or to eject other grains (Ungar & Haff, 1987). Creep and reptation are often used interchangeably (Mitha et al., 1986) and can be defined synonymous, and bedform migration can be considered creep as well since they migrate with a rate proportional to the bedform (Sherman, et al., 2019).

Figure 2.1. Saltation streamers (left) and sand strips (right) are common features of aeolian transport

Because natural settings, such as coastal winds, are unsteady and non-uniform it is hard to predict or model aeolian sand transport (Davidson-Arnott & Law, 1996). Besides, aeolian transport depends on multiple factors, including weather conditions and bed properties (Sherman & Hotta, 1990). Due to this dependency, strong wind velocities does not necessarily coincide with strong aeolian activities (Hage et al., 2018b), causing the understanding of aeolian transport to be hard and complexity is created when the factors interact with each other (Bauer, et al., 2009). Extensive field research is therefore desired, however, most of the fieldwork is short in time and long-term scales are then not included. Therefore, the effects of these factors on the long-term are unknown. It would require long-term observations with high temporal resolution to determine the causes and factors of aeolian activity (Hage et al., 2018a). Nield et al. (2011) have conducted the most extensive field research into aeolian sand strips. They measured sand strip patterns after a rain event for three and a half hours with a TLS and they related sand strip development not only to weather conditions, but also to bed roughness, moisture patterns and saltation.

2.1 Formation, shape and migration of the sand strips

Aeolian sand strips are slipfaceless bedforms and are classified as bedforms with a (i) low-amplitude; (ii) large wavelength and; (iii) rounded deposits, but without crestlines (Nield, 2011). They commonly have a wavelength in the order of 10 *m* and a height in the order of centimetres (Hage et al., 2018b; Baddock et al. 2018). They are often oriented alongshore, even with oblique regional winds, implying wind steering by the foredune (Hage et al., 2018b).

Sand strips commonly form on moist beds and start as patches of dry, moving sand that turn into thin strips over time (Kocurek et al., 1992). Initial bedforms are small, chaotic and close to each other. Over time, the length and the width of the sand strips became larger, while the wavelength remained constant. Hage et al. (2018b) found that the wavelength does not depend convincingly on the wind speed. Usually sand strips form close to the dune foot and spread towards the sea with falling tide (Hage et al., 2018b). They only form close to the waterline when the beach is wide and during offshore winds. When former sand strips still were present, the new formed strips had the same shape, size and most often also the same location as the former ones, but this changed when the new sand strips began to migrate.

For aeolian transport to occur, the wind speed should exceed a certain threshold velocity. For aeolian sand strip development, Hage et al. (2018a) suggest a threshold velocity equal to 8 *m/s*. The duration of the formation is inversely related to the wind speed. After a strong wind event of a certain length, it is more likely to see well-developed bedforms (Hage et al., 2018a). When the wind velocity drops below the threshold velocity, the already visible sand strips remain visible, but they do not grow or move (Hage et al., 2018b). One of the most common causes for the disappearance of sand strips is that the rising tide destroys the sand strips on the intertidal beach. Furthermore, Hage et al. (2018b) suggest that precipitation can cause a temporarily disappearance of sand strips. After the precipitation event, the sand strips can recover within an hour, given that the wind speed is above the threshold velocity.

Immediately after formation, sand strips do not necessarily migrate (Hage et al., 2018b). Furthermore, the migration rate, usually a few meters per hour, is weakly dependent on the wind velocity, given that the threshold velocity is exceeded (Kocurek et al., 2009; Hage et al., 2018a). Since the migration rate of bedforms is by approximation inversely proportional to the size of the bedform, smaller bedforms will migrate faster and overtake and interact with larger, slower bedforms. These interactions most likely occur when they have just developed when they are small, diverse in size and randomly spaced. Due to these characteristics of initial bedforms, their migration rate is different and therefore interactions are possible (Kocurek et al., 2009). Furthermore, most bedforms experience some deforming during migration, while Bauer et al. (2009) also concluded that sand strip migration is intermittent, which could be caused by the spatial patchiness of the sand strips. This spatial patchiness corresponds to a difference in moisture content between the sand strips and the surrounding bed surface. Altogether, the dynamics involved in bedform development is poorly understood. Because of the uniqueness of each bedform, it is important to determine boundary conditions for different stages and systems (Kocurek et al., 2009). Kocurek et al. (2009) studied interaction processes between bedforms and they recognized multiple processes that occur for approaching bedforms (Figure 2.2), while only a few of them appear for sand strips. The importance of these interaction processes is recognized, but since interactions are not studied in this thesis they will not be discussed in more depth and only the development will be discussed.

Since initial bedforms are small, chaotic and close to each other, constructive interactions should dominate for the pattern to develop. Constructive interactions cause fewer, larger and more widely spread bedforms. Regenerative interactions, on the other side of the spectrum, causes a more initial state, resulting in more and smaller bedforms. As bedforms grow, space widely, become more similar in space and migration rate, the number of interactions will decrease because a steady state will be approached (Kocurek et al., 2009). This steady state is, however, very difficult to reach for sand strips, as the boundary conditions are dynamic, unsteady and non-uniform. Ewing & Kocurek (2010) proposed the wind direction, the origin of the sand supply, the geometry of the sand source area, areal limits of the field, and antecedent conditions as the boundary conditions. They concluded that the orientation of the crest is a result of the wind direction, and the pattern of the sand strip is determined by the sand source. The density depends on the field area. The development of new bedforms is affected by older bedforms which may still be present (antecedent conditions) and the new formed bedforms will self-organize into a similar pattern as the older ones (Nield, 2011). The impact of these boundary conditions on the aeolian bedform development is little explored but not yet fully understood (Kocurek et al., 2009).

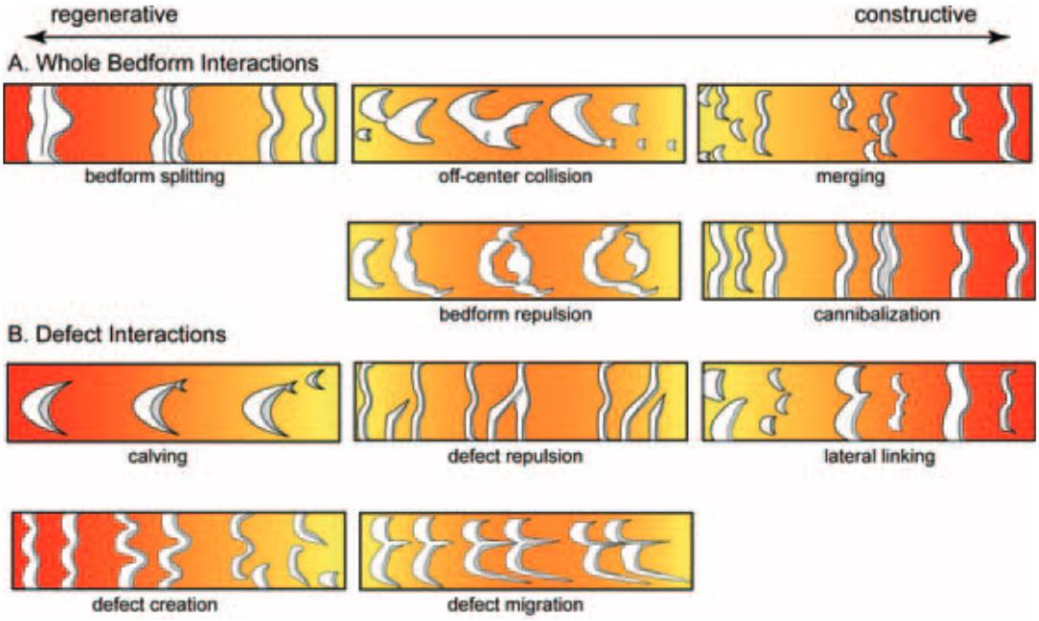

Figure 2.2. Idealized bedform interactions for (A) whole bedforms, and (B) bedform defects. Each box shows the streamwise (from left-to-right) evolution of the interaction (Kocurek, Ewing, & Mohrig, 2009)

2.2 Surface moisture

Bed properties affect the development of sand strips, and more general aeolian transport. The surface moisture is very important for the determination of sediment transport in aeolian beach systems. Aeolian transport can occur when the bed is not be inundated and when the gravimetric moisture content is below 10% (Nield et al., 2011; Hage et al., 2020). The transported sand is usually lighter in colour because it is less moist than the moist bed (Hage et al., 2018b). In Figure 2.1 it can be seen that the streamers as well as the sand strips (the transported sand) are lighter in colour, suggesting a lower surface moisture. These dryer sand particles are picked up and transported by the wind. In the case of sand strips, the sand is transported in an organized, stripped way perpendicular to the wind direction. Sand transport increases when the beach surface dries, with all other variables being equal (Nield et al., 2011). Aeolian sediment transport therefore depends on the changing moisture content and can result in the formation of sand strips. The formation of sand strips does not only depend on the surface moisture, but on other bed characteristics as well, such as bed roughness (Hage et al., 2018b). However, bed roughness is also related to moisture content since the moist surface is rougher than the dryer sand strips. The difference in bed roughness between the wet and dry beach surface is likely to influence the aerodynamic roughness and ultimately aid in differential saltation patterns. The water in the moisture surface creates a smoother surface and less drag on airflow, and the development of adhesion structures will likely increase aerodynamic roughness and reduces the ability for aeolian transport to occur (Nield et al., 2011).

Besides, moisture content also influences the fetch as it can constrain the width of the beach (Bauer, et al., 2009). Tides and waves influence the conditions on the foreshore, which can cause the bed being too moist for the sand particles to be picked up, resulting in a decrease in fetch length. Surface moisture also increases the shear velocity threshold, which reduces the transport and extends the critical fetch length (Nield et al., 2011), therefore it is more likely that the critical fetch will exceed the maximum fetch length, resulting in limited transport (Hage et al., 2020). Moisture content is therefore important for the controlling and releasing of sediment from the surface.

Besides hydrodynamics affecting the moisture content on the foreshore, atmospheric humidity and precipitation events are critical to understand aeolian transport occurring at the upper beach (Bauer, et al., 2009). In these dryer upper regions, the surface moisture content typically is less than 5% and these atmospheric conditions are the most prominent factors in aeolian transport rates (Nield et al., 2011). Precipitation can result in a sharp decrease in aeolian transport, since sand strips might disappear (Hage

et al., 2018b) and the intensity of streamers decrease (Davidson-Arnott & Bauer, 2009). However, streamers can remain visible with the presence of a wind speed of 10 *m/s* or more. Strong winds could also cause the reappearance of sand strips an hour after the precipitation stopped. Limited and unlimited events did not differ in the presence, duration and amount of precipitation (Hage et al., 2018a).

Jackson & Nordstrom (1998) conceptualized five conditions that describe transport over an initially moist bed that is drying. The first condition is the saltation of moist sediment across a moist bed surface under high wind speeds. The second condition begins with in-situ drying of the surface, followed by a saltating layer of dry sand. The second condition is therefore comparable with the streamers and is common when the shear velocity is between the wet and dry thresholds. Condition three involves the transport of dry sediment from bedforms (including sand strips), accumulated on the moist bed surface. These bedforms represent a secondary sediment source. The fourth condition involves entrainment from a dry upwind source and transport across a moist bed surface and the last condition is the sediment transport on a completely dry surface.

2.3 Sand strips affected by wind characteristics

Small changes in wind characteristics will have an immediate effect on the short-term variations in aeolian transport rate (Bauer et al., 2009). Aeolian sand transport in the form of sand strips only occurs if the wind speed exceeds a threshold velocity of around 8 *m/s* (Hage et al., 2018b). An exceedance of this threshold velocity does not significantly lead to an increase in intensity of the transport, only to more saltation events (Bauer et al., 2009). It leads therefore to a more continuous transport in terms of intermittency, but the mass flux will remain unsteady (Davidson-Arnott & Bauer, 2009).

There are two types of transport events: supply-limited and -unlimited transport. For supply-limited transport the transport is governed by the supply rate, while for unlimited transport, when upwind supply exceeds the transport capacity of the wind, the transport rate is determined by the capacity of the wind. Wind-driven equilibrium transport rates do not occur for limited events, and transport is governed by the supply. For unlimited events, wind-driven equilibrium transport rates exist and the transport is governed by the wind (de Vries et al., 2014). Limited and unlimited events both happen under a wide range of wind speeds. According to Hage et al. (2018a) high wind speeds are more common features for limited events and unlimited events show a somewhat lower average wind speed. However, De Vries et al., (2014) suggest that the transport capacity decreases with decreasing wind speed, resulting in sedimentation, and transport capacity increases with increasing wind speed, resulting in more aeolian transport and sand picked up by the wind. Hage et al. (2018a) suggest that the type of transport is more related to the duration of the wind event. When the beach is covered with sand strips, they consider the transport event as unlimited. When there is no aeolian transport visible, it is considered as a limited transport event because the wind speed was above the threshold velocity and it should result in visible signs of transport. Limited transport events also have a smaller transport rate, and the actual rate depends on the ratio between the critical fetch and maximum fetch (Hage et al., 2020).

The wind direction, however, cause changes in intensity in the appearance of sand strips. Well-developed bedforms form when the wind is (almost) alongshore directed, while cross-shore winds result in poorly developed bedforms (Hage et al., 2018b). This implies that the intensity of the transport is governed by the wind direction. Hage et al., (2018a) suggested that the wind direction could be more important than the wind speed, due to the fact that the maximum fetch length is determined by the wind direction and the beach width. More alongshore winds lead to an increase in maximum fetch length, while during onshore winds the maximum fetch will be smaller than the critical fetch and no full transport is reached. The critical fetch is the fetch at which aeolian transport has saturated at its potential volume and it is the distance from the leading edge of the transport surface to the point where maximum transport is achieved in downwind direction (Bauer & Davidson-Arnott, 2003). The critical fetch is governed by the wind speed as well as by the supply rates (de Vries et al., 2014). The limitation of supply could, however, dominate over fetch effects. As a result the concept of the critical fetch could be

argued to be unsuitable for supply-limited situations. With an increase in fetch length, the transport rate will evolve towards an equilibrium transport (Bauer et al., 2009). However, the actual fetch length is typically shorter than the critical fetch length and therefore it is rare to find equilibrium conditions on beaches. Therefore, the critical fetch can limit transport on a narrow beach as the beach width, and therefore the fetch, is small compared to the critical fetch length (Bauer & Davidson-Arnott, 2003).

Besides, an equilibrium transport rate is unlikely to occur because of the development of an internal boundary layer in the atmosphere immediately downwind of the ocean-beach transition with a steep vertical gradient in the horizontal velocity (Bauer et al., 2009). These steep gradients imply large shearing stresses acting on the foreshore, indicating large potential for sand transport, while the internal boundary layer causes a decrease in wind speed and shear velocity in dune-ward direction. Atmospheric turbulence has therefore an important role in the control of sand transport in aeolian environments (Baas, 2007). Measurements on the wind field alone would suggest that most transport would occur on the foreshore and decreases due to the internal boundary layer in downwind direction. This is, however, not 100% correct to say as there is no sand supply from the upwind direction resulting in less aeolian transport on the foreshore (Bauer et al., 2009). Nevertheless, it is correct that the transport potential decreases in dune-ward direction because of the development of this internal boundary layer, despite an increase in fetch length. This internal boundary layer causes a decrease in near-surface wind speed in dune-ward direction, which decreases the near-surface shear stress, but this decrease is not investigated in depth in coastal aeolian geomorphology (Bauer et al., 2009). This decrease in wind speed in dune-ward direction may possibly explain why sand strips move at different migration rates along the width of the beach, which may subsequently result in interactions between sand strips (Hage et al., 2018b).

Not only the wind direction determines the fetch length, also the tide, and therefore the moisture content affect the fetch length. Moist sand can increase the critical fetch length with 50% or more, and it is also possible that the bed is too moist for the sand to be picked up by the wind, resulting in a decrease in fetch length (Smit et al., 2018). During rising tide, the maximum fetch distance seems even more important than the moisture content. During falling tide, sand from the intertidal beach becomes available for aeolian transport since the sand dries below the moisture threshold for aeolian transport.

3. Data description

In this chapter, more information regarding the data is given. In section 3.1 the study area is explained, followed by an explanation of the data obtained with the terrestrial laser scanning (TLS) in section 3.2. Besides, sand samples are acquired on the beach as discussed in section 3.3 for the determination of the moisture content and grain size. To correlate sand strip behaviour to environmental conditions, weather and tidal data are obtained from the Royal Netherlands Meteorological Institute (KNMI) and Rijkswaterstaat respectively as presented in section 3.4.

3.1 Study area

The study site is the beach of Noordwijk aan Zee, the Netherlands, located near the middle of the Dutch coast (grey dot in Figure 3.1). The coastline has a straight orientation of 30° with respect to the North and faces the North Sea. The beach width depends on the tide and ranges between 100 *m* and 200 *m*. Noordwijk explores a semi-diurnal tide with a 1 *m* and a 1.8 *m* tidal range at respectively neap and spring tide (Walstra et al., 2012). The dominant wave direction for waves approaching the Noordwijk coast is southwest (SW) and north-northwest (NNW) (Quartel et al., 2007). The mean wave height along the Dutch coast is 1.2 *m* and the mean wave period is equal to 5 seconds. Since alongshore differences in wave climate are small, these conditions can also be applied for the Noordwijk coast (Wijnberg & Terwindt, 1995). Furthermore, the wind climate is dominated by winds coming from the southwest (SW) and are thus oblique-alongshore.

Figure 3.1. Location of the field site at Noordwijk (grey dot in the overview), along the Dutch coast. The blue dot in the inset shows the location of the laser scanner with the range of the laser scanner indicated with the orange rectangle. The locations of the two weather stations used relative to the study area in Noordwijk (grey dot) are shown with red dots, the water level stations are shown with yellow dots.

Figure 3.1 shows an overview of the study site showing (in the inset) the location of the laser scanner with the blue dot and the area covered by the scanner with the orange box. The laser scanner is located on top of Grand Hotel Huis ter Duin, and within its range are the beach, the dunes, the intertidal zone and the beach pavilion Breakers beach club (Figure 3.2). The laser scanner covers a distance of around 1 *km* in alongshore direction (500 *m* in both direction). In cross-shore direction, the laser scanner has a range of approximately 300 *m*.

Figure 3.2. The Riegl VZ-2000 on top of the balcony of Grand Hotel Huis ter Duin with its corresponding view over the beach

3.2 Data obtained with the terrestrial laser scanning (TLS) device

The Noordwijk beach is monitored as part of the CoastScan project since July 10th 2019 until June 21st 2022 using TLS (CoastScan, 2022a). Advantages of the TLS technique is that the data is acquired fast, the spatial coverage is large and the measurement accuracy is high (Soudarissanane et al., 2011). Due to the known and fixed location and orientation of the TLS 3D coordinates can be obtained. Due to its continuous and permanently scanning of the Noordwijk beach the TLS is referred to as permanent laser scanning (PLS), resulting in a 4D geospatial dataset due to the addition of the time dimension. This 4D geospatial dataset serves as basis to quantify changes over time (Vos et al., 2017). Short term morphological changes can be observed with point clouds (Figure 3.3), which can give a better understanding in long term coastal morphology. In the point cloud shown in Figure 3.3 the Noordwijk beach is visualized. The data gaps in the figure contain no data since they are shadow zones caused by obstacles in the range of the laser scanning device, e.g., due to the dunes (upper part), or the beach pavilion around $(x, y) = (-180,0)$. In the lower part of the figure parts with no data is caused by the water and not by a shadow zone.

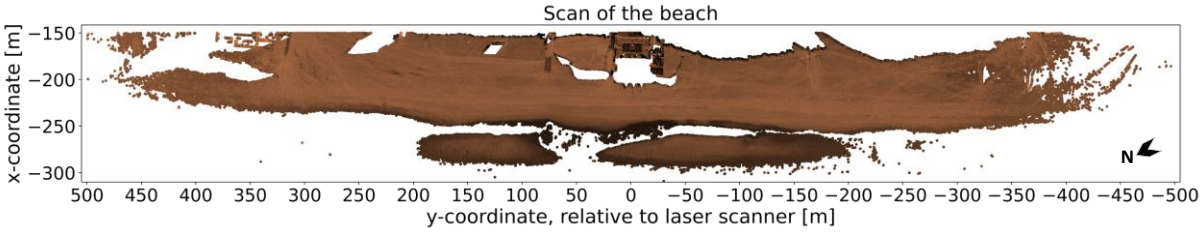

Figure 3.3. Point cloud of the beach. The data gaps are caused by shadow zones due to the presence of objects such as dunes/beach pavilion. Besides, the water contains no data points as well

The TLS that is used is a Riegl VZ-2000. The Riegl VZ-2000 integrates a Light Detection and Ranging (LiDAR) sensor with a rotating head and mirror to produce a 3D scan of the environment (Vos et al., 2017). The point clouds are obtained by measuring the distance to an object or surface with the time-of-flight (TOF) principle. The laser emits a pulse and the reflection of that pulse is also captured by the sensor (Figure 3.4). Using this two-way travel time (sending and receiving) the time gap is computed, which can be converted to a distance with an accuracy in the order of millimetres in combination with the speed of light (Soudarissanane et al., 2011; Angelopoulou & Wright Jr., 1999). Besides only determining the distance, and therefore the elevation profile, surface properties can be derived as well by measuring the intensity of the reflecting signal (Nield et al., 2011).

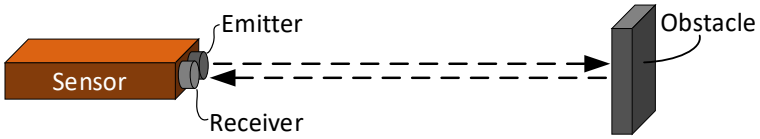

Figure 3.4. Time-of-flight (TOF) principle. Modified from Angelopoulou & Wright Jr. (1999)

Despite the high accuracy of the scanning technique, there are four main influences that can affect the quality of a point cloud. These influences are the scanner mechanism, the atmospheric conditions and environment, the object properties and the scanning geometry (Soudarissanane et al., 2011). For the set-up in Noordwijk the influence of the atmospheric conditions and environment, and the scanning geometry are most likely causes of detected errors (Vos et al., 2020). Due to its permanently scanning, there are varying atmospheric conditions present in the time period, which influences the repeated measurements.

The point clouds are provided in a local cartesian coordinate system. The original origin of the coordinate system is located at the laser scanner itself. The positive x-direction is directed land-inward, resulting in negative x-values at the beach. The positive y-direction is directed north-eastward (NE), parallel to the orientation of the beach and the positive z-direction is located upward. The elevation of the laser scanner is 55.76 *m* relative to MSL (mean sea level) (Di Biase et al., 2022), resulting in negative z-coordinates on the beach. The origin of the z-coordinate is therefore converted to +0 *m* MSL for a better interpretation of the z-coordinates while the x and y-directions remain unchanged, resulting in the location of the laser scanner at $(x, y, z) = (0; 0; 55.76)$ (Figure 3.5).

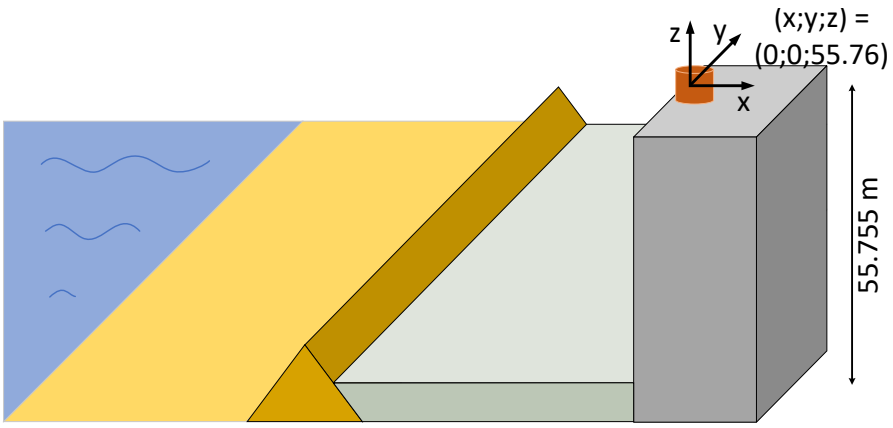

Figure 3.5. Local cartesian coordinate system of the laser scanner on top of the hotel. The figure shows schematically the position of the laser scanner compared to the sea, beach and dunes.

Due to the non-Lambertian behaviour of sand (Smit et al., 2018) a correction for the incidence angle between the laser scanner and the beach surface, i.e. the Lambertian cosine law, is not applied. The Lambertian cosine law states that the reflecting signal from the surface is proportional to the cosine of the angle between the direction of the incident laser beam and the surface normal (Gray, 1978). Sand acts as macroscopic irregularities within a laser footprint, and therefore there will always be sufficient sand particles perpendicular to the incident beam to neutralize the Lambertian cosine law. Smit et al. (2018) found that the reflectance values on the beach do not depend on the incidence angle up to an incidence angle of 88°, in correspondence with other literature. Even if the local slope of the beach is included in the consideration, the incidence angle is still below 88° for the full study area.

3.3 Sand sample acquisition during the fieldwork

Sand samples are acquired during fieldwork, executed at four different moments: February 4th, 17th and 18th and April 6th. The samples were obtained by scraping approximately the upper 3 *mm* of the sand with a spade with a vertical accuracy of roughly 2 *mm*, resulting in a sample weight of around 150 to 200 gram. Furthermore, each sample location is sampled once.

On February 4th, sand samples were taken from the crests of three sand strips, which were directed perpendicular to the waterline, in longitudinal direction (Figure 3.6). The longitudinal direction is mostly divided in three locations; one closest to the waterline, one closest to the dunes, and one in between them, with a distance of around 8 meters between each other. The transverse direction is divided into four different sample locations: the crest of the sand strip, the trough of the sand strip (the surrounding

beach) and both the windward and leeward side of the sand strip. On February 17th, two sand strips and the trough between them were sampled. The sand strips were directed more parallel to the waterline, and they were sampled in both transverse and longitudinal direction. On February 18th, two sand strips were sampled, also in both directions. Lastly, on April 6th three sand strips and four troughs were sampled in both directions. Besides, one large sand strip is sampled with more detail in longitudinal direction. The exact sample locations are determined with a GPS and they can be seen in Figure 3.7. In this figure all sample locations are visualized in the same figure, despite not being sampled on the same day. In appendix B every sample location is shown in more detail in a scan that is taken during the sample acquisition for a better visualization of the specific sand strip that is sampled.

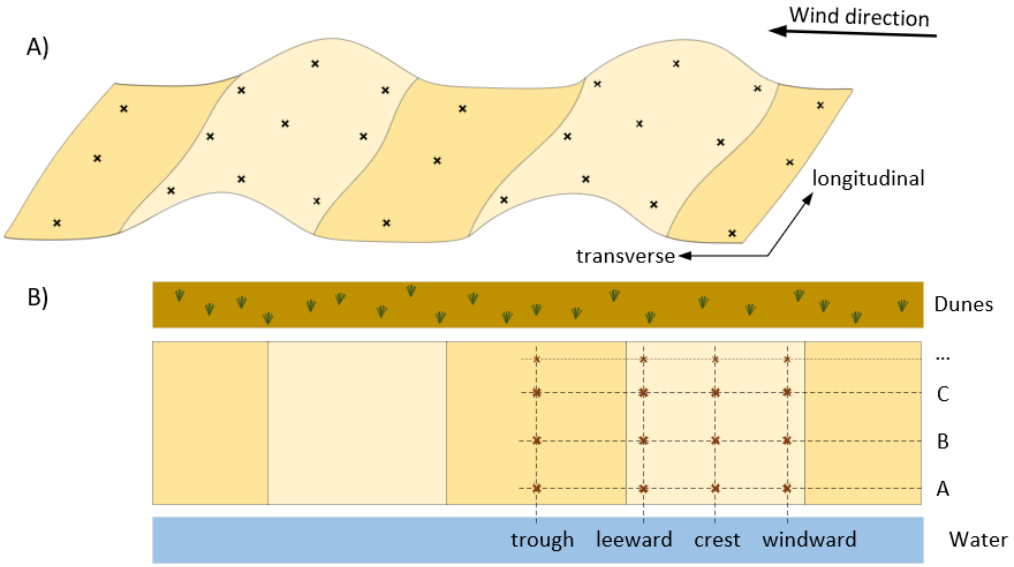

Figure 3.6. Overview of the locations of the sand samples that are taken. The lighter colour indicates the sand strips, the darker colour the surrounding beach. A) overview that shows the definition of the sample direction; B) letter code used for the longitudinal direction and the used terms for the transverse direction. The trough corresponds to the surrounding beach

The sediment samples were preserved in a sealed bag in a fridge, preventing evaporation and maintaining their original moisture content. Before the samples were oven-dried for about 14 hours, the in-situ (wet) mass is determined. After oven-drying, the samples are weighted again to determine the gravimetric moisture content according to equation 3.1.

$$w = \frac{m_{wet} - m_{dry}}{m_{dry}} \cdot 100\% \tag{3.1}$$

With:

- w: the gravimetric moisture content [$\%\ mass$];
- m_{wet}: the original mass of the sediment sample [g]
- m_{dry}: the dried mass of the sediment sample [g]

The grain size distribution of the samples is determined by dry sieving with twelve sieve screens ranging from 1.7 *mm* to 0.075 *mm*, based on BS1377-2 (1990). From the obtained grain size distributions, characteristic grain sizes are determined, such as the D_{50} (median grain size) as an indication of the primary grain size at each sample location. Furthermore, the D_{10}, D_{16}, D_{25}, D_{50}, D_{75}, D_{84} and D_{90} are determined to obtain information regarding the amount of finer and coarser particles. Comparing these characteristics for the different sample locations results in an analysis of the grain size variation over the sand strip.

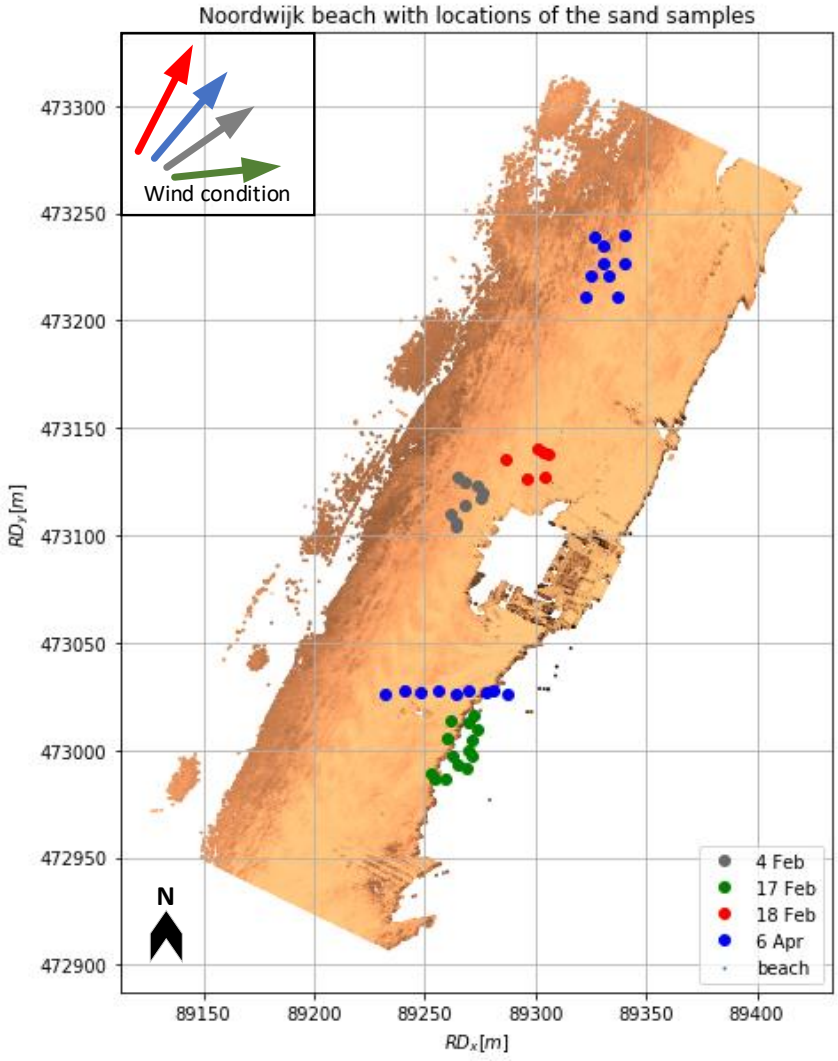

Figure 3.7. The sample locations on the beach. The coordinates are within the Dutch Rijksdriehoek (RD) system

3.4 Environmental data

The requested environmental data is official data rather than local amateur data due to the insufficiency of professional data at the study site. The requested environmental data are the wind conditions, consisting of both the wind direction and (hourly mean) wind velocity, precipitation and tidal data.

The wind conditions are acquired from the official KNMI station located in IJmuiden, and the precipitation from the KNMI station located in Voorschoten. The distance between the weather station in Voorschoten and the study area of the Noordwijk beach is approximately 11 *km* and is therefore the closest weather station to the study area. However, coastal winds occurring at Noordwijk differ from inland winds measured at Voorschoten. Therefore the wind conditions are acquired from the station located in IJmuiden, which is the closest coastal weather station to the Noordwijk beach (with a distance of approximately 25 *km*). The location of the stations of IJmuiden and Voorschoten are visualized with red dots in Figure 3.1.

Tidal data is requested from both the stations located in Scheveningen and IJmuiden. Scheveningen is located around 24.5 *km* from Noordwijk, whereas the water level station at IJmuiden is located 27.4 *km* from Noordwijk. Noordwijk is therefore roughly located in between these two water stations and the average water level of these two stations is used as estimation of the water level in Noordwijk. The locations of the stations of Scheveningen and IJmuiden are visualized with yellow dots in Figure 3.1, where the study area in Noordwijk is visualized with a grey dot.

4. Methodology

A Fourier transform (Cooley & Tukey, 1965) is applied for the detection of sand strips. Before this detection, some pre-processing steps for the raw point clouds are taken (section 4.1) as well as for the detection method (section 4.2). Thereafter, the detection method is applied as discussed in section 4.3. The workflow of the method including all the pre-processing steps can be seen in Figure 4.1. The sections in this chapter correspond to the grey boxes in the figure, and the sub-sections correspond to the orange boxes (except for the sub-sections in 4.3 where the characteristics for the detection as well as the differentiation between the 1D and 2D method are discussed while they are not detection steps).

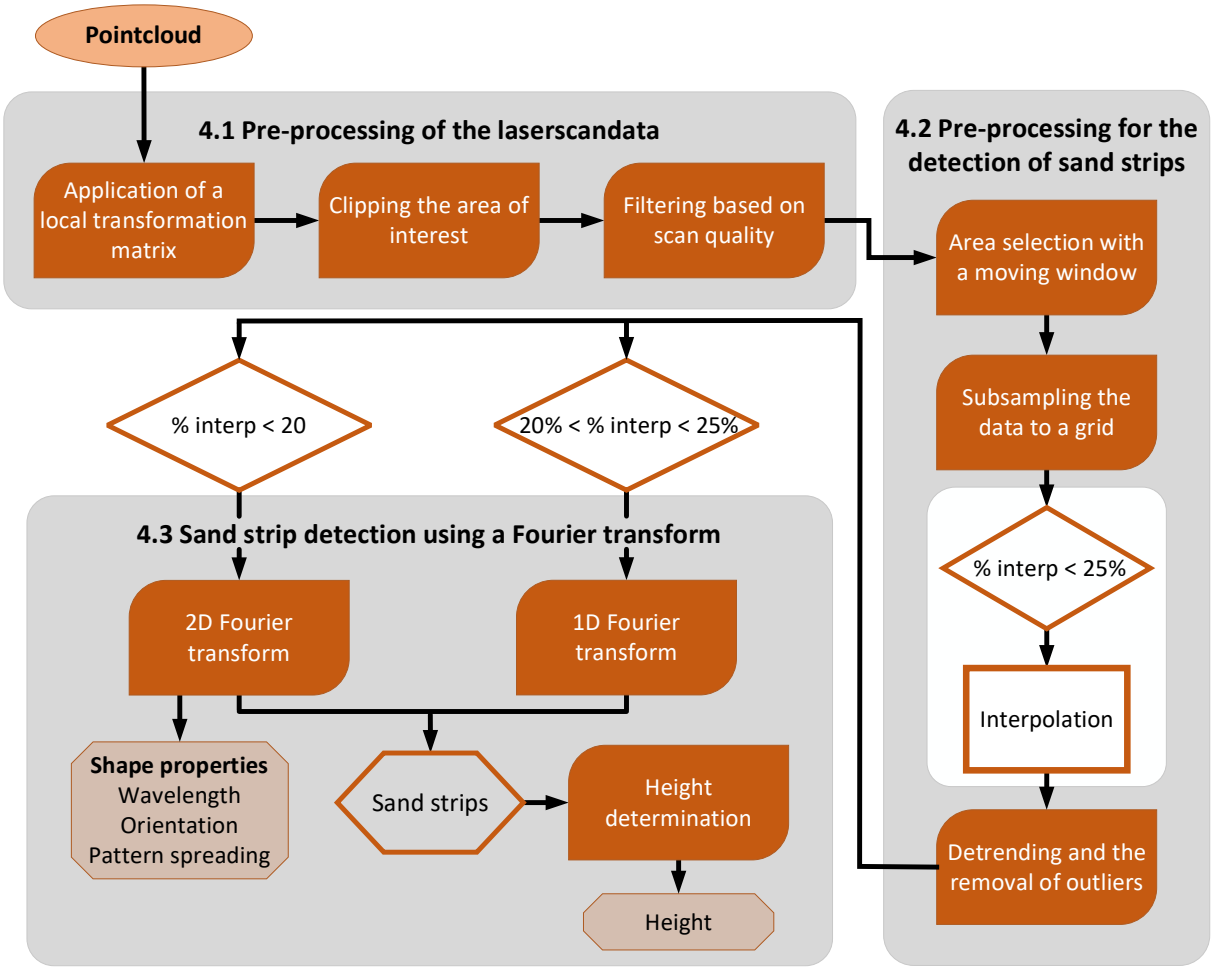

Figure 4.1. Workflow of the method, mainly divided in three parts shown in grey boxes. Each step that is taken has its own orange cell in the workflow. The light-orange cells are output variables

Furthermore, the detection, and therefore the surface plots as shown in this section, are based on the reflectance values. With the reflectance intensity of the used TLS-data, the surface moisture can be derived according to Di Biase et al., (2021), and the colour difference between the sand strips and surrounding beach (e.g., Figure 1.2) indicate a different moisture content between them.

Additionally, Riegl describes the reflecting intensity as a range-corrected amplitude, internally calculated by the scanner based on the calibration of the manufacturer. It is therefore important to note that the used reflectance differs from the target surface reflectance in the SI sense (Vos et al., 2022). This suggests that the used reflectance values are dimensionless. For clarification purposes the symbol *R* is therefore assigned at the reflectance values as internal unit.

4.1 Pre-processing of the laser scan data

Several pre-processing steps are executed on the raw point clouds in order to apply the detection method. First, the raw point clouds are aligned using a local, time-dependent, transformation matrix for the correction of small displacements. Secondly, the studied area is selected based on both the scanning geometry and the beach width, whereafter bad quality data is removed.

4.1.1 Application of a local transformation matrix

The laser scanner is subject to movements due to wind forcing resulting in small rotations of the laser head. These small variations affect the scanning geometry (Soudarissanane et al., 2011) resulting in measurement errors on the beach. To compensate for these errors, time dependent rotation matrices are calculated to minimize these measuring errors. These matrices are obtained by aligning georeferenced objects in the point cloud to known objects (and hence known locations) in the field. The beach pavilion in front of the hotel and the concrete access path to the beach north of the hotel are used as georeferenced objects. A more detailed explanation for obtaining these matrices is discussed in Joosse (2021).

4.1.2 Clipping the area of interest

Sand strips only appear at the beach, while the total area covered by the laser scanner also contains the dunes. Focussing on the beach only results already in a significantly smaller area of interest of 200 m by 1000 m in x- and y-direction respectively. The area of interest can be cropped even more based on the scanning geometry (in longshore-/y-direction) as well as the width of the beach (in cross-shore-/x-direction), positively affecting the computation time.

Clipping based on the scanning geometry

In longshore direction the area of interest is clipped based on the point density, which decreases with an increase in distance relative to the laser scanner. This decrease is caused by a combination of a small incidence angle and a large range (Smit et al., 2018). In Figure 4.2-A a point cloud of the beach with roughly constant reflectance values is visualized. The reflectance profile at the horizontal transect at x = -220 m with a width of 0.4 m is approximately constant (Figure 4.2-B), suggesting no sand strip occurrence on the beach. The point density decreases significant when the relative distance to the laser scanner exceeds 200 m. Furthermore, the reflectance values increase in absolute value when the distance exceeds 200 m, possibly caused by the large distance. Large distances can result in different values between the emitted and returned pulse, causing a lower accuracy (Smit et al., 2018). The area of interest is therefore limited to a range of -200 m to 200 m in y-direction relative to the laser scanner.

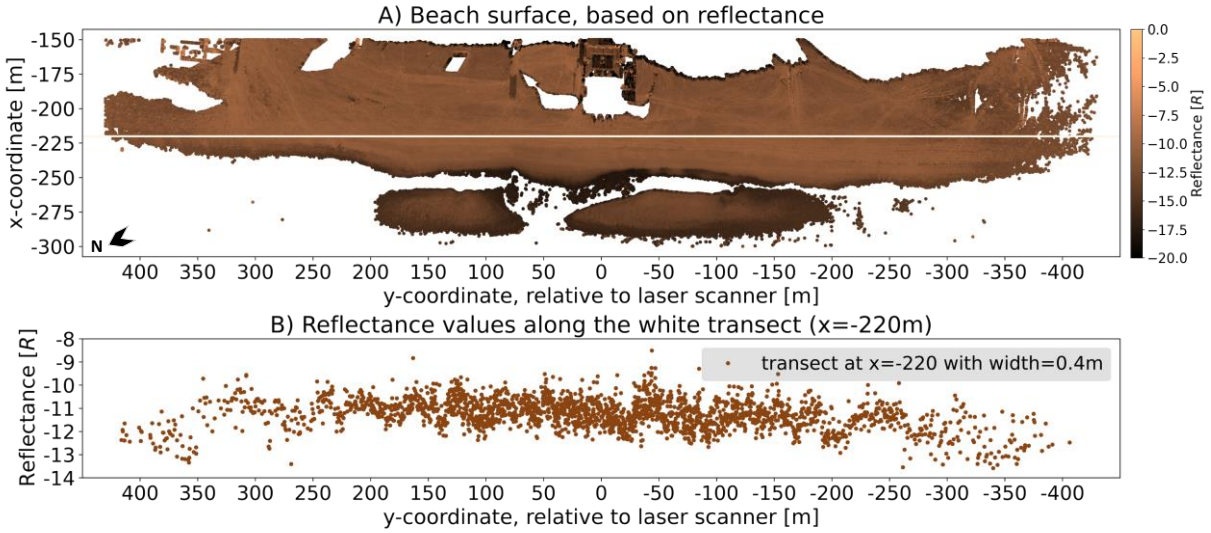

Figure 4.2. A) Visualization of the beach, based on reflectance with an horizontal line at x=-220m; B) The reflectance values along the white line at x=-220m in A

Clipping based on the beach width

The tidal cycle causes a variation in beach width over time due to the varying waterline. Therefore, the waterline is detected using the 1D point density of cross-shore profile lines every 20 m (Figure 4.3-A and B). As a result, the lower x-limit, and subsequently the total area of interest, can differ for each scan. In the example in Figure 4.3-C, the beach-water boundary is determined at x = -288.36 m (the black solid line in Figure 4.3-B and C). By this waterline detection, the area of interest is limited to the beach, preventing the application of the detection method on areas containing almost no data.

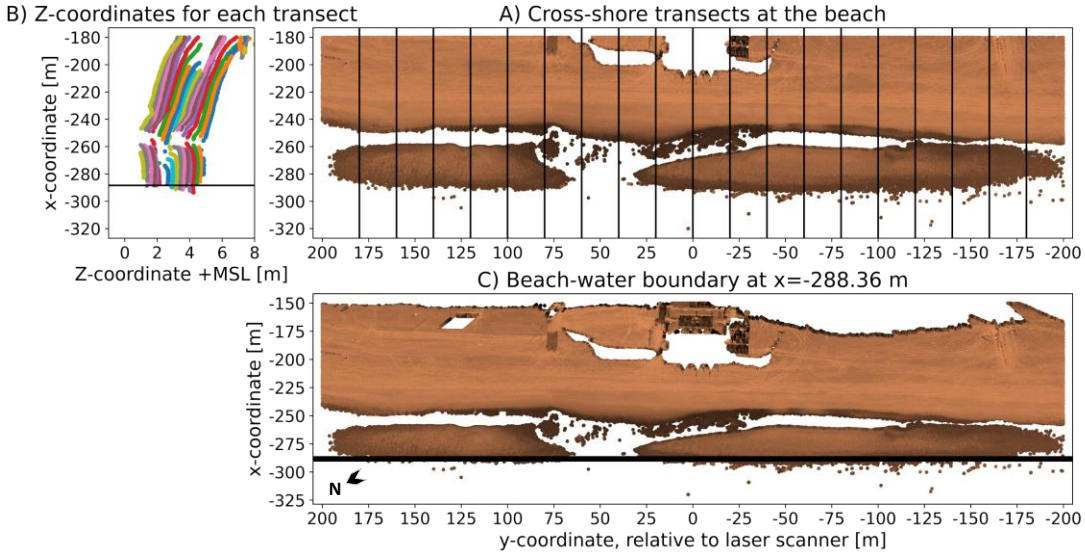

Figure 4.3. Detection of the end of the beach. A) Beach profile with cross-shore profile lines; B) Z-coordinates for each transect; C) Detection of the end of the beach (black line) using the point density for each profile line in B.

4.1.3 Filtering based on scan quality

The quality of the point clouds is determined according to three criteria, with two possible outcomes: good or bad quality data. The point clouds are considered bad quality if one of the three criteria is not met, and are then disregarded from the analysis. The first requirement is that a local transformation matrix should be provided with the point clouds. Furthermore, the point cloud should contain at least 1.000.000 data points in the area of interest with a beach-water boundary of at least x = -220 m, since the detection of sand strips in point clouds with too few points is not accurate. Most of the obtained point clouds contain around 8.000.000 data points and are therefore reliable and accurate. However, measurement errors or environmental conditions can cause notably less data points, resulting in less reliable and accurate data.

4.2 Pre-processing for the detection of sand strips

Sand strips are detected by a moving window in which the total area of interest is covered by smaller areas. Each window is subsampled to a grid that is detrended, and outlying points are removed.

4.2.1 Area selection with a moving window

The total area of interest is subdivided into several smaller windows by a moving window to maximize sand strip detection, since they do not necessarily occur at the full beach area. The windows have a fixed window size of 40 m in cross-shore (x) direction and 100 m in longshore (y) direction. They move over the complete beach to include all possible sand strips with a step size of 10 m in x-direction and 20 m in y-direction as visualized in Figure 4.4. Therefore, the windows are overlapping each other, preventing sand strips from being excluded during detection.

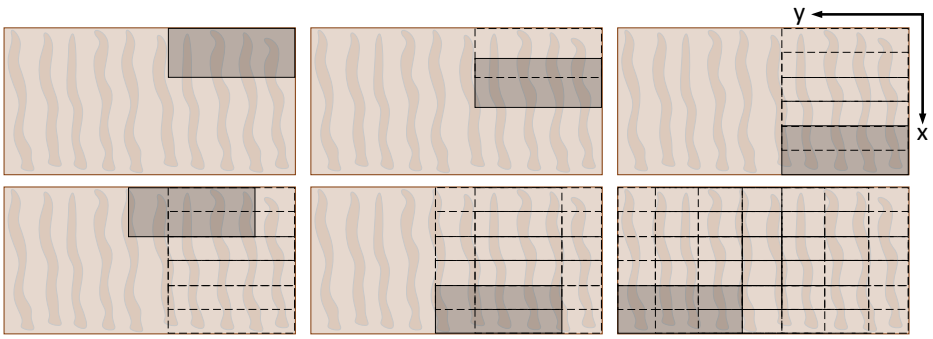

Figure 4.4. Visualization of the moving window

4.2.2 Subsampling the data to a grid

The data in each window is subsampled to a grid because a fixed grid size is needed for the application of the detection method and it reduces the computation time. Furthermore, it reduces the accuracy of the data since multiple neighbouring points are averaged. The quality of the resulting grid depends on the grid size. A too small grid size will result in much interpolation, increasing the computation time and decreasing the representativeness of the grid due to the caused errors by too much interpolation. Contrarily, a too large grid size results in very rough and less accurate data. Thus it is necessary to find an optimal grid size in order to keep the grid as representative as possible, while also constraining the computation time.

The optimal grid size is selected based on the percentage of interpolation required and on the footprint size of the laser pulse. A grid size of 0.40 *m* results in a percentage of interpolation required of 5.7% (Figure 4.5). Similar, a grid size of 0.30 *m* corresponds to an interpolation percentage of 22.5% and a grid size of 0.50 *m* to 1.5%. Therefore, a grid size of 0.40 *m* will save a lot of computation time compared to a grid size of 0.30 *m*, while a grid size of 0.50 *m* does not significantly improve the computation time. Thus, a grid size of 0.40 *m* is assumed best for the computation time, resulting in a squared cell area of 0.16 m^2. The footprint size of a laser pulse is estimated by the point density of different areas of interest. This is however a simplification since it is assumed that the areas are covered with evenly spread datapoints, and that the size of the footprint is constant despite their dependency on the range to the laser scanner and the incidence angle (Di Biase et al., 2022). Furthermore, the footprint has an elliptical form instead of squares. This simplified estimation resulted in an (elliptical) footprint size of 0.09 m^2. A grid size of 0.40 *m* leads thus to a slightly larger covered area, which is assumed acceptable due to the dependency of the footprint size on the distance to the laser scanner and incidence angle. Therefore, the applied optimal grid size is assumed to be 0.40 *m*.

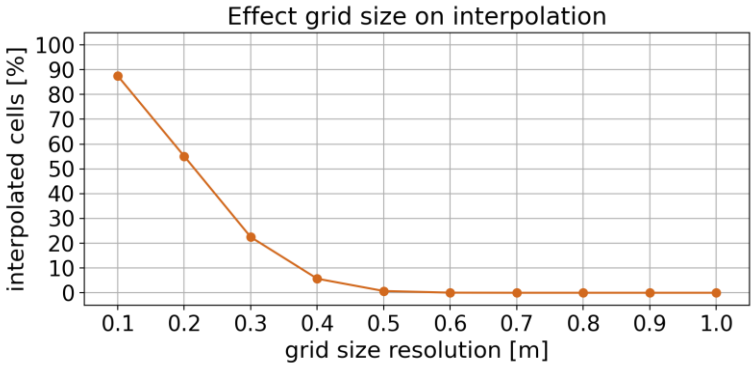

Figure 4.5. Effect of the grid size on the amount of interpolation required

4.2.3 Detrending and the removal of outliers

The dominant 2D linear trend is detrended from the data, which facilitates the detection of sand strips. Such dominant trend can be caused by the tide. High tide leads to an increase in moisture content in the intertidal zone, whereas the moisture content at the upper beach does not increase. This large spatial-scale difference in moisture content is not of importance since the presence of sand strips suggest a small spatial-scale difference in moisture content. Detrending the window causes the focus to shift towards moisture content differences on the smaller spatial-scale, hence facilitating the detection of sand strips.

Besides detrending the window, outliers are removed as well. Measurement errors or obstacles present on the beach (such as persons) induce outliers, leading to more difficulties in analysing the point cloud. A datapoint is considered an outlier if it has a value larger than the mean value plus five times the standard deviation or smaller than the mean value minus five times the standard deviation of the window. Outliers are replaced with a value equal to the mean value of the window.

The effect of detrending and the removal of outliers is visualized in Figure 4.6. In Figure 4.6-A, the original reflectance values are shown, where the dominant trend is clearly visible. At the top left corner, the reflectance values are larger in terms of absolute value than the values on the lower right corner (Figure 4.6-B). Detrending results in a window with more constant reflectance values where sand strips are still visible (Figure 4.6-C). The removal of outliers can also be seen in the figure. Around (x, y) = (-228, 97) a small area of outliers can be seen in Figure 4.6-A (less negative reflectance values) while they are not visible anymore in Figure 4.6-C.

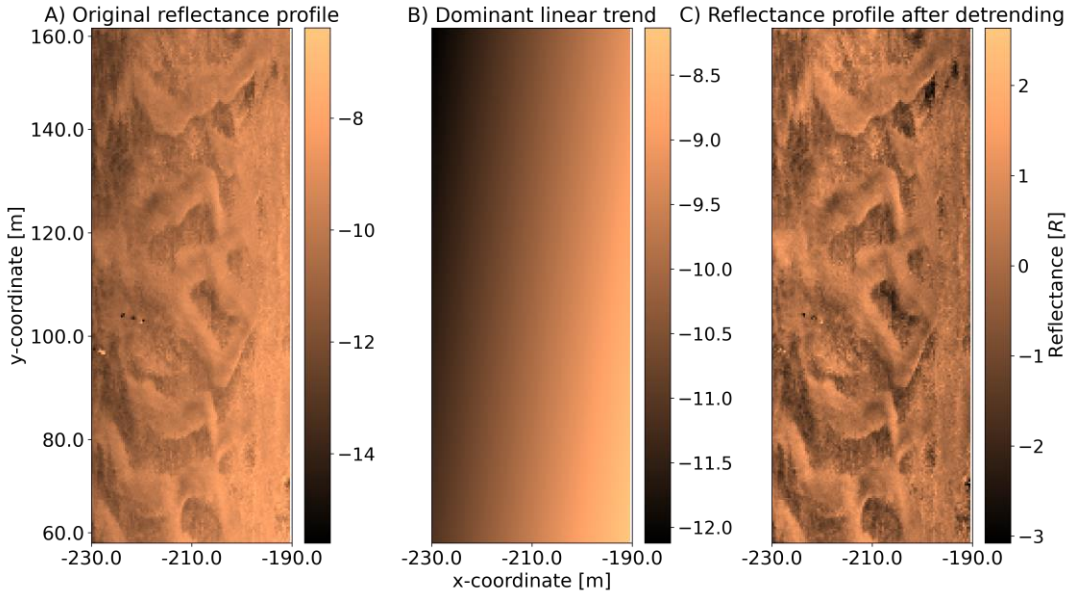

Figure 4.6. Application of detrending the data, A) the original window based on the reflectance values; B) the dominant trend present and; C) the resulting window after detrending and the removal of outliers

4.3 Sand strip detection using a Fourier transform

The application of either the 1D or 2D fast Fourier transform (FFT) (Oliphant, 2006) as detection method for sand strips is elaborated in this section. The characteristic parameters that are used for this detection are discussed first in section 4.3.1. The differentiation between the 1D and 2D method is discussed in section 4.3.2. The 1D method is presented in section 4.3.3, followed by the 2D method in section 4.3.4. Last, the height determination is elaborated in section 4.3.5.

4.3.1 Characteristics of the sand strip detection

The detection method is based on the reflectance values due to the derivation of the moisture content from the reflectance values. A less moist sand surface will lead to a less strong reflecting signal in terms of absolute value. If there are sand strips present on the beach, the reflectance values show a certain waveform with higher (less negative) reflectance values on the sand strip (crest) compared to the surrounding beach (trough), visualized in Figure 4.7 where the sand strips have a less strong reflecting signal in terms of absolute value. The differences in reflectance values is more pronounced than in elevation, since not all sand strips will have a significant height difference compared to the surrounding beach. A detection based on the z-coordinates, and therefore on the height of the sand strips, will not detect all sand strips due to present irregularities and the accuracy of the laser scanner being in the same order of magnitude. Only if sand strips are detected in a window based on the reflectance values, a Fourier transform based on the z-coordinates is applied to determine the height in the same window.

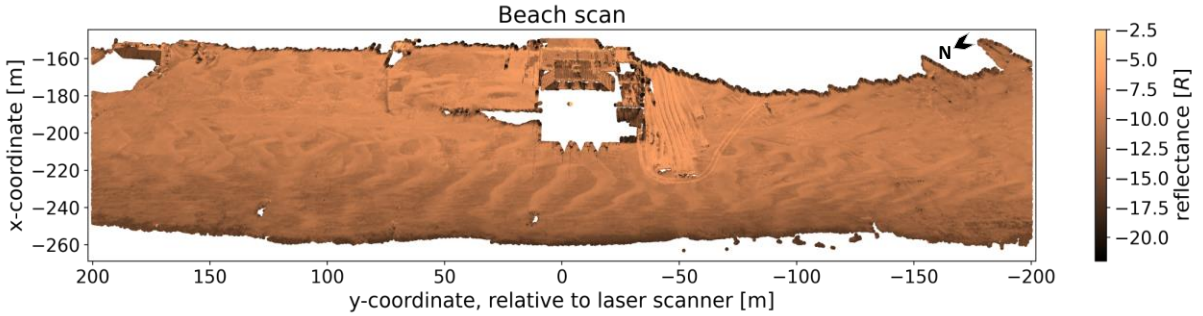

Figure 4.7. Point cloud of the beach based on reflectance values, sand strips are visible

Sand strips are detected based on the dominant waveform that is present caused by the different reflectance values. Additionally to this waveform, the reflectance values also contain irregularities due to natural processes on the beach. By applying a Fourier transform, the reflecting signal of the profile is decomposed into different waveforms with their corresponding wavenumber. The obtained variance density spectrum shows the distribution of the variance over the wavenumbers constituting the profile. A large peak in the spectrum coincides with a strong signal of the corresponding wavenumber. An advantage of a variance density spectrum is that it provides a complete statistical description of the waves and the definition is given in equation 4.1 (Holthuijsen, 2007).

$$E(k) = \lim_{\Delta k \to 0} \frac{1}{\Delta f} \frac{1}{2} {a_m}^2 \tag{4.1}$$

With:

- $E(k)$: the variance density spectrum;
- a_m: the mean amplitude of the wave-pattern and;
- Δk: the wavenumber bandwidth

The variance density spectrum will show a peak at wavenumber k of $E(k)$ if a wave pattern with wavelength L $(= 1/k)$ is dominant in the profile. Based on the height of this spectral peak and the corresponding wavenumber, sand strips are detected. When sand strips are present, a large peak will occur around k = 0.083 m^{-1} in the variance density spectrum. This wavenumber is observed by Hage et

al. (2018b), who observed an average wavelength of 12.0 m for sand strips in their study. Contrarily, irregularities result in a much smaller spectral peak height at larger wavenumbers due to their less significant difference in reflectance values and their wavelength of $O(cm)$, respectively. Furthermore, detrending causes a significant decrease in spectral peak height at very low wavenumbers of $O(\text{window size})$, facilitating the detection of the peak caused by sand strips. Therefore, the detection of sand strips is based on both the spectral peak height and the corresponding peak wavenumber.

4.3.2 Differentiation between the 1D and 2D Fourier transform as detection method

Sand strips are detected by either the 1D or 2D Fourier transform, while only the shape properties according to the 2D Fourier transform are analysed. The 1D Fourier transform does not consider the orientation of the sand strips, causing an overestimation of the wavelength. Since sand strips are detected for both methods dependent on a range of possible wavenumbers corresponding to sand strips, a rather rough upper boundary is applied for the 1D Fourier transform due to this overestimation. The range of wavelengths considered for the 1D Fourier transform is between 6.67 m and 25.0 m, or alternatively $0.04 < k < 0.15$ m^{-1}. For the 2D Fourier transform this range is more strict with a wavelength ranging between 8.00 m and 18.18 m, or alternatively $0.125 < k < 0.056$ m^{-1}.

For a proper determination of the shape properties, the 2D Fourier transform is only applied on more accurate data compared to the 1D Fourier transform. The accuracy of the data in each window is determined according to the amount of interpolation required. Windows with a required interpolation of at least 25% for the complete window area are not considered in the detection method. The 1D Fourier transform is applied on windows with a required interpolation between 20% and 25%, and the 2D method is applied when the required interpolation in the window does not exceed 20%. In comparison: the applied grid size of 0.40 m provides on average a required interpolation of 5.7% (section 4.2.2). The applied interpolation method is linear interpolation.

4.3.3 Sand strip detection using a 1D Fourier transform

The 1D method draws five vertical lines through the window that store the reflectance values along these transects. In Figure 4.8-A only one line is drawn for illustrational purposes. The reflectance profile of this transect is shown in Figure 4.8-B with the corresponding variance density spectrum according to the grey line in Figure 4.8-C. Sand strip occurrence in the window is assumed if at least four out of the five transects suggest their presence.

The detection of the spectral peak in the variance density spectrum that corresponds to sand strip occurrence is an iterative process. First the largest spectral peak is determined, and the wave pattern corresponding to this peak is approached with the inverse fast Fourier transform (IFFT), visualized with the orange spectrum in Figure 4.8-B corresponding to the orange variance density spectrum in Figure 4.8-C. This Fourier approximation is compared to the original reflectance profile by the root mean square error (RMSE). It is assumed that the Fourier approximation coincides with the original reflectance profile when the RMSE is below 0.5, and the corresponding wavenumber to the spectral peak is assumed as the wavenumber of the reflectance profile. If the RMSE is above 0.5, the next highest peak in the spectrum is considered, and again the profile is approached with the IFFT until the RMSE-criterion is met. Sand strips presence is suggested if the correct peak height (with a RMSE < 0.5) exceeds 10 $R^2 \cdot m$ and the corresponding wavenumber is in the range $0.04 < k < 0.15$ m^{-1}.

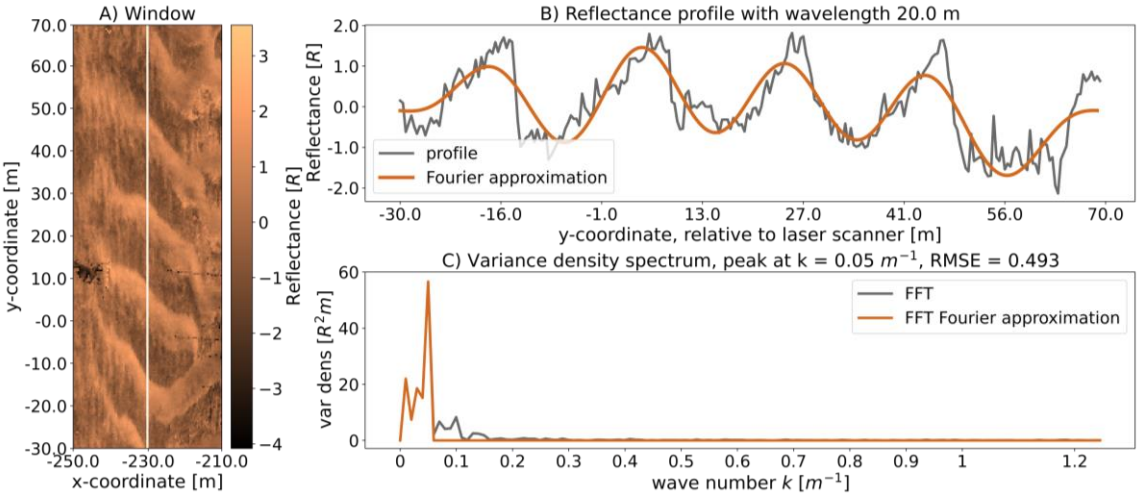

Figure 4.8. Example of the 1D Fourier transform. A) a window where sand strips are present, based on reflectance values; B) the reflectance values along the white transect in A (grey) and the Fourier approximation (orange); C) the variance density spectrum of the original profile (grey) and the Fourier transform which is used to approach the wave pattern (orange

4.3.4 Sand strip detection using a 2D Fourier transform

The 2D method includes two directions (the x- and y-direction), resulting in two wavenumbers; k_x and k_y. The resultant wavenumber is determined according to equation 4.2.

$$k = \sqrt{{k_x}^2 + {k_y}^2} \tag{4.2}$$

Due to the focus on the wavenumber range $0.125 < k < 0.056\ m^{-1}$, the energy in the variance density spectrum corresponding to other wavenumbers is removed (Figure 4.9-B, where the spectrum corresponding to the window shown in Figure 4.9-A is presented as a logarithmic for illustrational purposes). It is empirically derived that the detection method suggests sand strip occurrence if the total energy in the remaining spectrum exceeds 1000 $(R^2 \cdot m)^2$, for a total spectral energy below this threshold no sand strips are detected. In Figure 4.9-A sand strips are present and the total energy in the remaining spectrum is above the threshold (graph title of Figure 4.9-C), suggesting sand strip occurrence.

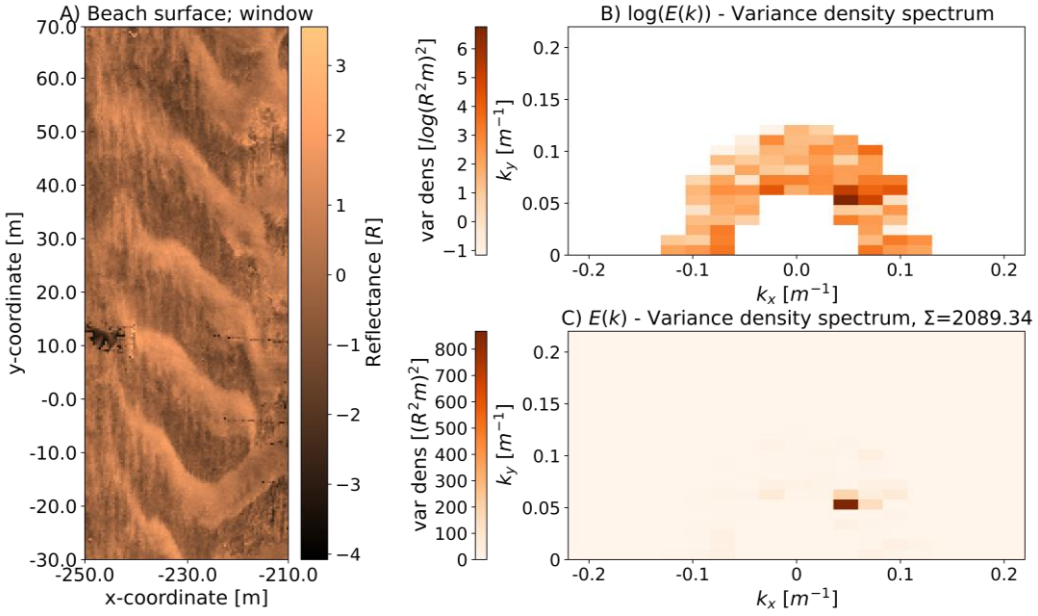

Figure 4.9. A) The beach surface profile based on reflectance values, sand strips are present; B) the variance density spectrum as a logarithmic to visualize the wavenumbers of interest; C) the variance density spectrum used to detect sand strips

If the interpolated cells are not evenly spread, i.e., due to data gaps, problems can occur. The distance between the valued-cells is then too large for the interpolation to be accurate and subsequently the interpolated cells do not correspond to the neighbouring values. E.g., Figure 4.10-A and Figure 4.10-B with B the interpolated window where the interpolated area does not coincide with the neighbouring values, caused by the too large percentage of interpolation along the x-axis (> 20%) for a width of roughly 7 m (Figure 4.10-C). For such data gaps the energy in the spectrum increases significant for low-valued k_y's, initiating a total energy above the detection threshold (Figure 4.10-D). By excluding these low-valued k_y's, the spectral energy decreases significant, preventing the detection of these pseudo-sand strips caused by interpolation (Figure 4.10-E). Therefore, the low-valued k_y's are removed from the wavenumber range of interest if the required interpolation along the x-axis is above 20% for a width of at least 2 m. Furthermore, if the amount of interpolation along the x-axis is at least 70% for four consecutive x-values (corresponding to a data gap of 1.6 m in x-direction and 70 m in y-direction), the window is disregarded instead of filtering the wavenumber range since this amount of interpolation is considered too much, resulting in no reliable results.

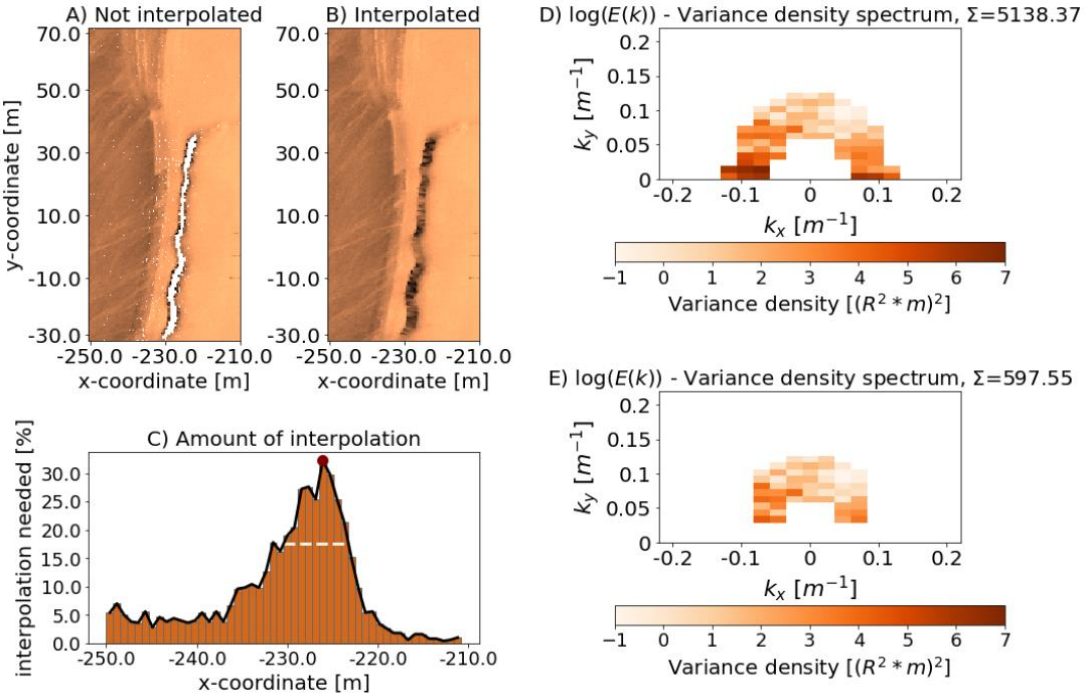

Figure 4.10. Effect of a lot of interpolation. A) and B) the area considered; C) the percentage of interpolation along the x-axis; D) the original variance density spectrum as a logarithmic; E) the variance density spectrum after taking into account the amount of interpolation

Only sand strip patterns with a clear orientation are considered for this study (referred to as a 1D/unimodal pattern). The amount of peaks in the spectrum is therefore also a requirement, determined by the distribution curves of both k_x and k_y. In Figure 4.9-A only one dominant orientation can be observed, resulting in one peak in the variance density spectrum in Figure 4.9-C. The distribution curves of both k_x and k_y for this spectrum are shown in Figure 4.11. The peaks of both distribution curves are determined, resulting in one peak per distribution. The spectrum, and the corresponding sand strip pattern, is therefore considered unimodal.

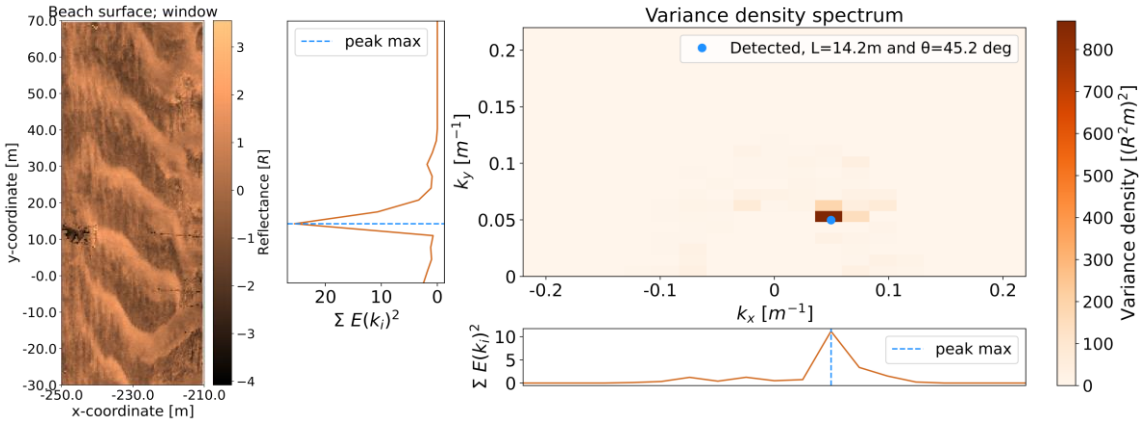

Figure 4.11. Variance density spectrum with corresponding distributions of k_x and k_y. Both curves show a clear uniform distribution. The blue dotted line represents the significant peak with their corresponding wavenumbers.

Less uniform oriented sand strips do also occur, resulting in a larger spectrum spreading (Figure 4.12; the sand strips are oriented less uniform, resulting in a larger spectrum spreading. However, the window is still considered unimodal). A larger spreading can result in more peaks in the distribution curves. Therefore, the significant peaks are determined for both the k_x and k_y distribution. Properties that are used to define significant peaks are the height and the prominence of the peak.

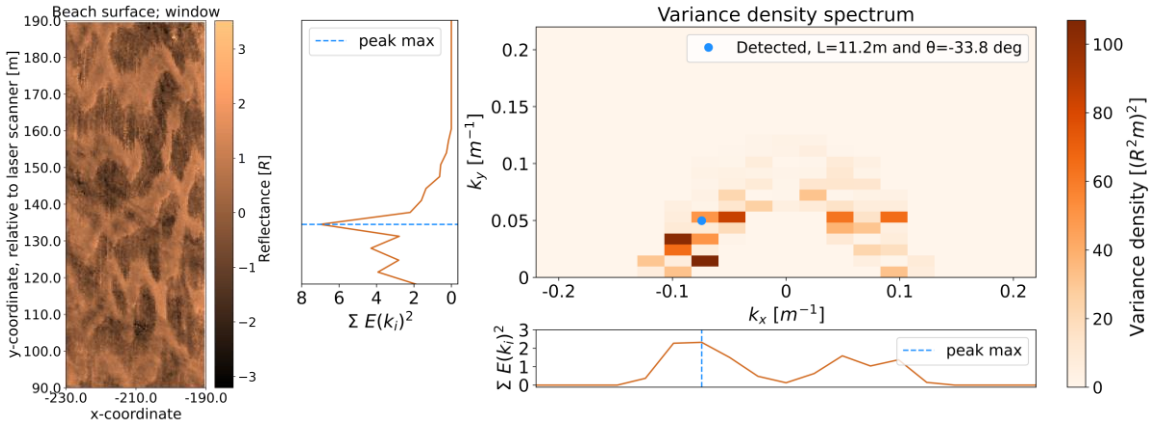

Figure 4.12. Variance density spectrum with corresponding distributions of k_x and k_y. Both curves contain a larger amount of spreading. The blue dotted line represents the significant peak with their corresponding wavenumbers and only one significant peak is detected for both curves

The prominence characterizes the tendency of a peak to dominate its surroundings. The prominence can be defined as the minimum vertical distance a mountain must descend from a point in order to reach a higher point. In other words: when walking downhill from peak A in order to reach a higher peak B, one probably reaches a minimum elevation which is called the saddle point (there are two paths leading uphill away from the saddle point; one path to peak A and the other path to peak B). The prominence of peak A is then equal to the peak elevation minus the elevation of its key saddle, illustrated in Figure 4.13. It can be shown that two peaks do not share the same key saddle (Kirmse & de Ferranti, 2017).

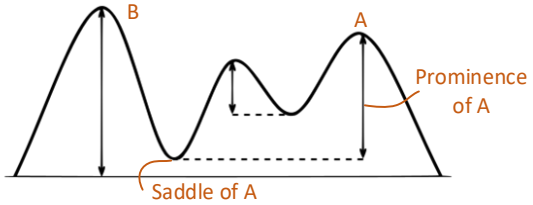

Figure 4.13. Definition of the prominence of a peak

Peaks in the distribution curves are considered significant if the peak height exceeds 3/4 of the maximum height of the distribution curve and when the prominence exceeds at least 1/3. These factors correspond best to multiple observations. The amount of significant peaks that are detected determine the modality of the distribution curve. A modality other than unimodal (bimodal or even multimodal) suggest that there is no clear, uniform orientation, resulting in a so-called 2D pattern. Due to the focus on 1D sand strip patterns only, these 2D patterns are not considered and only the unimodal 1D patterns are analysed.

Determination of the shape properties; wavelength, orientation and pattern spreading

For the 1D patterns, the wavelength, orientation and pattern spreading are determined. The resultant wavenumber can be determined using equation 4.2, with the values of k_x and k_y equal to $k_{x,peak}$ and $k_{y,peak}$ obtained with the distribution curves respectively. With the resultant wavenumber the corresponding wavelength can be obtained according to equation 4.3. The orientation (θ) can be determined according to equation 4.4, which is in degrees relative to the horizontal (Figure 4.14).

$$L = \frac{1}{k} \tag{4.3}$$

$$\theta = \tan^{-1}\left(\frac{k_y}{k_x}\right) \tag{4.4}$$

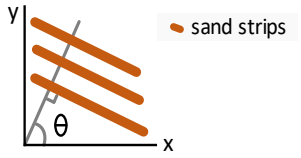

Figure 4.14. Definition of the angle θ which determines the orientation of the sand strips

The pattern spreading is determined with the width of the significant peak. The standard deviation, a common measure for the spreading of a distribution, is related to the full width at half maximum (FWHM) for a Gaussian distribution according to equation 4.5 (Locci-Lopez et al., 2018). Subsequently, the FWHM is a common measure for the spreading of a distribution too (Markevich & Gertner, 1989). Due to the bandwidth Δk_i (with i denoting either x or y) the wavelength and orientation are discrete values. The distribution curve is therefore also represented by discrete values. However, the values that represent the pattern spreading are continuous, caused by the interpolation to find both the left and right intersection points that determine the FWHM (Virtanen, et al., 2020).

$$\Gamma = 2\sqrt{2\ln(2)}\,\sigma \tag{4.5}$$

With:

- Γ: FWHM, full width at half maximum and;
- σ: standard deviation

The shape properties and characteristics of the two windows visualized in this section that are used as example (Figure 4.11 and Figure 4.12) are summarized in Table 4.1 (with respectively 'left' and 'right' in the table). Besides, the detected orientation for both windows is shown in Figure 4.15 with two blue arrows. For both windows the detected orientation represents the orientation of the sand strips accordingly. The detected orientation is therefore considered an appropriate representation of the orientation of the sand strips in the window.

Table 4.1. Shape properties of the two windows used as example. 'left' and 'right' correspond to the windows of Figure 4.15

	$k_{x,p}$ $[m^{-1}]$	$k_{y,p}$ $[m^{-1}]$	$k_{res,p}$ $[m^{-1}]$	L $[m]$	θ [°]	$FWHM_x$ $[m^{-1}]$	$FWHM_y$ $[m^{-1}]$
left	0.050	0.050	0.070	14.2	45.2	0.031	0.013
right	-0.075	0.050	0.089	11.2	-33.8	0.072	0.011

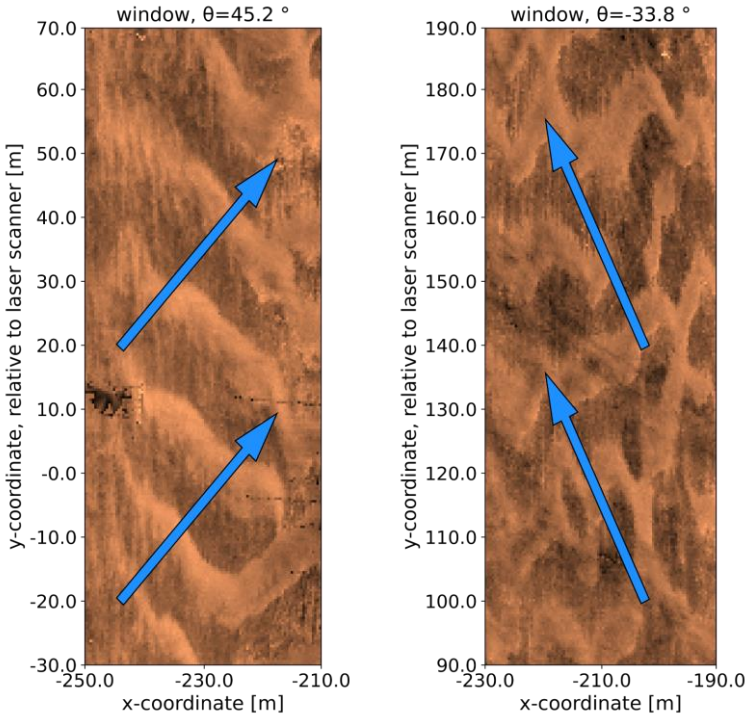

Figure 4.15. Detected orientation of the sand strips (blue arrows) compared to the real orientation for the windows shown in Figure 4.11 (left) and Figure 4.12 (right)

Besides, the detected wavelength and orientation of Figure 4.11 as summarized in Table 4.1 ('left') are compared to the result from the 1D Fourier transform (Figure 4.8). The detected wavelength according to the 1D method is equal to 20.0 *m*. When taking the orientation of 45.2° into account, the wavelength of 20.0 *m* becomes $20.0 \cdot \cos(45.2) = 14.1$ *m*, which is in correspondence with the obtained wavelength of 14.2 *m* using the 2D Fourier transform.

4.3.5 Height determination of detected sand strips using a 1D Fourier transform

Only if sand strips are detected in a window, either with the 1D or 2D method, the height of the sand strips is determined with a 1D Fourier transform based on the z-coordinates. The height determination is therefore comparable to the 1D detection method based on reflectance, however, the main focus is on the height of the spectral peak rather than the corresponding wavenumber. Similar to the 1D detection method, five lines are drawn through the window (based on the detrended z-coordinates) that store the z-coordinates along these transects (only one line is shown in Figure 4.16-A and Figure 4.16-D for illustrational purposes with the corresponding height profile according to the grey line in Figure 4.16-E). Although this grey profile is already detrended, it still contains a slope and therefore the third polynomial best fit (the orange line in Figure 4.16-E) is subtracted from the detrended profile (the grey line in Figure 4.16-E), resulting in the grey profile line in Figure 4.16-F. The variance density spectrum corresponding to the height profile is obtained for each transect and is shown with the grey line in Figure 4.16-G. Identifying the peak corresponding to the height profile is an iterative process, similar to the 1D detection (section 4.3.3). The IFFT is used to approach the height profile according to the peak in the spectrum and a correct profile is assumed for a RMSE below 0.02. The zeroth order spectral moment (m_0) can be determined from the height of the spectral peak according to equation 4.6 (Holthuijsen, 2007). With the zeroth order spectral moment the significant wave height is determined according to equation 4.7.

$$m_0 = \int_{\Delta k}^{\infty} E(k)\ dk \tag{4.6}$$

$$H_{m_0} = 4\sqrt{m_0} \tag{4.7}$$

The height of the sand strip is assumed to be equal to the determined significant wave height according to equation 4.7. This may seem contradictory because sand strips are described as low-amplitude bedforms (Nield, 2011), but it should be noted that the beach profile does actually not contain a trough but only a crest. Therefore, the surrounding beach is considered as the trough in the height profile, and the crest of the sand strip is equal to the crest of the height profile, resulting in a sand strip height equal to the significant wave height. In the example of Figure 4.16 the sand strip height is therefore equal to 7.4 *cm* (as described in the graph-title of Figure 4.16-F).

Furthermore it can be observed in the title of Figure 4.16-F that the detected wavelength is equal to 20 *m*. This corresponds to the detected wavelength of the same window based on the reflectance profile (which is shown in Figure 4.16-A), as computed in section 4.3.3, and also to the detected wavelength and orientation according to the 2D detection method as computed in section 4.3.4.

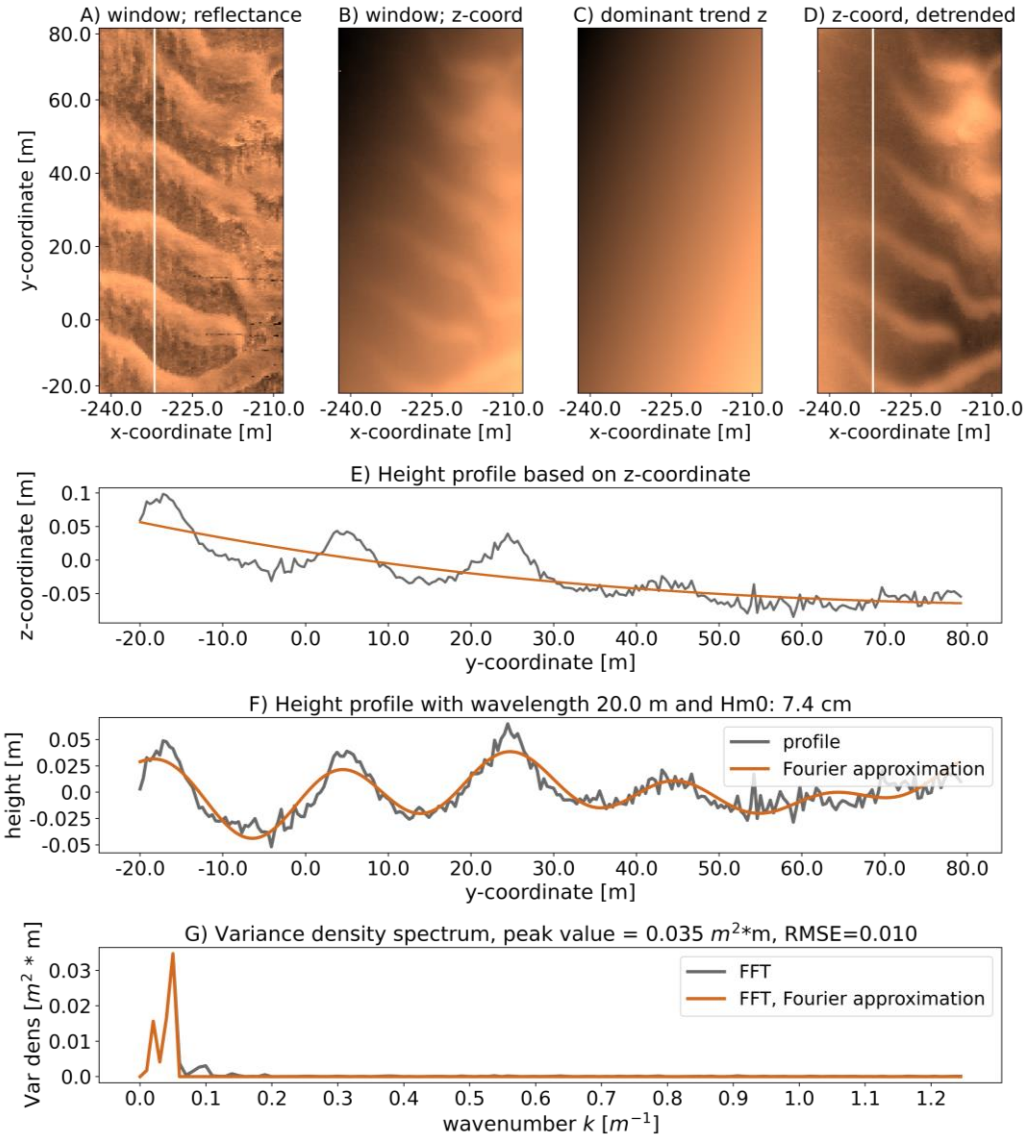

Figure 4.16. Example of the height determination of the sand strip; A) the sand strips based on the detrended reflectance values; B) the original z-coordinates; C) the dominant trend of the z-coordinates and; D) the detrended z-coordinates. E) all the z-values are plotted along the white transect in figure A and D (grey), together with the best fit (orange). F) the wave pattern due to the sand strips in combination with the Fourier approximation and; G) the Fourier transform of both the original profile (grey) and the Fourier transform which us used to approach the wave pattern (orange).

5. Results

In this chapter, both the results from the detection method as well as the grain size analysis will be discussed. In section 5.1 a description of the results acquired with the detection method is presented. In section 5.2, some characteristic properties of the sand strips are discussed that followed from either the detection method or the grain size analysis. The environmental conditions that appeared during sand strip occurrences are elaborated in section 5.3. In section 5.4 some dynamic properties of the sand strips, such as changes over time, are analysed.

5.1 Description of the detection results

In this section, the results of the detection method are presented. First, an overview of the results is given in section 5.1.1. The time period is discussed in combination with the amount of scans and the scans on which the detection method is applied. Some information regarding the accuracy of the output is shown in section 5.1.2. In section 5.1.3, the results are validated visually with two qualitative quantities.

5.1.1 Overview of the results

The detection method is applied on the period of January 30th, 2022 until February 28th, 2022. For the majority of this period the beach is scanned on an hourly interval, resulting in 24 scans per day (visualized with black dots in Figure 5.1). From February 16th 8:40*h* until February 26th 23:59*h* the beach is scanned every 20 minutes, resulting in 72 scans per day. During this specific period three storms passed over the Netherlands (section 1.2), resulting in more detailed information regarding aeolian sand strip behaviour during extreme environmental conditions. The laser scanner scanned the beach 1215 times during the complete time period, while the detection method is applied on 943 scans (77.6%). The other 272 scans (22.4%) (visualized with red stars in the figure) were filtered out according to the described requirements in section 4.1.3. Possible causes for the failure of the laser scanner can be derived with the environmental conditions that are requested, but is beyond the scope of this study and will therefore not be discussed. Out of the 943 scans that are checked, sand strips were detected in 261 scans (27.7%) (visualized with blue dots in Figure 5.1). Sand strips were detected with only the 1D Fourier transform in 72 scans. In the other 189 scans the sand strips were detected with the 2D method at least once. Therefore, the wavelength, orientation, height and pattern spreading are based on these 189 scans, while the environmental conditions for sand strip occurrence are based on all 261 scans.

The average wavelength, height, orientation and pattern spreading of each scan are used in the analysis rather than multiple values of these shape properties for one scan. Each scan contains around 150 windows due to the moving window, where the exact amount of windows is governed by the beach width. It is time demanding and genuinely difficult to compare the windows individually, among others due to overlap between the windows. Therefore, the detected shape properties which are analysed are averaged for each scan.

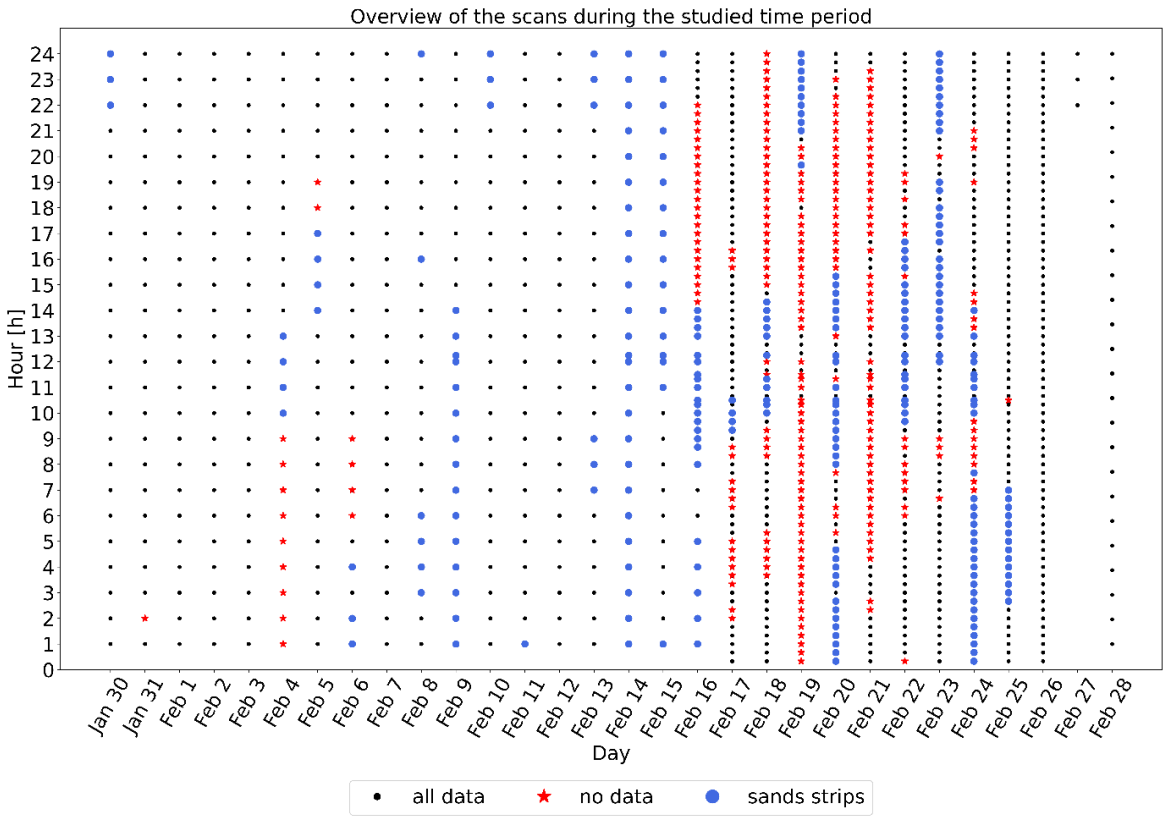

Figure 5.1. Overview of the scans during the studied time period. All the scans are marked with black dots, scans where sand strips were detected are marked with blue and the bad quality data are marked with red stars.

5.1.2 Accuracy of the determined orientation and wavelength

The accuracy of the wavelength and orientation is mainly determined by the bandwidth in the wavenumber domain, and therefore subsequently on the window size according to equation 5.1 (with i denoting either x or y, in correspondence to the direction). With a window size of 100 m by 40 m in y- and x-direction respectively, the bandwidths of the wavenumber domain in the Fourier transform are Δk_x = 0.025 m^{-1} and Δk_y = 0.010 m^{-1}.

$$\Delta k_i = \frac{1}{\text{window size in } i\text{-direction}} \tag{5.1}$$

Due to the bandwidth, the wavenumbers in both x- and y-direction are discrete variables, affecting the accuracy of the determined wavelength as well as the orientation. The resulting wavenumber (and wavelength) and the resulting orientation are also discrete since the two input variables (k_x and k_y) are discrete (according to equations 4.2 to 4.4). The accuracy of both the wavelength and orientation are therefore governed by the bandwidths Δk_x and Δk_y. The mean wavelength and orientation of the scan, which are used in the analysis, are however considered continuous since they are the mean value of multiple discrete values. The pattern spreading is also considered continuous due to the interpolation used to determine the width of the significant peak in the distribution curve (section 4.3.4).

5.1.3 Visual validation

The detection method is examined qualitatively with two quantities based on the percentage false positives (FP) and false negatives (FN) with a visual validation. The area is considered a false negative when some sand strips are not detected as sand strips by the detection method and it is considered a false positive when an area without sand strips is detected as an area where sand strips are present according to the detection method. The first quantity is epoch-based, and the second area-based. The epoch-based method determines the amount of false positive and false negative scans of a certain time period. The area-based method focusses on the total beach area and the area where sand strips are detected.

The results of the detection method for four scans are visualized in Figure 5.2. In Figure 5.2-A (February 15th) the complete beach area is covered with sand strips and the sand strips over the complete area are detected. Therefore the scan is considered correct according to both the epoch- and area-based method. In Figure 5.2-B (February 14th) almost the complete beach is covered with sand strips, while they are not all detected by the detection method, resulting in an area-based false negative ($A\text{-}FN$) larger than zero. Areas without sand strips are not detected, and thus the area-based false positive ($A\text{-}FP$) is equal to zero. In Figure 5.2-C (February 26th) no sand strips can be seen in the scan and the detection method has also not detected any sand strips, implying that the scan is correct according to both methods. In Figure 5.2-D (January 30th) no sand strips are present on the beach. However, a small area is detected where sand strips are present according to the detection method, implying $A\text{-}FP$ bigger than zero. Besides, the scan will be considered in the analysis due to the detection of sand strips while they are not present, and therefore the scan is also considered an epoch-based false positive ($E\text{-}FP$). A scan is considered an epoch-based false negative ($E\text{-}FN$) when sand strips are present while they are not detected in the scan, resulting in the scan being disregarded in the sand strip analysis while it should be included due to the presence of sand strips.

A possible cause for false negatives could be the requirement set for the amount of interpolation. In this way, it is possible that some sand strips are not detected because the detection method is not applied at these areas due to the too large amount of interpolation required, while these areas are included in the determination of the percentage false negatives. Besides, false positives that are detected usually have an orientation smaller than 15° or larger than 165° relative to shore-normal where 0° and 180° correspond to shore-normal (Figure 5.2-D). On the other hand, sand strips with an orientation smaller than 15° or larger than 165° are not observed during the visual validation. Therefore, the detected windows with an orientation smaller than 15° or larger than 165° are considered false positives and are disregarded in the analysis.

Epoch-based

February 23rd is used for the epoch-based assessment of the detection method since the PLS scanned the beach every 20 minutes on this day resulting in 72 scans. From these 72 scans, 5 scans were considered bad quality, resulting in the application of the detection method on 67 scans (Figure 5.1). Furthermore, sand strips were present on the beach for the majority of the day since they were detected in 29 scans. A scan is considered $E\text{-}FP$ when the detection method detects sand strips while they are not present in the scan, and it is considered $E\text{-}FN$ when sand strips are present while they are not detected in the scan. The percentage $E\text{-}FP$ and $E\text{-}FN$ are determined according equations 5.2 and 5.3, and they are equal to 3.9% and 3.6% respectively (Table 5.1).

$$E\text{-}FN = \frac{N_{FN}}{N_{sand\ strips}} \cdot 100\% \tag{5.2}$$

$$E\text{-}FP = \frac{N_{Fp}}{N_{no\ sand\ strips}} \cdot 100\% \tag{5.3}$$

With:

- $E\text{-}FN$: epoch-based false negatives;
- $E\text{-}FP$: epoch-based false positives;
- N_{FN}: number of scans where present sand strips are not detected;
- $N_{sand\ strips}$: number of scans where sand strips are present;
- N_{FP}: number of scans where sand strips are detected while not present and;
- $N_{no\ sand\ strips}$: number of scans where sand strips are detected while not present

Area-based

For the computation of $A\text{-}FP$ and $A\text{-}FN$ 20 random scans are selected. In these scans, the total area is computed as well as the area with and without sand strips. The area where sand strips are detected is known, and the percentage of both the area-based FP as well as the FN can be computed according to equations 5.4 and 5.5. An example of the computation for one scan can be found in appendix D. The average percentage of the $A\text{-}FP$ and $A\text{-}FN$ of the 20 random scans are 3.8% and 3.4% respectively, summarized in Table 5.1.

$$A\text{-}FN = \frac{(A_{sand\ strips} - A_{detected})}{A_{sand\ strips}} \cdot 100\% \tag{5.4}$$

$$A\text{-}FP = \frac{(A_{false\ detected})}{A_{no\ sand\ strips}} \cdot 100\% \tag{5.5}$$

With:

- $A\text{-}FN$: area-based false negatives;
- $A\text{-}FP$: area-based false positives;
- $A_{sand\ strips}$: area where sand strips are present;
- $A_{detected}$: area where sand strips are detected according to the detection method;
- $A_{no\ sand\ strips}$: area where no sand strips are detected and;
- $A_{false\ detected}$: area where sand strips are detected while sand strips are not present

Table 5.1. Percentage false positives and false negatives for the two applied quantities

Percentage FP and FN	**False negative [%]**	**False positive [%]**
Epoch-based	3.6	3.9
Area-based	3.8	3.4

The percentages of both the epoch- and the area-based FP as well as FN are considered small enough that the detection method works accordingly. Further analysis can therefore be executed with the results obtained from the detection method.

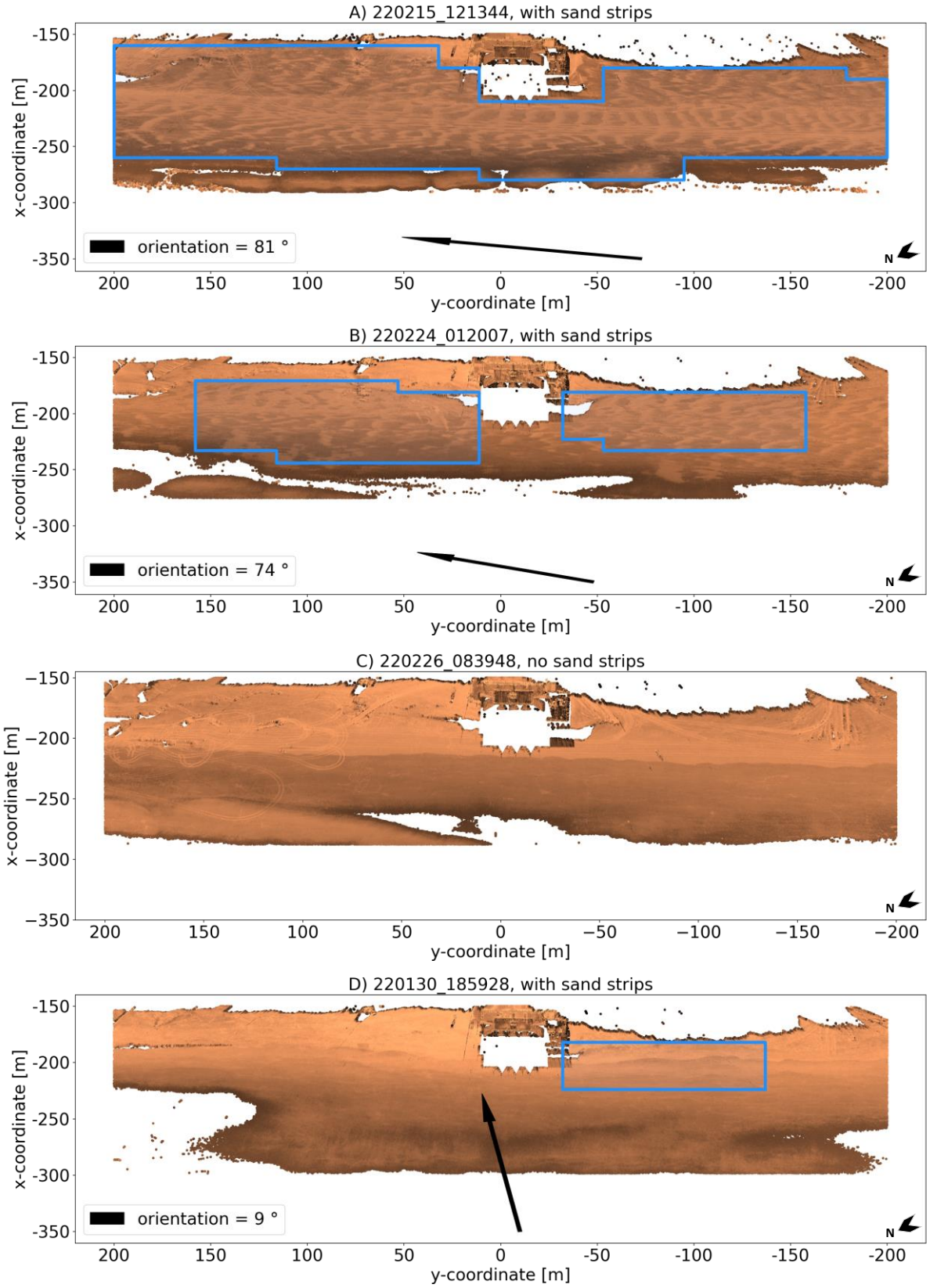

Figure 5.2. Results of the detection method. The detected sand strips are framed in blue and the average detected orientation of these sand strips is shown with the black arrow, for A) Feb 15th, 2022 at 12:13h with an orientation of 81°; B) Feb 24th, 2022 at 01:20h with an orientation of 74°; C) Feb 26th, at 08:39h where no sand strips are detected and; D) Jan 30th at 18:59h where no sand strips are present, despite being detected with an orientation of 9°, which indicates a false positive due to the uncommon orientation for sand strips.

5.2 Characteristic properties of the sand strips

In this section, some characteristic properties of the sand strips are discussed. In the sections 5.2.1, 5.2.2, 5.2.3, and 5.2.4 the wavelength, orientation, pattern spreading and height are discussed respectively. These four properties are output variables of the detection method. The variation in grain size is elaborated in section 5.2.5, and the moisture content in section 5.2.6. Finally, correlations between the characteristic properties are discussed in section 5.2.7.

5.2.1 The wavelength of the sand strips

The wavelength of the detected sand strips varies between 8.9 *m* and 17.6 *m*. The distribution follows a Gaussian profile with a median (M) and mean (μ) wavelength of 13.3 *m* and 13.2 *m* respectively (Figure 5.3), a standard deviation (σ) of 1.5 *m* and a variance of 2.1 m^2:

$$N(\mu;\ \sigma^2) = N(13.2; 2.1)$$

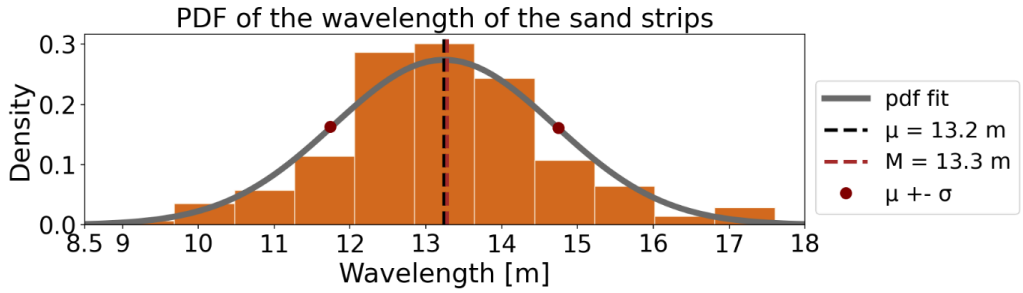

Figure 5.3. Histogram and probability density function of the wavelength according to the detection method. The bin width is equal to 0.80 m, corresponding to the Nyquist rate which is equal to twice the grid size. The grey line represent the probability density function (pdf). The mean and median wavelength are visualized with the black and red dashed line respectively. The standard deviation is indicated with the red dots

In Figure 5.3, the grey line represents the probability density function (pdf) that fits the distribution best. The mean and median values are visualized with respectively black and red dashed lines. The 68% confidence interval corresponds to the values between the standard deviation, visualized with the dots. Characteristic values that describe the distribution of the wavelengths are summarized in Table 5.2.

Table 5.2. Characteristic values for the distribution of the wavelengths

	Wavelength [*m*]
Mean; μ	13.2
Median; M	13.3
Standard deviation; σ	1.5
Variance; σ^2	2.1
Minimum	8.9
Maximum	17.6

The first quartile (Q1; the 25th percentile) is equal to 12.3 *m* and the third quartile (Q3; the 75th percentile) is equal to 14.0 *m*. The interquartile range (IQR) is the difference between the first quartile and the third quartile and is a measure of the spread of the middle 50% of the data and is therefore equal to 1.7 *m*. Considering the size of the IQR, there are outliers at both ends of the distribution since outliers are defined according to the $1.5 \cdot IQR$-rule. Wavelengths that are considered outliers have therefore a value above 16.5 *m* ($Q3 + 1.5 \cdot IQR$) or below 9.8 *m* ($Q1 - 1.5 \cdot IQR$), resulting in one outlier at the lower limit and four outliers at the upper limit.

5.2.2 The orientation of the sand strips

The orientation of the sand strips are almost parallel to the beach. Figure 5.4 visualizes the scan of February 24, 04:00*h*, where sand strips are detected within the blue window. The present sand strips have slightly different orientation, ranging from alongshore to more oblique-alongshore. The mean orientation of the detected sand strips is equal to 62°, also visualized with the black arrow. The black arrow is comparable to the orientation of the sand strips, and the detected orientation is therefore assumed a representative orientation of the sand strips. Other comparisons between the detected orientation and the orientation of the sand strips can be seen in Figure 5.2.

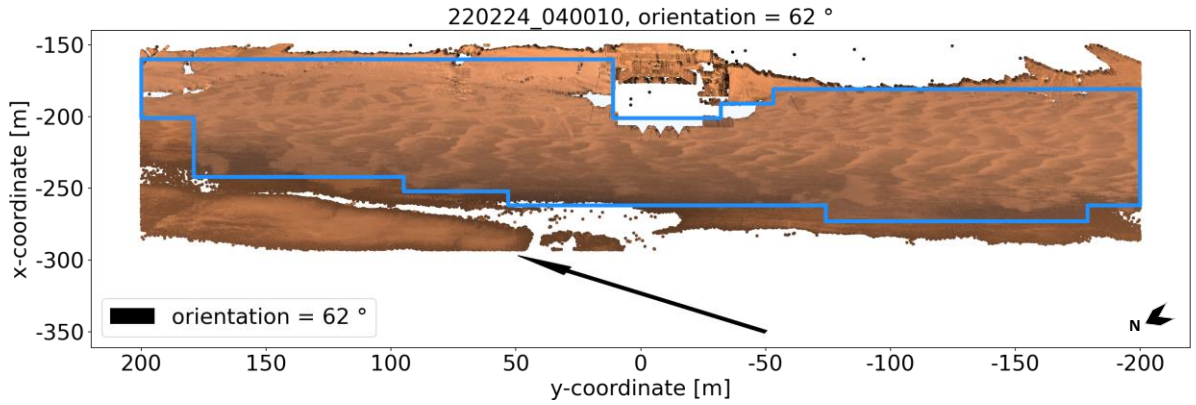

Figure 5.4. Comparison of the orientation of the sand strips and the detected orientation. The detected sand strips are framed with blue and the detected orientation is shown with the black arrow, equal to 62°

In Figure 5.5 the orientation is given, where the colour of the bins indicate the corresponding wavelength (section 5.2.1). In Figure 5.5-A the orientation is given relative to shore normal, where 0° corresponds with a cross-shore orientation, and 90° with a longshore orientation. The orientation of the beach is in this local coordinate system equal to the solid black line at 90°. In Figure 5.5-B the orientation is given relative to North, and the orientation of the beach in this coordination system is equal to the solid black line at 30°. The values for the orientation of the sand strips that are discussed in this section are given in the local coordinate system according to Figure 5.5-A, and are therefore relative to shore normal. The radial axis indicates the amount of scans of the detected orientation.

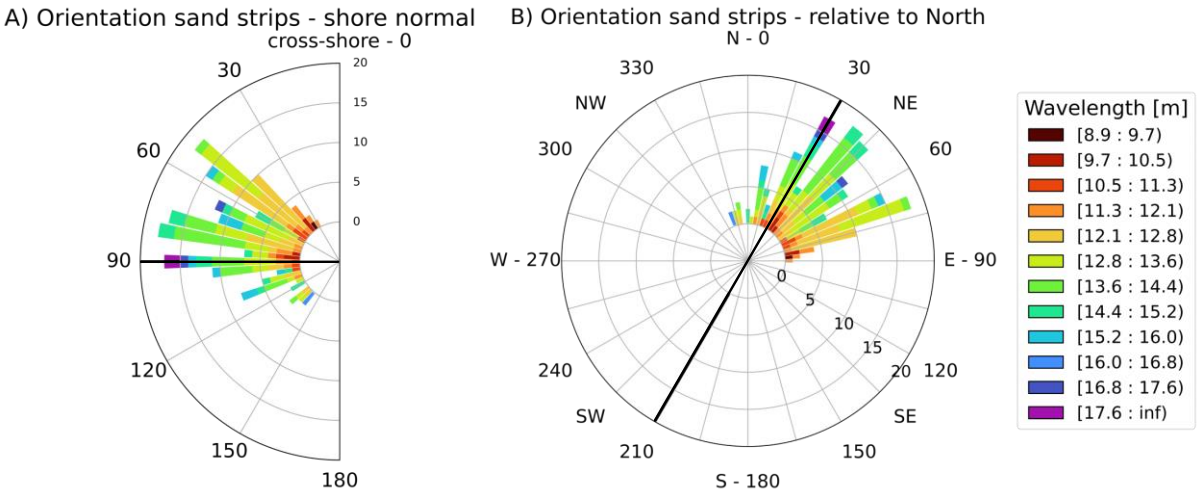

Figure 5.5. Orientation of the sand strips; A) the orientation relative to shore-normal; B) orientation relative to North. The radial axis represents the amount of scans that the detected orientation appeared.

The orientation of the detected sand strips varies between 29° to 142°. Both the mean and median orientation are equal to 75°, and are therefore alongshore-oblique. The first quartile is equal to 55° and third quartile is equal to 90°. The IQR is therefore equal to 35° (Table 5.3), and considering its size, there are no outliers in the detected orientation according to the $1.5 \cdot IQR$-rule resulting in a lower limit of 2.5° and an upper limit of 142.5°.

Table 5.3. Characteristic values for the distribution of the orientations

	Orientation [°]
Mean	75
Median / second quartile (M / Q2)	75
First quartile (Q1)	55
Third quartile (Q3)	90
Interquartile range (IQR)	35

5.2.3 Pattern spreading in the sand strip orientation

The pattern spreading is an indication of the uniformity of the sand strips and the pattern occuring in the window. A small spreading suggests a clear pattern with one dominant orientation (e.g. Figure 4.11), while a larger spreading suggests more randomness where the sand strips are not oriented uniform (e.g. Figure 4.12). Furthermore, when the spreading is large the accuracy of the computed orientation and wavelength is less than with a small spreading due to the non-uniform orientation. For each window, the spreading of the distribution of both k_x (FWHM_x) and k_y (FWHM_y) are determined. The resultant spreading is computed according to equation 5.6.

$$FWHM_{res} = \sqrt{FWHM_x{}^2 + FWHM_y{}^2} \tag{5.6}$$

In the two windows in Figure 4.15 it can be seen that the left-sided window has a dominant uniform orientation compared to the less uniform orientation of the right-sided window. This difference can also be observed when focussing on the FWHM. The FWHM for the left window in Figure 4.15 is smaller than the FWHM for the right window (Table 4.1), especially in x-direction while it is comparable in y-direction. In order to put the values in more context, it should be noted that both k_x and k_y vary between 0 m^{-1} and 0.12 m^{-1} in terms of absolute value with a bandwidth of respectively 0.025 m^{-1} and 0.010 m^{-1}. The resultant wavenumber (k_{res}) varies between 0.0564 m^{-1} and 0.125 m^{-1}.

In Table 4.1 it can also be observed that the spreading in x-direction (FWHM_x) is larger than the spreading in y-direction (FWHM_y). This is in correspondence to all spreading-values, visualized in Figure 5.6 where all the obtained values for both FWHM_x and FWHM_y are shown as a histogram as well as the resultant 2D histogram. The median values for FWHM_x, FWHM_y and FWHM_{res} are respectively 0.056 m^{-1}, 0.024 m^{-1} and 0.063 m^{-1} (Table 5.4), and, in general, the spreading in x-direction is therefore larger than the spreading in y-direction. It is important to acknowledge that no conclusion can be drawn with this spreading difference due to the different bandwidths Δk_x and Δk_y. Therefore, both values for the spreading cannot be compared to each other. Such comparison can only be applied when the bandwidth is equal for both directions, c.q. with a square window size.

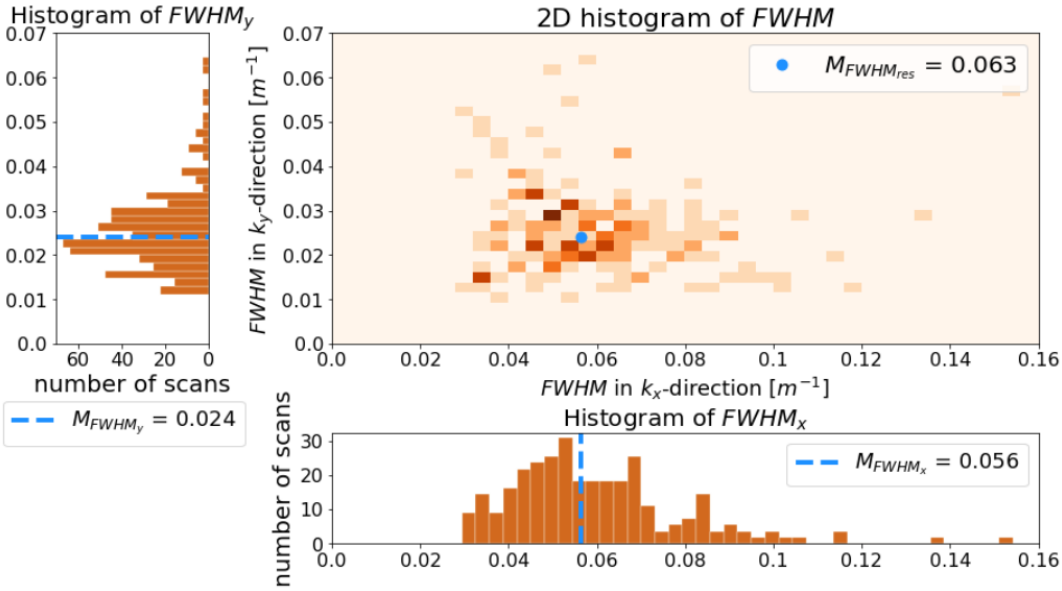

Figure 5.6. the values for FWHM in both x- and y-direction visualized as histograms. The lower histogram shows $FWHM_x$, the left-sided histogram represents $FWHM_y$ and the 2D histogram represents the total combination of both. The median values are marked with blue dashed lines for both directions separately and the blue dot represents the median resultant spreading. The values of FWHM are considered continuous due to the interpolation applied (Virtanen, et al., 2020), and therefore smaller bin widths than the bandwidths are considered.

Table 5.4. Mean and median values of the FWHM

	$FWHM_x$ [m^{-1}]	$FWHM_y$ [m^{-1}]	$FWHM_{res}$ [m^{-1}]
Mean; μ	0.060	0.026	0.066
Median; M	0.056	0.024	0.063

The computed orientation and wavelength partly depends on the spreading. A large spreading, and therefore a less uniform orientation, will result in a less accurate determined orientation since more directions are present in the window. The spreading is therefore compared to the orientation and the wavelength. There is however, no dominant trend for a range of wavelengths or orientations with a significant difference in spreading values, neither for the x- or y-direction nor the resultant spreading (Figure 5.7). All the orientation- and wavelength-values show similar spreading values. The colour bars are based on a boxplot, where the IQR is visualized with both green and yellow. The median value corresponds to the value at the boundary between yellow and green and it is visualized with a white horizontal line in the colour bar.

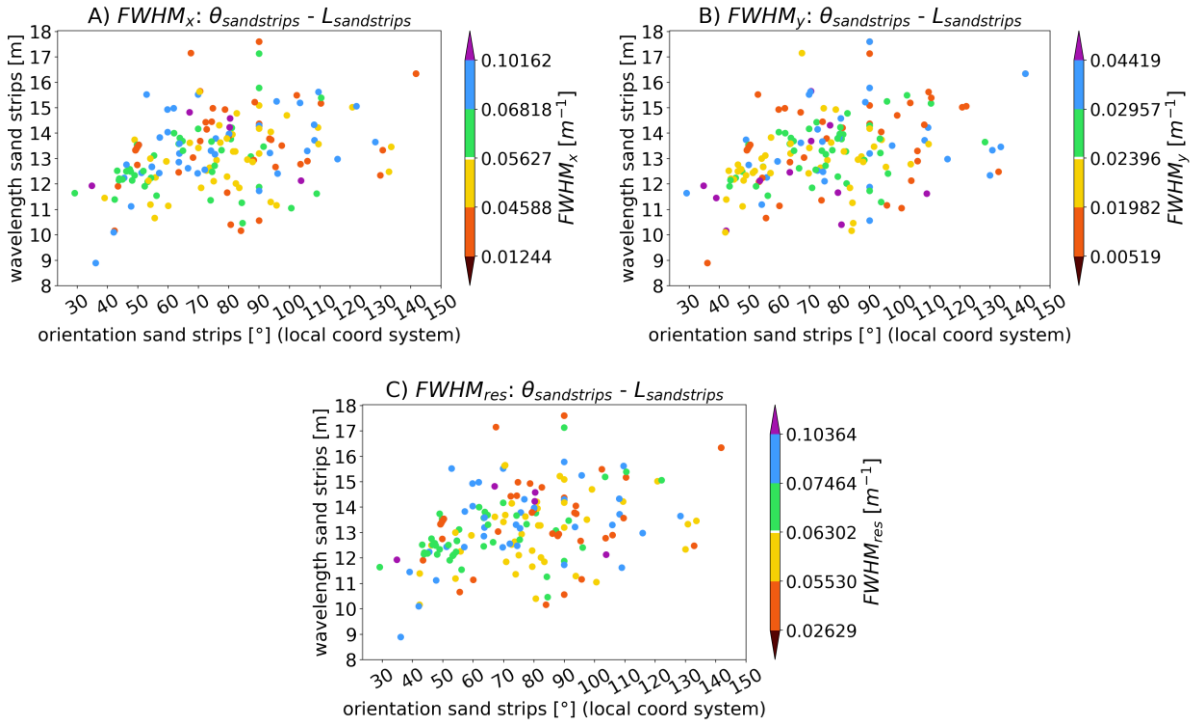

Figure 5.7. The detected orientation against the detected wavelength; the colour represents in A) $FWHM_x$; B) $FWHM_y$ and; C) $FWHM_{res}$. The colourbars are distributed according to the same boxplot method. Black and purple indicate outliers, red indicates the values ranging from Q1 to Q1-1.5·IQR, yellow corresponds to the values ranging from Q1 to Q2, green from Q2 to Q3, and blue indicates the values ranging from Q3 to Q3+1.5·IQR. The median value (Q2) corresponds to the white horizontal line in the colourbar

5.2.4 The height of the sand strips

The height of the detected sand strips varies between 2.0 *cm* and 12.0 *cm*. The median height of the sand strips is equal to 3.8 *cm* and the mean is 4.0 *cm*. The distribution of the detected heights is positively skewed, which can be seen in Figure 5.8 where the tail of the distribution is on the right-hand side of the curve. In the figure, the grey line represents the probability density function that fits the distribution best. The mean and median values are visualized with respectively black and red dashed lines.

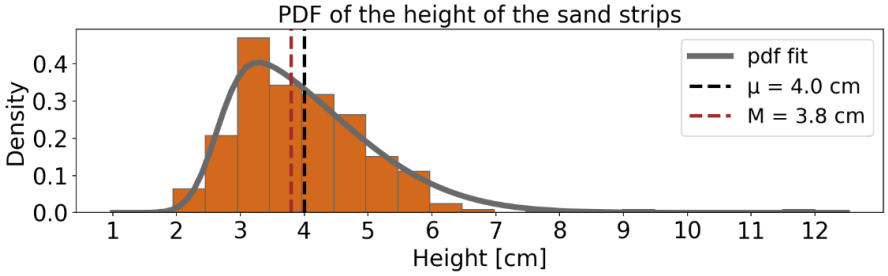

Figure 5.8. Histogram and probability density function of the height of the sand strips according to the detection method. The bin width is equal to 0.5 cm. The pdf is represented by the grey line, and the mean and median height by the dashed black and red lines respectively

The IQR is equal to 1.4 *cm* since the first quartile is equal to 3.2 *cm* and the third quartile is equal to 4.6 *cm* (Table 5.5). According to the $1.5 \cdot IQR$-rule there are outliers since the upper limit, according to this rule, is equal to 6.7 *cm*. Besides, most of the detected sand strips have a height in the range of 2.0 *cm* to 6.0 *cm* roughly.

Table 5.5. Characteristic values for the distribution of the height

	Height [*cm*]
Mean	4.0
Median / second quartile (M / Q2)	3.8
First quartile (Q1)	3.2
Third quartile (Q3)	4.6
Interquartile range (IQR)	1.4

5.2.5 Grain size variation over the sand strips

The variation over both the transverse and longitudinal direction of the sand strip are studied, with the directions according to Figure 3.6-A. First, the variation in transverse direction will be discussed, followed by the longitudinal direction of the sand strip.

Variation in transverse direction of the sand strip

Based on the studied samples, it is observed that the grain size varies in transverse direction. The surrounding beach had much variation in grain size compared to the sand strip. When focussing on the sand strips only, it is observed that the largest grains are located at the crest of the sand strip, followed by the windward side. The leeward side contains the smallest grains of the sand strip, visualized in Figure 5.9 for the D_{50} (upper graph) and D_{10} (lower graph). The three days when the samples are taken are shown individually in order to exclude variations caused by the location on the beach (note that during the sample acquisition on February 4th only the crest is sampled (section 3.3), therefore the results cannot be used in this analysis). Each day suggests the same variation in transverse direction with the largest grains on the crest and the smallest grains on the lee-side. All measurements are within the coloured box for the specific day, with the standard deviation more dark-coloured. The solid line represents the mean.

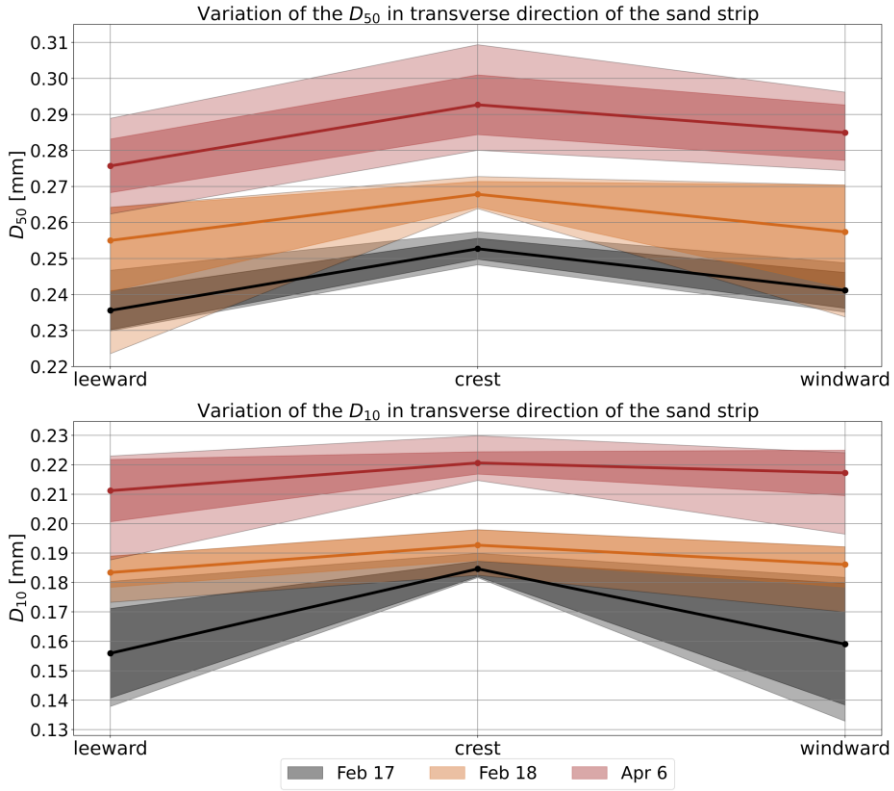

Figure 5.9. Variation in grain size over the transverse location of the sand strips for the D_{50} (top) and; D_{10} (bottom). The mean values correspond to the solid lines, the light-shadowed areas correspond to all the determined grain sizes and the dark-shadowed area to the standard deviation

These patterns are normalized in Figure 5.10 for the D_{10} by the corresponding characteristic grain size of the crest for a better interpretation. The normalized grain size at the crest is therefore equal to 1.0 for all samples, and the values at both the leeward and windward side can be seen as a fraction of the grain size at the crest. Based on these normalized values, the D_{10} shows the strongest signal compared to other characteristic grain sizes (Table 5.6). The normalized mean values are equal to 0.93 for the leeward side and 0.95 for the windward side:

- $D_{10\text{ leeward side}} = 0.93 \cdot D_{10\text{ crest}}$
- $D_{10\text{ windward side}} = 0.95 \cdot D_{10\text{ crest}}$

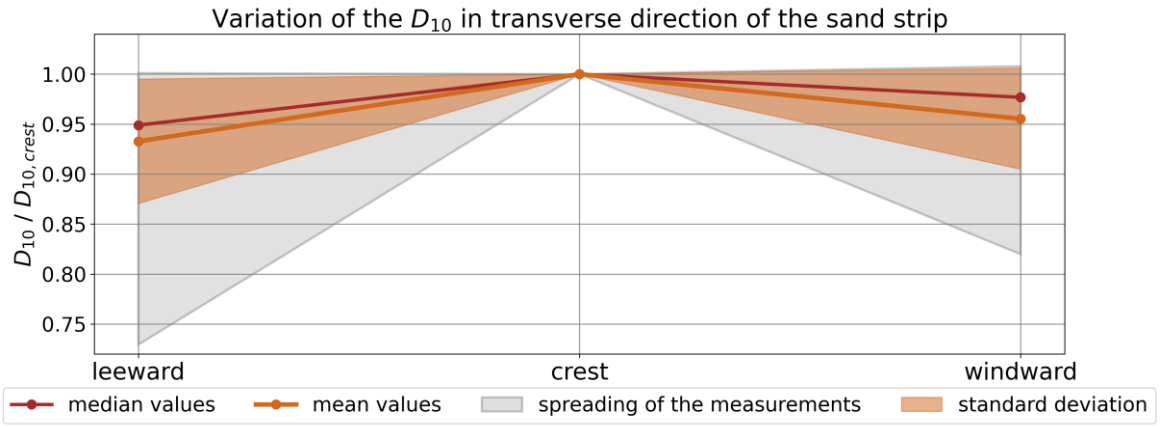

Figure 5.10. Grain size variation in transverse direction for the D_{10}. All data is shown in the grey box, the standard deviation in the orange box, and the mean and median values are visualized with respectively red and orange dots

Table 5.6. Fractions of the grain size on the leeward and windward side compared to the crest for the D_{90}, D_{50} and the D_{10}

	D_{90}	D_{50}	D_{10}
Leeward	0.98	0.94	0.93
Windward	0.99	0.97	0.95

Variation in longitudinal direction of the sand strip

In longitudinal direction, no clear dominant variation in grain size is observed. The grain size varies, there is however not a dominant pattern in grain size variation in longitudinal direction (Figure 5.11). Besides, the differences are small, with a difference of approximately 0.01 *mm* in general based on the mean values. In the figure, the characteristic grain sizes D_{50} and D_{10} are visualized for the samples taken at February 17th and 18th and April 6th. All measurements for one day are within the coloured box, and the mean is represented by the solid line. The sample days are shown individually since the samples are taken on different locations on the beach (Figure 3.7). By this differentiation, the variability in grain size due to the different sample locations on the beach is excluded. The letter '*A*' along the x-axis corresponds to the sample location closest to the water, *'C'* closest to the dunes, and *'B'* between *A* and *C*, distanced approximately 8 meters from the *A* and *C* (Figure 3.6-B).

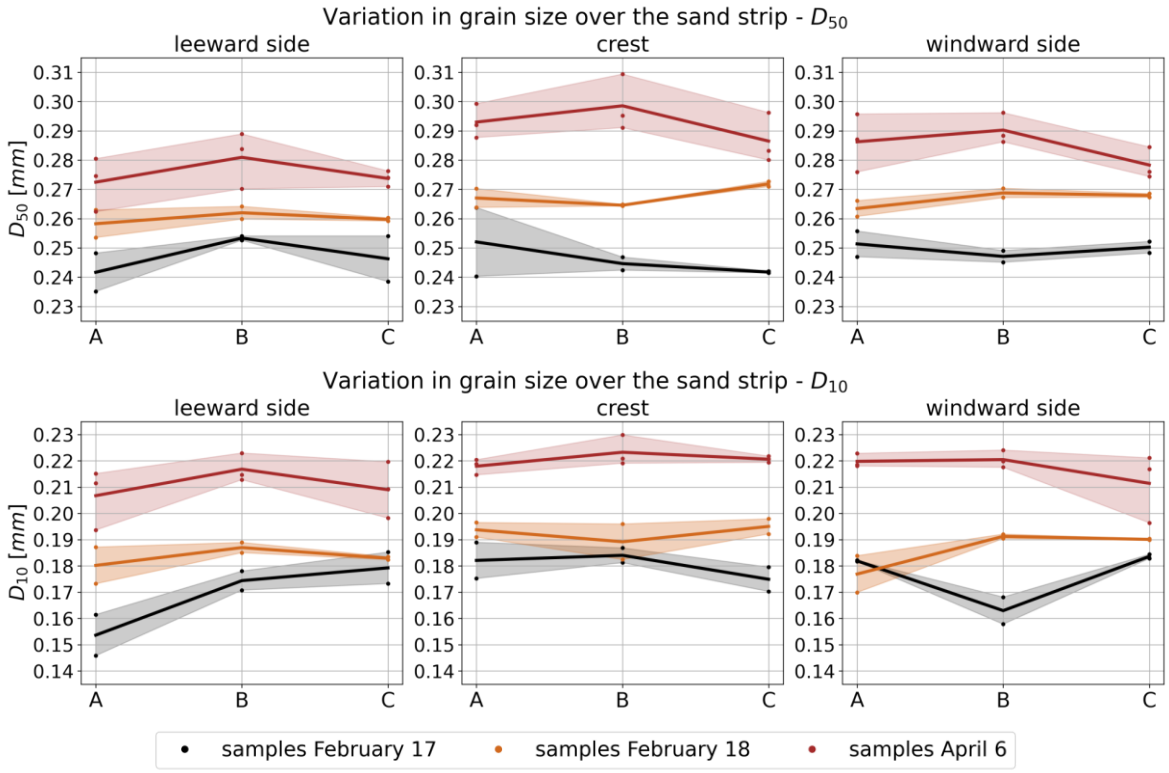

Figure 5.11. Variation in grain size over the sand strip for the D_{50} (top) and; D_{10} (bottom). All the samples taken on the specific day are within the corresponding coloured box. The mean values correspond to the solid lines

Besides the small difference in longitudinal direction, the spreading can be larger than this difference of 0.01 *mm*. Therefore it cannot be concluded whether there is a variation in longitudinal direction. It is suggested that more samples need to be taken (in more detail) in future studies in order to draw a conclusion regarding the variation in grain size in this direction. More detailed samples will lead to less spread results since outlying points then stand out, resulting in the possibility to disregard these outliers in the analysis. The amount of sand samples taken for this study is too small for the detection of possible outlying points.

5.2.6 Variation in moisture content between the sand strips and the normal beach

The gravimetric moisture content is determined according to equation 3.1, and it is concluded that the moisture content of the sand strips is less than the surrounding beach, referred to as trough (Figure 5.12). There is no variation in longitudinal direction since all values in this direction are comparable to each other. In transverse direction there is a significant difference with a median moisture content at the surrounding beach area equal to 8.6% and at the sand strip of around 2.5%. The median values for the leeward side, crest and windward side are respectively 2.8%, 1.6% and 3.1%, also summarized with other characteristics in Table 5.7. In Figure 5.12, these characteristics are visualized for the leeward side, the crest and the windward side of the sand strip as well as for the surrounding beach surface (trough). The inset in the figure shows the same results, focussed on the values of the sand strips.

Table 5.7. Characteristic values for the moisture content

Moisture content [%]	**Leeward**	**Crest**	**Windward**	**Trough**
Mean	3.08	1.69	3.12	9.36
Median	2.81	1.60	3.07	8.62
Standard deviation	0.98	0.71	0.87	3.51
Minimum	1.87	0.82	1.76	6.00
Maximum	5.25	3.99	5.26	19.33

With the minimum and maximum values for the moisture content as given in Table 5.7, it can be observed that the moisture content of the sand strips was below 6% for all samples, while it was at least 6% for the surrounding beach surface when sand strips occurred. This shows that there is a significant difference in moisture content between the sand strips and the surrounding beach. Based on the measurements, the sand strips have a moisture content of around 2% to 3%, while the surrounding beach has a moisture content of around 8% to 10% when sand strips were present on the beach.

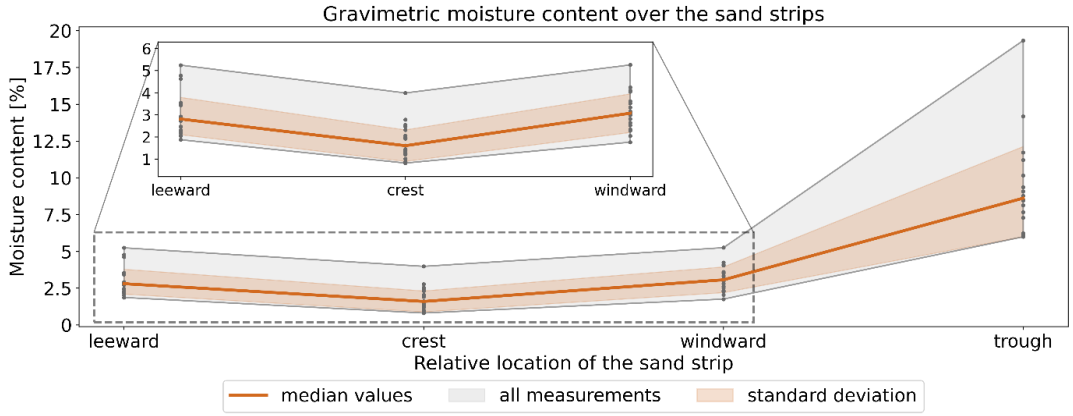

Figure 5.12. Gravimetric moisture content of the sand strip compared to the surrounding beach surface. The inset shows the same results, but zoomed-in

5.2.7 Correlations between the characteristic properties

The colour differences in Figure 5.5 indicate the mean wavelength of the detected sand strips. These colour differences imply a smaller wavelength for more inland oriented sand strips and a larger wavelength for more alongshore orientations. The Pearson correlation coefficient (Benesty et al., 2009) between the orientation and the wavelength is, however, equal to r = 0.36 (Figure 5.13-A). The height of the sand strips is not directly correlated to neither the orientation nor wavelength, since the correlation coefficient for the height with both the orientation and wavelength is equal to r = 0.12 as shown in Figure 5.13-B and C.

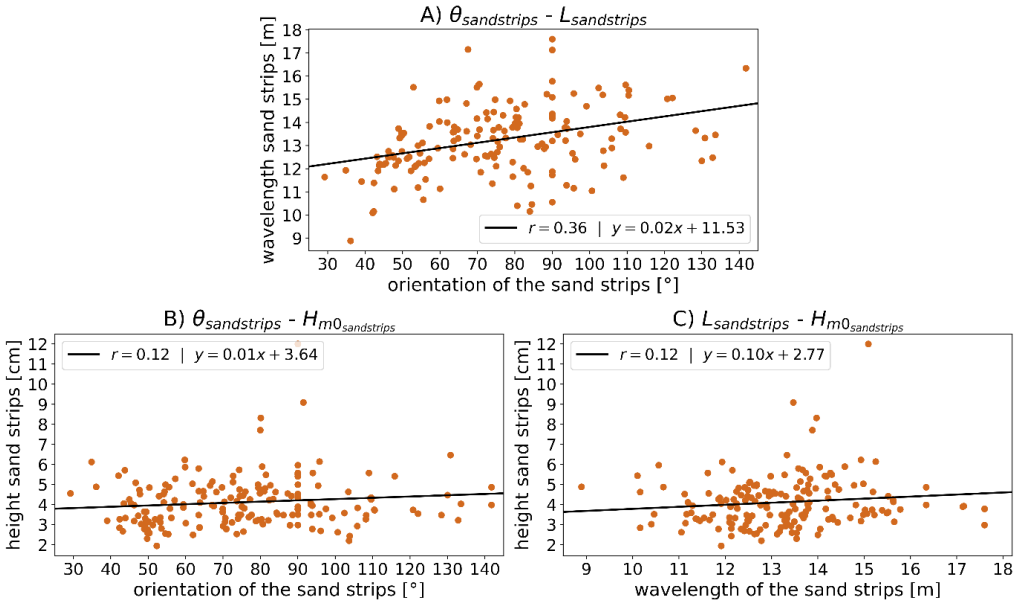

Figure 5.13. Correlations between the orientation, wavelength and height of the sand strips; A) orientation and wavelength with r=0.36; B) orientation and height (r=0.12) and; C) wavelength and height (r=0.12)

5.3 The environmental conditions for sand strip development

In this section, some environmental conditions during sand strip occurrence on the beach are discussed. In section 5.3.1 the wind conditions, such as the wind direction and wind velocity, are presented. The influence of precipitation is elaborated in section 5.3.2, and the influence of the tide in section 5.3.3. In section 5.3.4 influences of the environmental conditions on the shape properties are analysed.

5.3.1 The wind conditions during sand strip detection

One of the most important variables for aeolian sand strip development is the wind. Throughout the study period, the wind direction came mainly from the southwest (Figure 5.14, where the orientation of the Noordwijk beach is illustrated with the black solid line). Wind events coming from the west to northwest also occurred, but less often compared to south-westerly winds. Furthermore, some wind events appeared with a south-south-easterly orientation, coming from inland. These inland winds had a wind velocity below 7 *m/s* which is smaller compared to other directions. The wind velocity ranged between 2 *m/s* and 26 *m/s* for the total period, with a median of 12 *m/s*. In Figure 5.14-A the wind rose for the studied time period is shown, and in Figure 5.14-B all the studied wind data is shown. The difference between the two figures are the wind events that occurred during bad quality data. Due to the importance of both the wind direction as well as the wind velocity on sand strip occurrence, both will be discussed separately in this section.

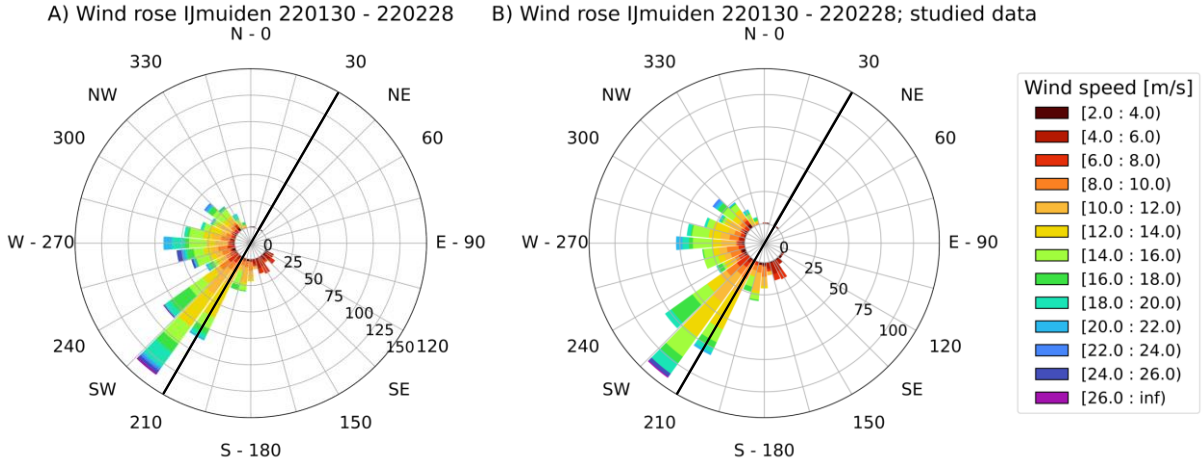

Figure 5.14. Wind rose for the studied time period. A) the total wind rose; B) the wind rose for the good quality data only. The solid black line represents the orientation of the coast, the colors of the bins indicate the wind speed

Wind direction

Sand strips mostly appeared with south-westerly winds (Figure 5.15), corresponding to alongshore winds. Wind events coming from inland (with a direction smaller than 180° with respect to North) did not lead to sand strip development, which can either be caused by the small fetch, the low wind velocity or a combination of both. Furthermore, wind events coming from the west to northwest, and therefore more oblique-onshore winds, did only lead a few times to sand strip development compared to the total amount of wind events that occurred with this oblique-onshore direction. With these oblique-onshore wind events, the wind velocity was much stronger compared to wind events coming from inland.

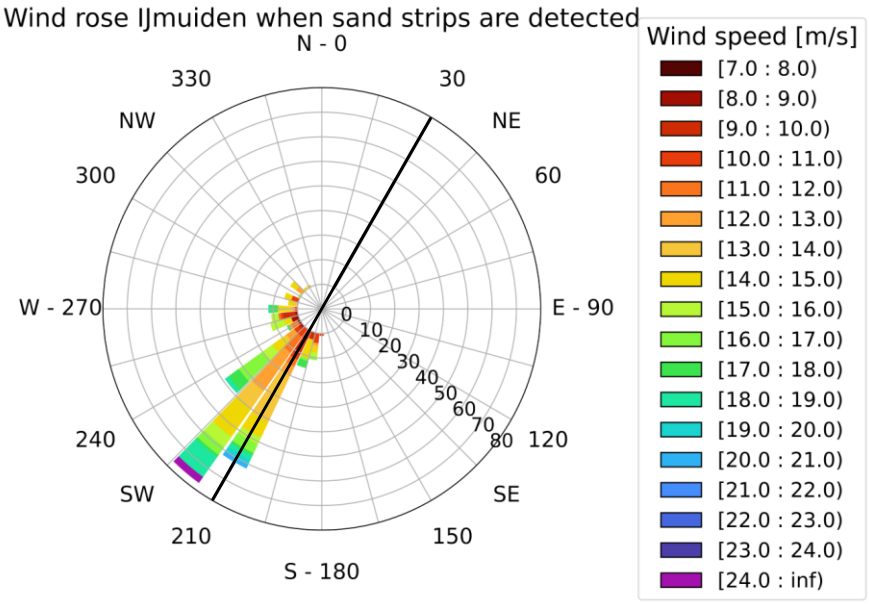

Figure 5.15. Wind rose with only the wind events when sand strips are detected

The alongshore to slightly oblique-alongshore winds that appeared during sand strip occurrences correspond to a wind direction of 210° to 240°. The median wind direction is equal to 220° with respect to North. The first and third quartile are respectively 210° and 230°. Although the dominant wind direction is a south-westerly wind (ranging between 210° and 240°), there are some westerly winds which also led to sand strips. Out of the 261 times that sand strips were detected, the wind was 202 times directed (almost) alongshore (190° to 240°). Once, the wind velocity was equal to 180°, and 58 times the wind had a more oblique (> 240°) direction with a maximum of 320°, equal to shore normal. Characteristic values for the wind direction are summarized in Table 5.8.

Table 5.8. Characteristic values for the wind direction during sand strip occurrence

	Wind direction [°]
Median / second quartile (M / Q2)	220
First quartile (Q1)	210
Third quartile (Q3)	230
Maximum	320
Minimum	180

Wind velocity

The minimum appeared wind velocity when sand strips were detected is *7 m/s*. For the studied time period, the wind velocity varied between 2 *m/s* and 26 *m/s* (shown in light-orange in Figure 5.16). The wind velocity during the studied scans are shown in darker-orange in Figure 5.16. During sand strip occurrence the wind velocity varied between 7.0 *m/s* and 24 *m/s* (grey bars in Figure 5.16), with a median of 14 *m/s*. Characteristic values that describe the distribution of the wind velocity during sand strip development are summarized in Table 5.9. Sand strips only appeared once out of the 27 times that a wind velocity of 7 *m/s* was measured (3.7%), while this percentage is equal to 20.5% for a wind velocity of 8 *m/s*. Due to this difference with a factor of almost six, a wind velocity of 8 *m/s* is a good threshold when sand strips can occur on the beach based on these results.

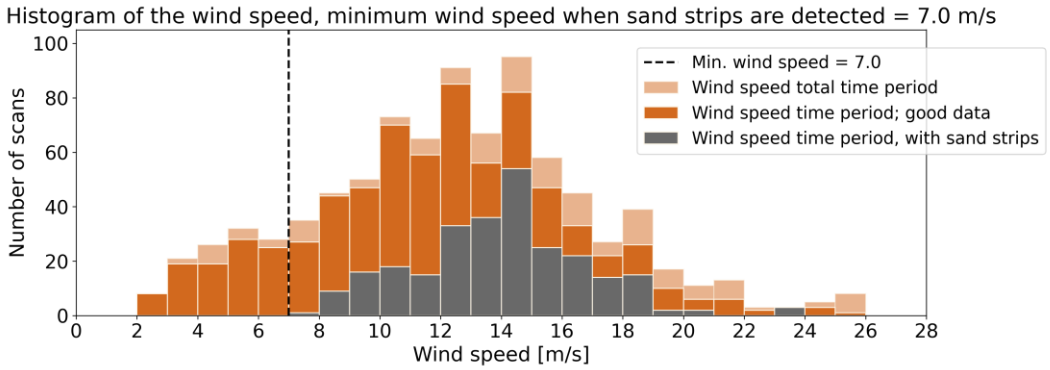

Figure 5.16. Histogram of the occurred wind speed during the studied time period. All the data is shown in light-orange, while the studied data is shown in orange. The bins were sand strips were detected are shown in grey. The dashed vertical line represents the minimum wind velocity when sand strips were detected and is equal to 7 m/s

Table 5.9. Characteristic values for the wind velocity during sand strip development

	Wind velocity [*m/s*]
Median / second quartile (M / Q2)	14
First quartile (Q1)	12
Third quartile (Q3)	15
Maximum	24
Minimum	7

The wind velocity during sand strip formation is however larger than the determined threshold of 8 *m/s*. In Figure 5.17 the wind velocity over time is visualized, with the orange dots corresponding to the detection of sand strips. The median wind velocity during sand strip formation is equal to 13 *m/s*, and the minimum and maximum were respectively 10 *m/s* and 16 *m/s*. These values are obtained by only considering the formation events when at least 3 consecutive scans prior to the first detection are of good quality. When at least 3 consecutive scans prior to the first detection are considered bad quality (bad quality data is visualized with dark red dots in the figure), there is a possibility that the sand strips formed during these bad quality data. In Figure 5.17, the minimum wind velocity for sand strip formation (10 *m/s*) is plotted as a blue dashed horizontal line, and the threshold wind velocity of 8 *m/s* for sand strip occurrence is plotted as a sandy-coloured dashed line.

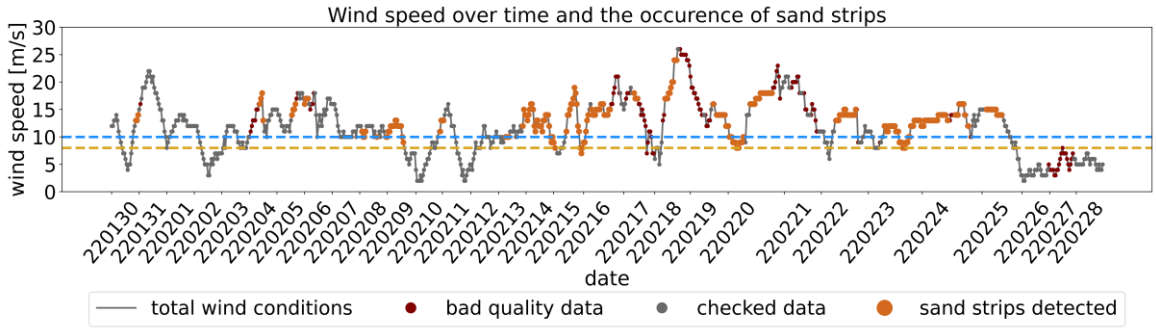

Figure 5.17. Wind velocity over time during the studied time period. The bad quality data is shown in red while the detected sand strips are marked orange. The blue line corresponds to the minimum occurred wind velocity of 10 m/s for the formation of sand strips. The yellow line corresponds to the threshold of 8 m/s for aeolian activity

Around January 31st, the wind velocity was at least 10 *m/s* every hour of the day. However, no sand strips appeared on the beach, probably caused by the wind direction which was onshore directed. In appendix F, all the environmental conditions considered over time are visualized in an overview. This overview eases a comparison between certain periods regarding sand strip occurrence. The other considered environmental conditions (besides the wind conditions) are the precipitation and the tide.

5.3.2 Precipitation events during sand strip detection

During the studied time period, several precipitation events occurred as visualized in Figure 5.18. In the figure, the orange dots correspond to the scans where sand strips were detected and the red dots correspond to bad quality scans.

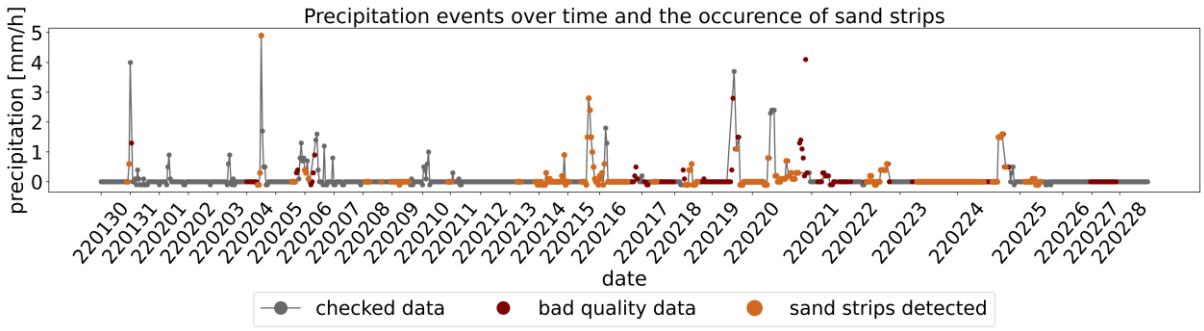

Figure 5.18. Precipitation events over time for the studied time period. The bad quality data is shown in red while the detected sand strips are marked orange.

The precipitation event of February 4th is probably being noticed almost immediately in Figure 5.18. Sand strips were detected in the two consecutive scans prior to the precipitation peak, and during the precipitation peak of 4.9 *mm/h*. The appearance of sand strips at these times is confirmed, since fieldwork is executed from 11:00*h* until 13:00*h* on this day. The disappearance of the sand strips after the precipitation peak cannot be explained by precipitation only since the wind direction also increased from 220° to 320° abruptly (corresponding to an alongshore wind towards a shore-normal wind). Therefore, the change in wind direction could cause the disappearance of the sand strips.

There occurred also precipitation events during alongshore winds of at least 10 *m/s*. During these wind conditions sand strips could occur according to section 5.3.1. However, they are not always detected during these precipitation events, while they are detected before the precipitation started. This implies that precipitation could be a limiting factor for sand strip development. Three of these events are the events on January 30th, February 16th and February 20th. For these precipitation events, sand strips were detected in at least three consecutive scans prior to the precipitation peak. Besides, for two of the three events (February 16th and February 20th), the sand strips were detected again within one hour after the precipitation stopped.

On the other hand, precipitation does not immediately imply the disappearance of sand strips, given the presence of sand strips during and after a precipitation event at February 15th. During this precipitation event, the precipitation increased almost linearly from 0 *mm/h* at 13:00*h* to 28 *mm/h* at 16:00*h*. After 17:00*h*, the precipitation decreased to 0 *mm/h* at 22:00*h*. Sand strips did not disappear for the complete duration of this precipitation event. This event seems therefore contradictive with the other three events where the sand strips disappeared. It should however be noted that the detection method is based on the reflectance, which is related to the surface moisture. The surface moisture can increase during rainfall, subsequently resulting in a smaller difference in surface moisture between the sand strips and the surrounding beach. This, eventually, can prevent the detection of sand strips using the reflectance values. It can, therefore, not be concluded that the sand strips disappeared and when applying a height based detection (section 4.3.5), it can be seen that the sand strips can remain present during precipitation.

For the precipitation event of February 16th, multiple windows are compared to each other for the time period of 05:00*h* until 08:00*h*. In these windows, there was still a height difference present according to the 1D Fourier transform based on the *z*-coordinate. It can therefore be concluded that precipitation not necessarily causes the disappearance of sand strips. For all the studied windows, the sand strips were still present with a comparable height. An example is visualized in appendix G, with one of the figures shown in Figure 5.19. At 05:59*h*, the precipitation intensity was equal to 18 *mm/h* and no sand strips

were detected based on the reflectance values (Figure 5.19-A). Based on the *z*-coordinate, the window had an average significant height of 4.5 *cm*. The specific transect which is drawn in Figure 5.19-B has an significant height equal to 5.1 *cm* (Figure 5.19-C). This detected height on this profile line is comparable with the height before the precipitation started and after the precipitation stopped at the same transect (Table 5.10). For the event of February 20th, the height-based detection did not result in sand strip detection, while February 6th sand strips were detected for two more hours during the event. It should be noted that both events are shorter in duration than the event of February 15th (where the sand strips remained present at the beach) and they had a lower intensity than the event of February 15th.

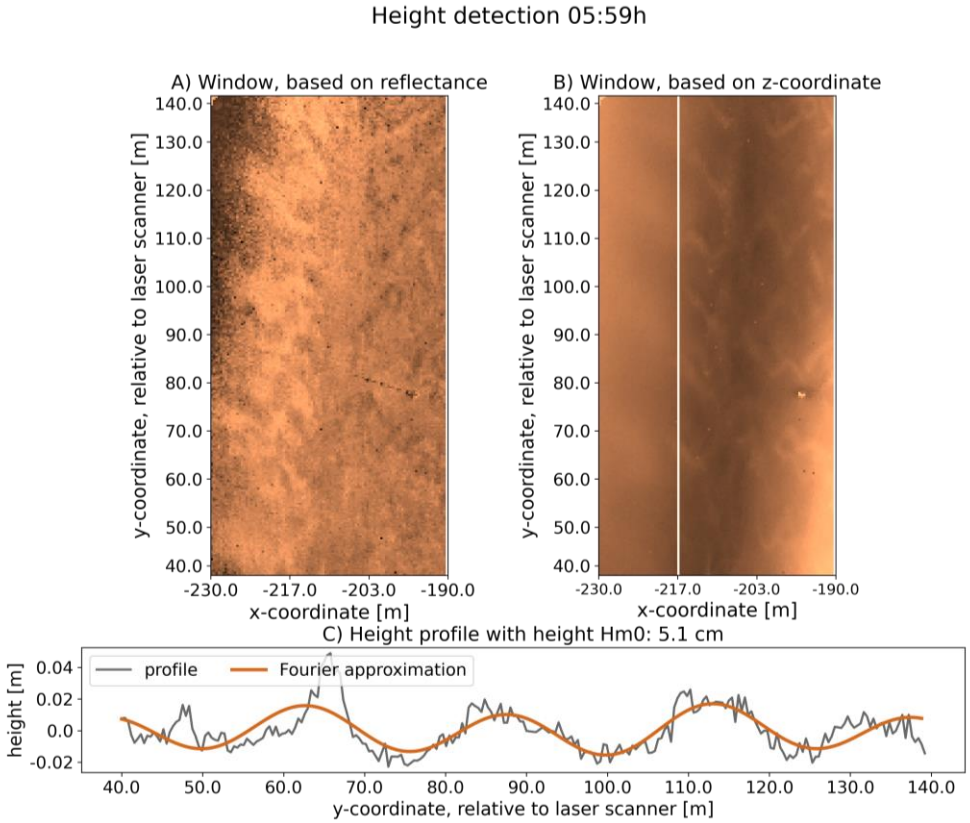

Figure 5.19. Sand strips present in a window which are not detectable with the reflectance values but only with the z-coordinate

Table 5.10. Detected sand strip height for the precipitation event occurring at February 16th

Hours	**Precipitation [*mm/h*]**	**Detected based on reflectance?**	**Height [*cm*]**
05:00	6	Yes	6.0
06:00	18	No	5.1
07:00	13	No	4.9
08:00	0	Yes	5.6

5.3.3 The tide during sand strip detection

The tide affects the moisture content, and therefore it could affect sand strip development. Another limitation of the influence of the tide is observed during the visual validation of the results. During high water (probably spring tide in combination with a storm surge) the waterline rises, sometimes even resulting in a beach width smaller than 40 *m*, preventing the application of the detection method (section 4.1.3). The amount of scans with a the width smaller than 40 *m* and where sand strips are present is however not investigated and only the scans which are marked good quality are considered.

The tidal data is visualized in Figure 5.20, where it can be observed that most of the times sand strips have formed during falling tide. It can be argued whether the sand strips have formed 20 times, however

it is assumed that they have formed 17 times. The 'disappearance' of February 6th, February 20th and February 16th are probably caused by precipitation (section 5.3.2) since the sand strips were detected with the height for February 16th. For February 6th, they were detectable with the height until 20:00*h* (where the precipitation started between 16:00*h* and 17:00*h*), and for February 20th the sand strips were not detectable with the height after precipitation started. They were detected again after the precipitation peak, and it is therefore unknown whether they remained present or disappeared temporarily. These re-appearing events are therefore not considered a new formation.

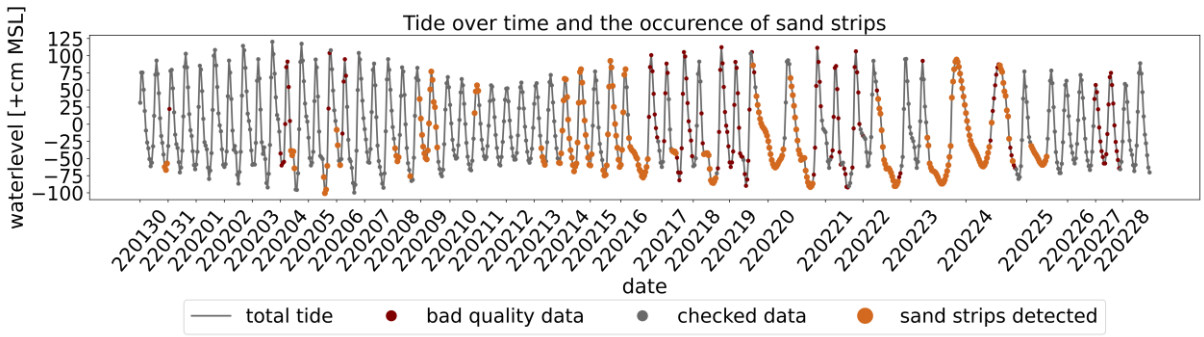

Figure 5.20. Tidal data during the studied time period. The bad quality data is shown in red while the detected sand strips are marked orange.

Out of these 17 times, sand strips have formed 10 times during falling tide (58.8%), 4 times during low tide (23.5%), whereas for rising tide and high tide this percentage is equal to 5.9%. Furthermore, the corresponding tidal period during formation on February 4th is unknown, caused by the nine bad quality scans prior to the first detection. These percentages are summarized in Table 5.11. Besides the formation, they also disappeared 17 times. They disappeared once during hight tide, and three times during low tide as well as during falling tide. During rising tide they disappeared eight times, and two times this is unknown due to the amount of bad scans (Table 5.11).

Table 5.11. Percentage of formation and disappearance of the sand strips during the tidal cycle

	High water	Falling tide	Low water	Rising tide	Unknown
Formed [%]	5.9	58.8	23.5	5.9	5.9
Disappeared [%]	5.9	17.6	17.6	47.1	11.8

Based on the results the sand strips mainly disappeared during rising tide and they mainly formed during falling tide, where the relative time in falling tide differs. Sometimes they formed right at the beginning of falling tide, while other times they formed right before low water. The disappearance during rising tide is mostly right after low water, at the beginning of rising tide. However, they do not necessarily disappear during rising tide or high tide since they have survived rising tide and high tide seven times.

5.3.4 Correlations between the environmental conditions and the characteristic properties

Shape properties of the sand strips, such as the wavelength, orientation and height, are affected by environmental conditions. One of the most obvious shape property that is affected by an environmental condition is the orientation by the wind direction. This dependency is discussed in some more detail compared to the other correlations. In addition, in section 5.1.1 it was mentioned that the environmental conditions are based on 261 scans where sand strips were detected. However, the shape properties are only determined when sand strips are detected with the 2D Fourier transform, and they are thus based on less scans. As a result, the correlations discussed in this sub-section are based on the same amount of scans where sand strips are detected according to the 2D Fourier transform. This sub-section focusses therefore on less scans than the other sub-sections of section 5.3.

The angle between the wind direction and the sand strip orientation

The sand strips were mainly oriented in the range of 55° to 90° relative to shore normal (section 5.2.2), which is in correspondence with a range between 30° and 65° with respect to North. The orientation of the sand strips is shown again in Figure 5.21, with the colour-scale based on the wind direction in the left wind rose, and in the right rose based on the difference between the wind and sand strips. The largest difference is 100° and occurred with a wind direction of 320° (shore-normal) while the sand strips had an orientation equal to 40° (almost alongshore) (the purple bar Figure 5.21).

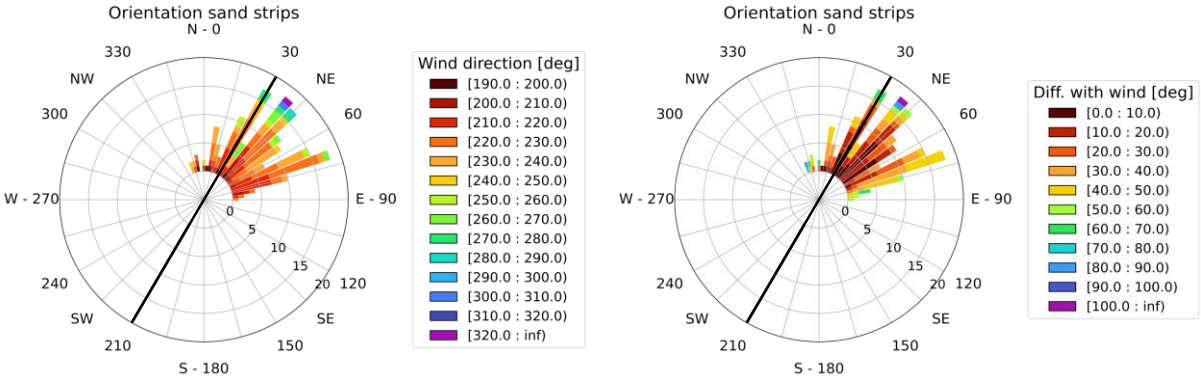

Figure 5.21. Orientation of the sand strips. The solid black line corresponds to the orientation of the Noordwijk beach. In the left figure the colours indicate the wind direction, in the right figure they indicate the difference in angle between the sand strips and wind direction

The orientation of the sand strips is mostly perpendicular to the wind direction, as visualized in Figure 5.22. In the figure the differences are shown in absolute values where 0° corresponds to a perpendicular orientation. Based on these values, the median angle of the difference is equal to 20°. The first quartile is equal to 10°, and the third quartile to 40°. A difference of at least 50° occurred only thirteen times. Five times, they occurred during longshore winds (≤ 240°), which were measured 157 times, and eight times during onshore oblique winds (> 240°), which were measured 24 times (Table 5.12). In the table it can be seen that a difference between the wind direction and the orientation of the sand strips of at least 50° is more common for onshore-oblique winds than for alongshore winds. Besides, during the 24th of February alongshore winds already led 4 times to a difference of at least 50° (out of the total 5 occurrences for alongshore winds).

Table 5.12. Difference between wind direction and sand strip orientation for alongshore and onshore-oblique wind events

	Number of occurrences	**Number of occurrences that $\Delta\theta \geq 50°$**
Alongshore (≤ 240°)	157	5 (3.2%)
Onshore-oblique (> 240°)	24	8 (33.3%)

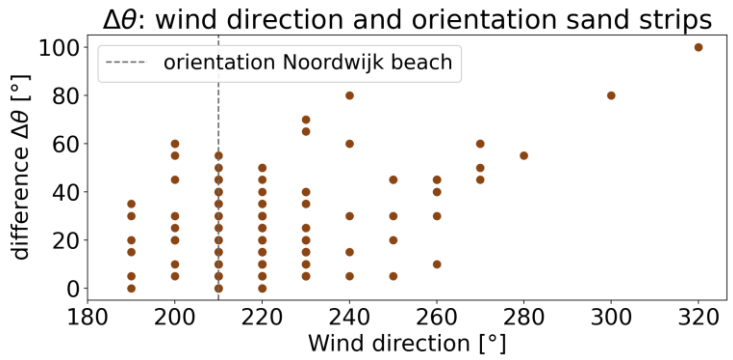

Figure 5.22. The wind direction and the difference in angle between the wind direction and the sand strip orientation. 0° corresponds to a perpendicular orientation of the sand strips compared to the wind. The orientation of the Noordwijk beach is visualized with the dashed vertical line

Correlations between the wind velocity and the shape properties

The wind velocity is correlated with other shape properties of the sand strips as well. The wind velocity and the wavelength have a correlation coefficient of r = 0.29, suggesting a slight increase in wavelength for an increase in wind speed. The wind velocity and the height are correlated with a Pearson correlation coefficient of r = 0.11, and the wind velocity and orientation with r = 0.05, implying that they are not correlated. These weak correlation coefficients imply that other environmental factors affect the shape properties as well. In Figure 5.23 and Table 5.13, these correlation coefficients are summarized.

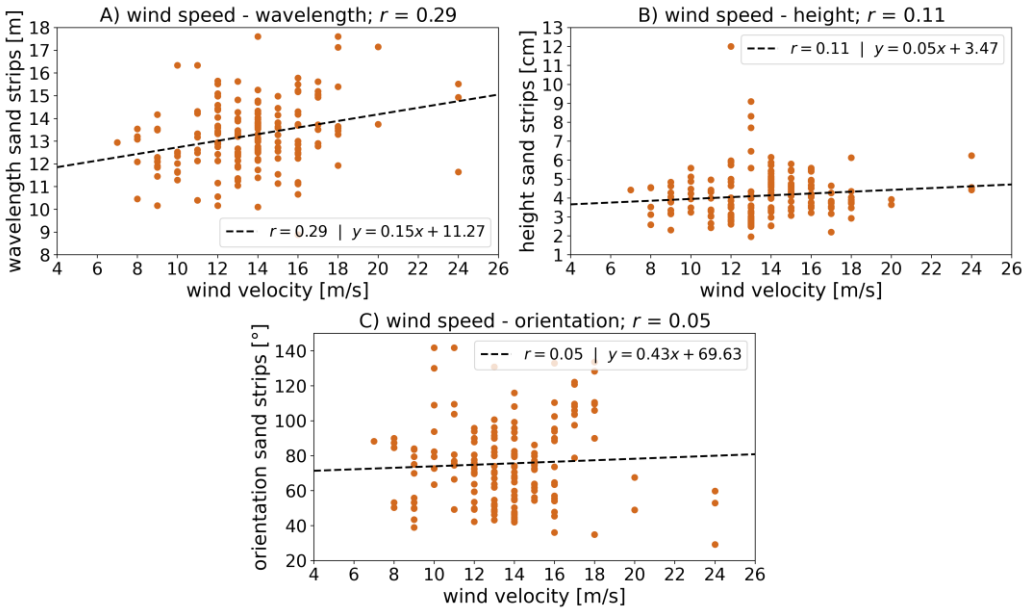

Figure 5.23. Correlation of the shape properties with the wind velocity. The shape properties that are considered are the wavelength (A), height (B) and orientation (C)

Table 5.13. Correlation coefficients - wind velocity and shape properties (wavelength, height and orientation)

Pearson correlation coefficient r	**Wind velocity**
Wavelength	0.29
Height	0.11
Orientation	0.05

5.4 The dynamic properties of the sand strips

In this section the dynamic properties for one life cycle of the sand strips are analysed. First, the shape properties over time are analysed for February 23th 21:40*h* until February 24th 12:00*h*. In this period sand strips were present without interruption and beach is scanned every 20 minutes, resulting in accurate and detailed information regarding temporal changes. In section 5.4.2 the horizontal migration rate of the sand strips is analysed for February 23th 22:00*h* until February 24th 06:00*h* due to the beach width as limiting factor caused by the tide. Since the observations discussed in this section are based on only one life cycle, the observations might not be applicable for all situations and it is thus important to note that no generic conclusions can be drawn regarding the dynamicity of the shape properties.

5.4.1 The shape properties over time

Although the two scans prior to the first scan of the time period (the scans of 21:00*h* and 21:20*h*) have detected sand strips, these scans are not considered since sand strips in these scans are only detected with the 1D method, thus no information of the wavelength and orientation are known. Sand strips were not detected in the three scans prior to 21:00*h*, implying the formation between 20:40*h* and 21:00*h*. Since the shape properties are determined first at 21:40*h*, the analysis will start at this time. In the last

scan of the considered period, February 24th 12:00*h*, sand strips appeared, while at 12:14*h* until 14:00*h* the scans were considered bad quality. Therefore information on the disappearance is missing and the analysed period stops at 12:00*h*.

During the life cycle, the environmental conditions remained approximately constant (Figure 5.24). The wind was oriented alongshore with a median velocity of 13 *m/s*, and increasing towards 16 *m/s* at the end. No precipitation occurred and the time period was something longer than one tidal cycle, starting at high tide and ending at falling tide.

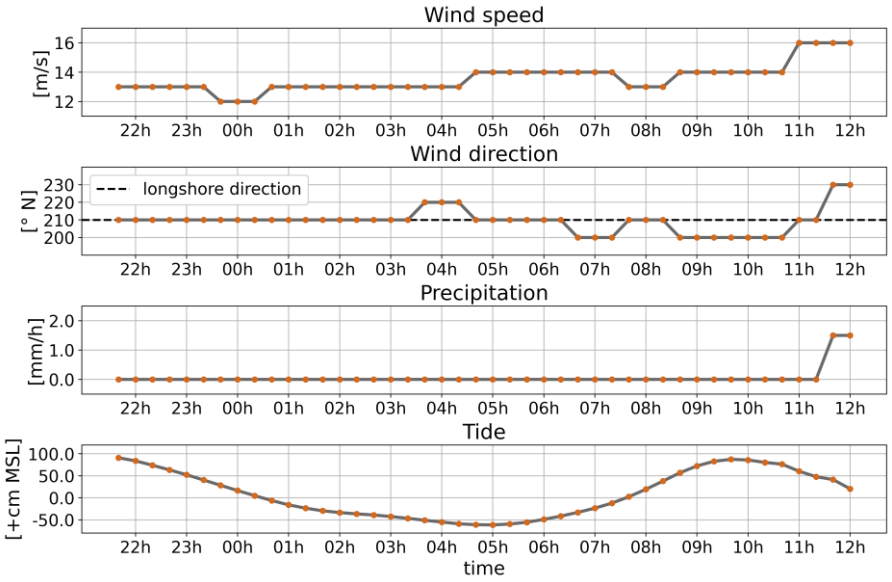

Figure 5.24. Environmental conditions during the considered life cycle of the sand strips

It took a few hours before the wavelength stabilized, whereafter it decreased slightly over time (Figure 5.25). In the beginning the sand strips were oriented alongshore, and thus perpendicular to the wind direction. After a few hours, the orientation increased and stabilized between 70° and 80° relative to North, while the wind direction remained constant with a deviation of 10°. This increase corresponds to more inland directed sand strips. This implies, in combination with a constant wind direction, a different migration rate of the sand strips over the width of the beach and is therefore discussed in section 5.4.2. Furthermore, the height also increased over time from around 3.0 *cm* to 4.0 *cm* at the beginning between 23:00*h* and 01:00*h* to 6.0 *cm* around 10:00*h*.

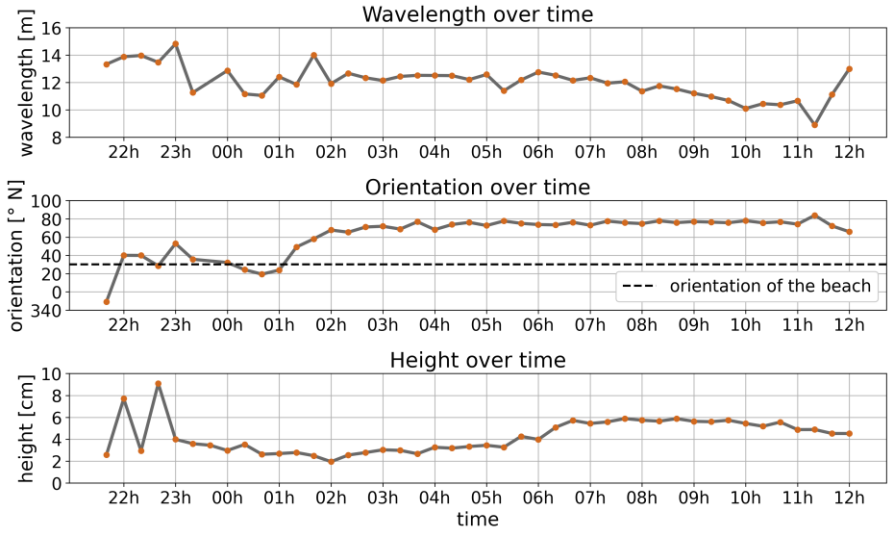

Figure 5.25. The shape properties over time for the studied time period

It should be noted that an increase in orientation relative to North corresponds to a decrease in orientation relative to shore-normal (see e.g., Figure 5.5). Therefore, this increasing orientation corresponds to the correlation coefficient between the wavelength and orientation of r = 0.36 (as derived in section 5.2.7). Since the other two correlation coefficients between the shape properties are weak (both equal to r = 0.12, section 5.2.7), not much can be said regarding the correspondence of these results to the derived correlation coefficients. However, the wind velocity and the wavelength have a correlation coefficient of r = 0.29 (section 5.3.4) which is still weak, yet statistically significant. In the analysed period, the wind speed increases near the end of the time period, while the wavelength decreases over time, contradictive to the positive correlation coefficient.

5.4.2 The migration rate of the sand strips

The variation in migration rate over the width of the beach is analysed by drawing multiple lines in longshore direction at different x-coordinates. The lines are drawn within the two boxes shown in Figure 5.26-A. The wind had an alongshore direction for the analysed time period, visualized with a black arrow. The sand strips migrated in the same direction as the wind, which is to the left in the figure. The orange box is therefore upwind and the grey box is downwind from the beach pavilion, where the pavilion could act as an obstacle in the wind field. The wind field in the grey box might therefore be different compared to the orange box. The range in x-direction of the grey box is equal to $-226 \leq x \leq -184$ *m*, and the orange box is within $-243 \leq x \leq -189$ *m*. In each box a line is drawn every six meter, resulting in eight lines in the grey box and ten lines in the orange box.

By storing the reflectance values along these transects, the migration rate is determined according to the y-coordinates of the sand strip crests and the known time interval between the scans. The migration rate varies over the width of the beach and decreases in duneward direction (Figure 5.26-B, where the colour of the dots correspond to the box in which they are determined). The maximum migration rate was equal to 3.3 *m/h*, occurring at x = -237 *m* upwind from the beach club (orange box). The minimum measured migration rate is equal to 0.3 *m/h*, occurring twice at x = -189 *m* and x = -190 *m* (both upwind and downwind from the beach pavilion). The mean migration rate and the median migration rate are both equal to 1.2 *m/h*. Furthermore, the migration rate and the beach width are correlated with r = 0.69, implying an increase in migration rate near the waterline.

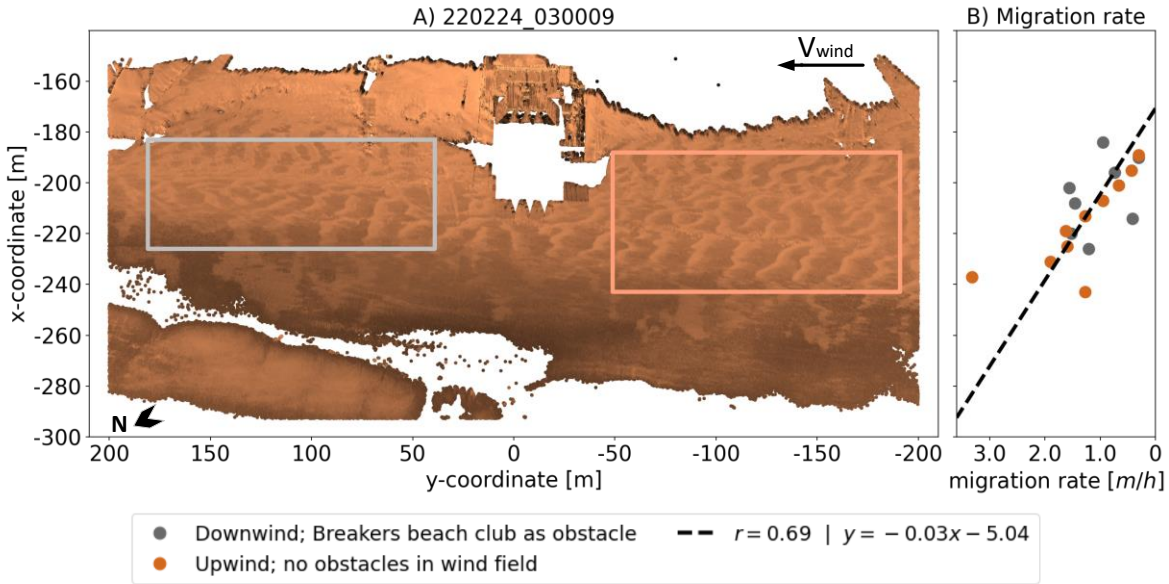

Figure 5.26. Migration rate determination, A) The locations of the two boxes, within these two boxes the migration rates over the width are determined; B) Variation in migration rate over the width of the beach with x=-180m closest to the dunes and x=-245m closest to the waterline. The colour of the dots in B correspond to the colour of the box in A

6. Discussion

The discussion consists of three parts. First, the quality of the available data is elaborated in section 6.1. In section 6.2, the detection method and methodology is discussed. In section 6.3, the obtained results are related to processes of sand strips and aeolian transport.

6.1 Quality of the available data

In the study period the TLS scanned the beach 1215 times while the detection method could be applied on 943 scans (77.6%) (with sand strips detected in 261 scans). The other 272 scans (22.4%) were considered bad quality (this is visualized in Figure 5.1). The developed method is therefore not applicable on all data due to its dependency on the quality of the input data. Furthermore, in Figure 5.16 and Figure 5.17 it can be observed that bad quality data appeared more often during high wind speeds compared to low wind speed events. In Figure 5.16 this can be observed by the difference in bin height between the light-orange bins and the darker-orange bins, which increases for higher wind speed events. Since scans were considered bad quality more often during high wind speed events in combination with the dependency of sand strips on a wind velocity threshold, sand strips could be present in these bad quality scans. Therefore, the amount of scans with sand strips could possibly be larger, although the detection method is not applied on these scans.

Furthermore, weather and water level data was not available for Noordwijk. For the wind conditions the station of IJmuiden is used, while wind conditions can differ locally and therefore the wind conditions occurring in Noordwijk may differ to some degree (van Tuyll, 2020). From a comparison between the occurring wind conditions at the Noordwijk beach (according to www.windguru.cz) and the analysed wind conditions measured at IJmuiden (Figure 6.1) it is concluded that the wind conditions differ slightly. The median wind velocity in Noordwijk was equal to 12 *m/s* ant the median direction 220°, and for IJmuiden these were 14 *m/s* and 220° respectively. Considering the accuracies of the measurements, which are 10° and 1 *m/s* for the wind direction and velocity respectively (KNMI, 2001), the differences in wind conditions between IJmuiden and Noordwijk are small. Therefore it is assumed that the wind conditions measured at IJmuiden are representative for Noordwijk.

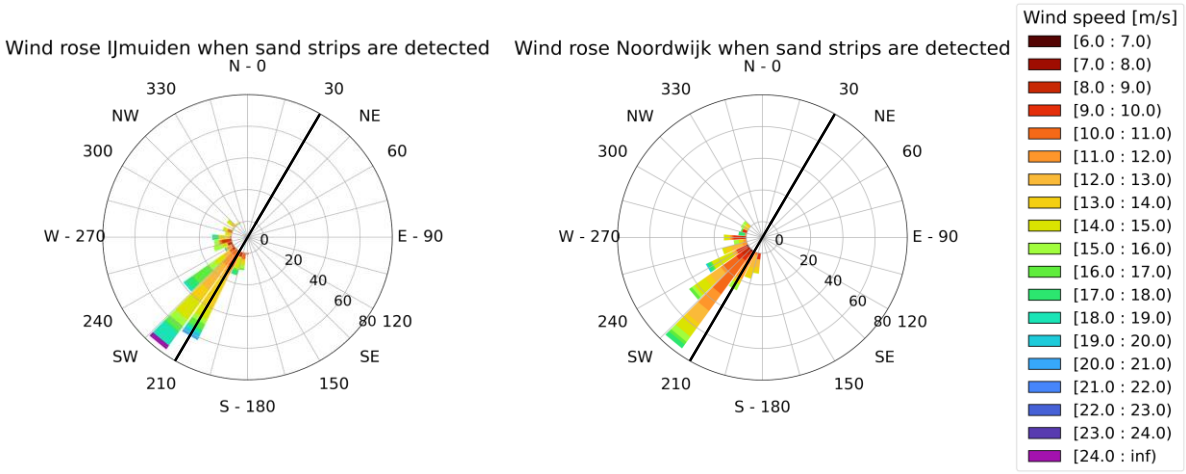

Figure 6.1. Wind rose for IJmuiden (left) compared to the wind rose of Noordwijk (right)

The analysed tide is assumed by the average of the water levels measured in Scheveningen and IJmuiden. Noordwijk is not located exactly in between these two locations and therefore the analysed tide will somewhat differ from the real appeared tide. The propagation of tidal waves depend on the water depth and along the centre of the Dutch coast the propagation varies slightly (Bosboom & Stive, 2021). Besides, the differences in tidal curve between Hoek van Holland (south of Scheveningen) and IJmuiden are small (especially compared to the differences between Vlissingen and Hoek van Holland or IJmuiden and Den Helder, figure 5.55 in Bosboom & Stive, (2021)). Due to the small differences along the centre

of the Dutch coast compared to the differences at the Wadden coast or the Southwest delta coast, the difference between the estimated and the real appeared tide is assumed small and the tide used is therefore assumed representative. Nevertheless, it is better to use local data if available.

6.2 The detection method and methodology

Since sand strips have a different moisture content compared to the surrounding beach (section 5.2.6), which can also be derived from the reflectance values of the laser scanner, the detection method is based on the reflectance values. However, the Fourier transform based on height differences detected sand strips that were not detected with the reflectance during precipitation events. This suggest that during these precipitation events the difference in moisture content decreases, rendering the reflection based method less useful for these events. Therefore, a detection based on either the reflectance or the z-coordinate is preferred instead of focussing on one parameter, despite the increasing computation time. For such detection, the amount of FN's might decrease since they are either detected with the reflectance or height. Due to this extra assessment the amount of omitted sand strips is minimized (e.g., precipitation can cause that sand strips are not detected with the reflectance, while they are detected with the height, preventing that these sand strips are counted as FN). Similar, such method could cause an increase in FP. As well as the reflectance-based detection, a height-based detection will have its own FP too. Since a detection based on both parameters is a 'either-detection' rather than a 'both-detection', these FP's of both individual parameters will add up (a 'both-detection' will still prevent the detection of sand strips during precipitation, since then they will not be detected by reflectance).

Hage et al., (2018b) studied sand strips on only the upper beach using Argus imageries that were converted to greyscale. The presence of sand strips was suggested by colour differences, resulting in a wave-signal with dark (surrounding beach) and light (sand strips) colours, and therefore their detection was also based on surface moisture differences. Hage et al. disregarded events on beforehand, resulting in the consideration of 41 and 43 events for the wavelength and migration rate respectively in a seven-year period. For instance, they only considered events with hourly mean wind velocities in excess of 8 *m/s* and they avoided circumstances that could reduce the quality of the imageries, whereas in this study such environmental filters are not applied. In this study, the detection method is applied on all available scans that are marked good quality without any further filtering. Although the bad quality scans are disregarded, it is not similar to Hage et al. since they filtered based on the circumstances that could reduce the quality, without having evidence that they are reduced.

Furthermore, Hage et al. (2018b) focused on areas of approximately 100 *m* by 25 *m* in alongshore and cross-shore direction respectively with a pixel size of 0.5 *m*. In this study a moving window over the complete beach area is applied, rather than focusing on the upper beach only, to maximize the detection of all present sand strips on the complete beach area. The used window size was 100 *m* by 40 *m* in longshore (y-) and cross-shore (x-)direction respectively with a grid size of 0.40 *m*. For the detection it is important that the wave-signal, caused by the presence of the sand strips, is high enough. Hage et al. observed mainly alongshore oriented sand strips, and by applying a rather long than wide window in combination with alongshore oriented sand strips, the wave-signal in this direction is high when sand strips are present. Although the signal in cross-shore direction is limited, the window width is considered wide enough for a proper determination of the orientation and corresponding wavelength. However, if cross-shore oriented sand strips appeared, their detection may be prevented by the too small wave-signal. The disregarding of detected orientations smaller than 15° or larger than 165° (relative to shore-normal, Figure 5.2-D) would possibly contribute to the absence of cross-shore oriented sand strips. However, since the detected orientations range between 29° and 142° (and therefore not between 15° and 165°) their occurrence is assumed unlikely. Therefore it is assumed that they did not occur and hence the applied window size is appropriate.

Sand strips are detected based on the spectral energy in the variance density spectrum for a range in wavenumbers that corresponds to possible wavenumbers for sand strips. Hage et al. (2018b) studied

sand strips on the beach of Egmond aan Zee (the Netherlands), distanced approximately 40 *km* from the Noordwijk beach and found a mean wavelength of 12.0 *m* (σ = 2.8 *m*). The same order of magnitude for the wavelengths is expected in Noordwijk, since the environmental conditions and the bed properties between the beach in Egmond and Noordwijk are comparable. Therefore, the applied wavelength range of interest (8.00 < *L* < 18.18 *m*) is based on the 95% confidence interval found by Hage et al. Due to this pre-proposed wavenumber range not all wavelengths can be detected, possibly preventing the detection of outlying wavelengths. However, the detected sand strips had a smaller wavelength-range (8.9 < *L* < 17.6 *m*, section 5.2.1) than the pre-proposed range and followed a Gaussian distribution, and hence the pre-proposed range seems appropriate.

Perhaps the biggest difference between Hage et al. (2018b) and this study is the applied method to determine the shape properties. In this study the wavelength and orientation, are determined according to the 2D Fourier transform whereas Hage et al. applied autocorrelation on horizontal pixel rows, similar to the 1D method in this study. They corrected the orientation manually to display the sand strips as vertical lines. By this manual rotation the orientation is taken into account, however, it still might cause an overestimation of the wavelength caused by an alignment where the sand strips are not fully perpendicular to the horizontal pixel rows. Although the accuracy of the numerical determination of this study is governed by the bandwidths and therefore the window size, it is less vulnerable to manual errors and small differences in individual observations. The numerical determination is therefore considered more consistent than the method of Hage et al. (2018b) although it is recognized that the accuracy of the numerical determination is governed by the bandwidths.

6.2.1 The applicability of the method on other sandy beaches

From June 25th to July 30th 2020, the used Riegl VZ-2000 was removed temporarily from its location for maintenance activities (CoastScan, 2022b), including the recalibration of the reflectance intensity. This recalibration did not cause difficulties with detecting sand strips before the summer of 2020. 14 point clouds were selected acquired before the summer of 2020, from February 9th 05:00*h* until 17:00*h* 2020, where sand strips were present, and detected, from 07:00*h* onwards (e.g., Figure 6.2 where sand strips are present, and they are all detected within the blue box). Therefore the detection method is applicable on laser scan data acquired with the same TLS before the recalibration.

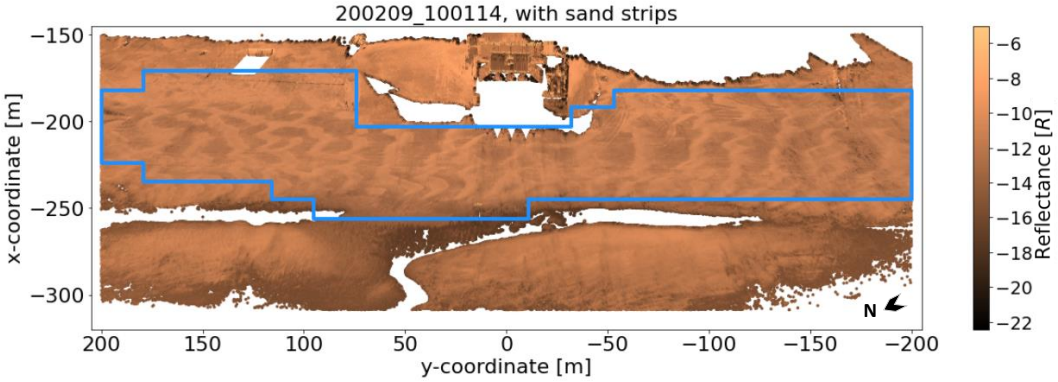

Figure 6.2. Point cloud of February 9th, 2020 (10:00h). Sand strips are present and detected (blue box)

However, the determined threshold is not necessarily applicable on other datasets. Nield et al., (2011) also derived the moisture content on a beach using the reflectance intensity of a TLS (a Leica Scanstation). Their obtained calibration curve between the reflectance and moisture was different compared to the calibration curve for the used scanner (Di Biase et al., 2021), despite other characteristics such as grain size being comparable. A different calibration curve implies different densities in the variance density spectrum, resulting in a different threshold. This is observed by applying the detection method on 22 point clouds of the beach at Mariakerke-Bad (near Oostende, Belgium), from January 16th 17:00*h* to January 17th 11:00*h* 2018. The method did not detect the present sand strips

(Figure 6.3-A), despite small adjustments of the window size due to a different beach geometry. The window that contains sand strips is visualized in Figure 6.3-B and its corresponding variance density spectrum in Figure 6.3-C with the spectral energy below the determined threshold for detection. However, the determined orientation represents the sand strips accordingly (blue arrow in Figure 6.3-B) and the method is thus applicable after calibrating the threshold for sand strip detection.

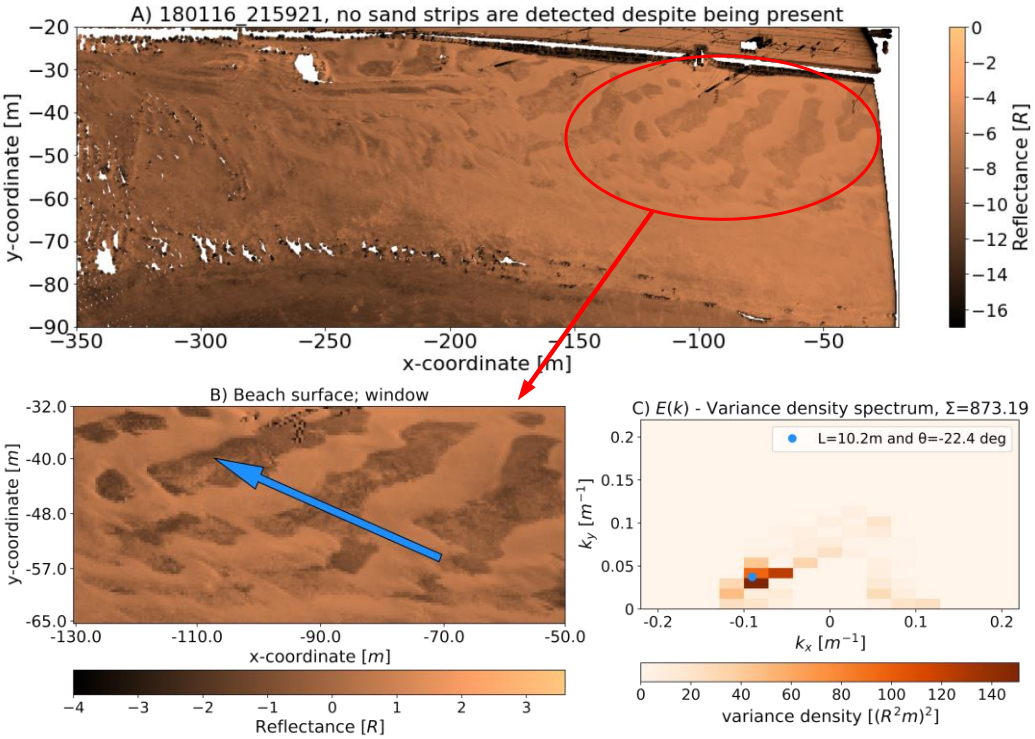

Figure 6.3. Point cloud from Mariakerke-Bad (February 16th 2018, 21:59h). No sand strips are detected despite their presence (e.g., in B). The small reflectance differences causes the energy in the spectrum (C) below the threshold for detection. Although the energy is below the threshold, the determined orientation, as shown with a blue arrow in B, is representative

6.3 Processes related to sand strips and aeolian transport

The sand strip detection resulted in almost alongshore oriented sand strips with a mean wavelength of 13.3 *m* (with σ = 1.5 *m*) and a mean height of 4.0 *cm*. The sand strips mainly appeared with alongshore winds of at least 8 *m/s*. The detection of the height gives new insights since this is not studied in depth yet. Baddock et al. (2018) only described the height of the sand strips being a few centimetres without mentioning any exact values. The wavelength and orientation as well as the occurring environmental conditions can be compared in more depth to similar sand strip-related studies.

Hage et al. (2018b) observed alongshore oriented sand strips with a mean wavelength of 12.0 *m* (σ = 2.8 *m*). The larger standard deviation compared to this study could be explained by the pre-proposed wavelength-range applied in this study, resulting in limited wavelengths that are detectable. Hage et al. did not apply a pre-proposed range and detected outlying wavelengths of $O(30\ m)$, which were not detectable in this study. However, as already mentioned in section 6.2, the pre-proposed range is considered appropriate. Furthermore, a wavelength of 30 *m* is significant larger (factor of two) than wavelengths found in this study. It should however be noted that Hage et al. only applied a horizontal (1D) method where the sand strips were rotated manually, which could still cause an overestimation of the determined wavelengths. Although they mentioned that the sand strips were mainly oriented alongshore, resulting in a limited overestimation, this observation might be based on visual observation since they did not mention the determination of the orientation. Therefore, the wavelengths might still be overestimated, but it is unlikely that this could explain the significantly larger wavelengths found by Hage et al. (2018b).

The orientation of the sand strips was mainly oriented alongshore to oblique-alongshore, in correspondence to the observed orientation by Hage et al. (2018b). Although alongshore wind events resulted in sand strips more often ($O(200\ \text{times})$) than onshore-oblique events ($O(50\ \text{times})$), these oblique directed wind events did not necessarily lead to more-inland oriented sand strips. During these more oblique wind events, a large difference in angle between the wind direction and sand strip orientation appeared. This angle between the wind direction and the orientation of the sand strips could be caused by topographic steering due to the present dune. Bauer et al. (2012) observed that during oblique wind events the near-surface wind flow had a strong tendency for an alongshore alignment, eventually resulting in sediment transport in alongshore direction, which corresponds to alongshore oriented sand strips.

The topographic steering effect caused by the dune might also explain the varying migration rate over the width of the beach. The wind velocity and shear velocity might decrease in landward direction (Bauer et al., 2009), which subsequently might explain the decreasing migration rate in duneward direction. Bauer et al. (2012) observed a larger sediment transport rate at the beach compared to close to the dune and related this to the presence of the dune. Contrarily, Davidson-Arnott et al., (2008) observed for alongshore winds a lower transport intensity at the upper beach compared to the lower beach. Furthermore, Hage et al. (2018b), who focused on the upper beach only, found an average migration rate of 1.24 *m/h* (σ = 0.78 *m/h*), which is in the same order of magnitude as the migration rates found in this study. It is however important to note that Hage et al. only considered migration rates that excessed 0.5 *m/h* due to their pixel size of 0.5 *m*, disregarding events with a lower migration rate. Nield (2011), who modelled bedforms after a precipitation event, found a lower migration rate of 0.176 *m/h* (σ = 0.076 *m/h*). Nield did neither discuss the exact location relative to the beach width nor grain size characteristics, causing difficulties when comparing the migration rates found in this study with the model. Since Nield modelled the migration rate after a precipitation event and Hage et al. focused on the upper beach, the difference may be caused by moisture content. This would suggest an increasing migration rate in duneward direction, in correspondence as the observed migration rate by Davidson-Arnott et al., (2008). This is however contradictive to the decreasing migration rate in duneward direction found in this study and the occurring decreasing near-surface wind speed (and thus a decreasing transport potential) in duneward direction (Bauer et al., 2009).

Altogether, moisture content is an important feature for sand strip development. Hage et al. (2018b) even suggested that sand strips disappeared temporarily during precipitation events and that they could recover within one hour after the precipitation stopped. However, since a significant height can still be detected during precipitation, the sand strips do not necessarily disappear during such events. Besides, sand strips were commonly destroyed by the increasing water level during rising tide, which is in correspondence with the results obtained by Hage et al. (2018b). Sand strips mostly formed during falling tide, which could be caused by the decrease in moisture content, since the maximum gravimetric moisture content for aeolian transport is determined at 10% (Hage et al., 2020). During falling tide the surface can dry, resulting in a decreasing moisture content. The time period for moisture content to decrease is considered largely important for sand strip formation, since it is observed that rapid surface drying can lead to the formation of sand strips (e.g., Jackson & Nordstrom (1998); Yang & Davidson-Arnott (2005); Wiggs et al. (2004)). Due to this rapid surface drying it may be suggested that sand strips most likely occur only in humid climates.

Furthermore, the moisture content affect the shear velocity (u_*) that is important for aeolian sediment transport to occur. Since the movement of sand strips is considered creep (Sherman, et al., 2019), the applicability of the transport regimes in the active bed surface layer (ABSL) as described by Uphues et al. (2022) is checked for sand strips. These regimes are based on field measurements at the dry, supratidal beach area at the same study site (Noordwijk). Uphues et al. described that transport in the ABSL occurs as creep for $1 < {u_*}/{u_{*t}} \leq 4$, whereas it occurs as saltation for ${u_*}/{u_{*t}} > 4$, with u_{*t} the threshold shear velocity where grains start to move. The shear velocity is computed according to the

Law of the Wall equation, in combination with Charnock's (1955) relation for the roughness height (the equations are presented in appendix G) and is visualized for different wind speeds with the orange line in Figure 6.4. The threshold shear velocity can be computed according to Bagnold's (1935) model. However, Bagnold's model does only consider dry sand, whereas moisture content is important for sand strips. Therefore the formula described by Hotta et al. (1984) is used for the determination of the threshold shear velocity. Assuming a sediment density of 1600 kg/m^3 and a grain size diameter of 0.20 *mm*, which is approximately equal to the D_{10} of the sand strip crest (section 5.2.5), and a moisture content of 3% (roughly equal to the mean moisture content of the sand strip, section 5.2.6), the threshold shear velocity for wet surfaces (u_{*tw}) is equal to 0.385 *m/s*. The boundaries for creep according to Uphues et al., (2022) are visualized with black horizontal lines in the figure, with corresponding measured wind speeds for this study as shown with vertical grey lines. The derived wind speeds that are important for sand strip development (section 5.3.1) coincide with these boundaries. Additionally, Hage et al. (2018b) observed that a wind velocity below 8 *m/s* (measured at the same height as the used wind velocities in this study) prevents the movement of sand strips whereas they remain visible, suggesting that the observed sand strips for wind velocities of 7 *m/s* and 8 *m/s* do not migrate. This is in correspondence with the lower boundary of 8.6 *m/s*, it is however not verified.

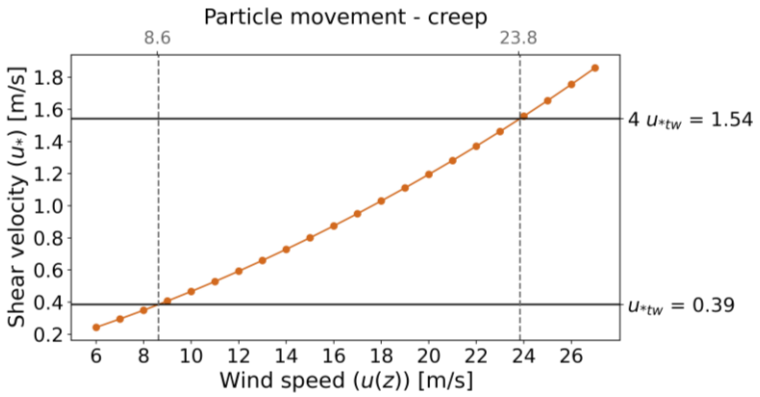

Figure 6.4. Shear velocities for the corresponding wind velocity measured (orange line). The boundaries for creep movement according to Uphues et al., (2022) are shown with horizontal black lines, the corresponding wind velocities are shown with vertical grey dashed lines

To verify this statement, it can be helpful to measure some parameters in the field for a better understanding of the local dynamics of sand strips. Firstly, the near-surface wind vectors can be measured since turbulent airflow is important for aeolian transport. Baas (2007) describes the aeolian sediment transport system by non-linear interactions between the wind forcing (airflow components), saltation flux, reptation, and bedform development (and therefore bed properties). Furthermore, the experiments of Baas & Sherman (2005) showed that moisture is not a necessary condition for the formation of streamers, while it is for sand strips since rapid surface drying can lead to the formation of sand strips. This suggest that the time-scale of the surface drying is an important parameter for the formation of sand strips, while there are no field studies that report the time-scales of surface drying on an initially too moist bed (Jackson & Nordstrom, 1998). Therefore, most important measurements for a better understanding of sand strips are probably related to (changes in) (i) airflow components; (ii) surface properties and; (iii) transport rates (both creep and saltation). It is already known that for moist surfaces the transport rate close to the bed is much larger than at saltation heights, and this transported sediment has a larger moisture content compared to the transport at the saltation heights (Swann et al., 2021). Besides, for these wet surfaces this near-surface transport rate is larger compared to dry surfaces.

It is expected that process-based modelling of sand strips is possible, but difficult due to the interdependency between different processes (e.g., the local bed topography affects the near-surface turbulent airflow), and not every relation between the components are known (i.e., the effect of bedforms on saltation (Baas, 2007)). However, Nield (2011) modelled sand strips after a precipitation event where

the complex interactions are explored using a cellular automaton model based on an algorithm for dune simulation developed by Werner (1995). The capillary action of the moisture content overpowers other forces, since a threshold moisture of 10% is applied for sediment entrainment. The moisture was updated by a feedback function based on sediment availability and transport properties. This resulted in a decrease in moisture for deposited sand, while eroded or neutral sand increased in moisture. Furthermore, the atmospheric conditions were assumed constant during the simulation time. In addition, Wang (internal PhD candidate in Coastal Systems and Nature-Based Engineering at the University of Twente) plans to model saltation characteristics by a grain-scale model, and subsequently model sand strips based on a transport model. In this way, relevant parameters such as moisture, bed roughness and bed slope can be included in the transport equation. Surface moisture is probably included as a function of factors that lead to drying, which allows updating the surface moisture during the simulation. By applying different initial conditions, they might be able to update the topography and model the aeolian sand strips. However, in this way the time-dependent turbulence effect will not be included in the model (personal communication, November 8, 2022).

The impact of the local bed topography on the near-surface airflow could be explained by the presence of a low-amplitude bedform. At the bedform crest, the streamlines converge and the wind shear velocity reaches a maximum just before the crest. At the troughs the streamlines diverge and the wind shear velocity reaches a minimum (Duran et al., 2011). Bagnold (1937) related this airflow to the variation in grain size over aeolian sand ripples, similar to the found variation over the sand strips in this study. The largest grains are transported towards the crest, given that the wind shear velocity is large enough to transport the coarser grains to the crest. From the crest, the wind shear velocity decreases in downwind direction, preventing the transport of these larger grains in downwind direction, and causing these larger grains to remain at the crest. The smaller grains can be transported at lower wind shear velocities, resulting in the transportation of these small grains towards the lee-side and the trough of the bedform. The small grains located at the windward side, which are not sheltered from the wind, could be transported, exposing the bigger grains at the surface. These exposed larger grains might be slowly transported to the crest of the bedform (Bagnold, 1937).

7. Conclusion

Laser scanning data for the period January 30th until February 28th 2022 was studied in order to determine the properties, and the factors that determine the properties, of aeolian sand strips on a sandy beach. The research question of this thesis was therefore as follows:

Which factors determine the properties of the aeolian sand strips on a sandy beach, and to what extent?

This research question is answered according to six sub-questions, which are answered below separately.

How should the data obtained with the permanent laser scanner be processed to detect sand strips?

Before the detection method is applied, several pre-processing steps are executed. First measurement errors are minimized by the correction of small displacements via the application of a local transformation matrix. Thereafter the area of interest is cropped by both the point density and the beach width. Bad quality data does not result in reliable and accurate results and is therefore disregarded. Scans are considered bad quality when either (i) the correction for small displacements is not possible; (ii) the area of interest contains less than 1.000.000 data points or; (iii) the beach width is smaller than 40 *m*. In order to assess the complete beach area a moving window is applied with a window size of 100 *m* (longshore direction) by 40 *m* (cross-shore direction; related to the minimum required beach width) with a grid size of 0.40 *m*. With these window characteristics, the window size is large enough to obtain a strong wave-signal when sand strips are present, whereas the grid size is optimal regarding the combination of the representativeness and the computation time. The dominant trend is subtracted from the original profile in the window, and outliers are removed and replaced with the mean value of the window, to facilitate detection. Sand strips are detected by applying either the 1D or 2D Fourier transform on the reflectance values of the TLS-data, and the detection depends on the spectral energy in the variance density spectrum in combination with the corresponding wavenumber. Since the shape properties are obtained with the 2D method, the windows for the 2D method should be reliable, c.q. less than 20% required interpolation. The 1D method is only applied when the required interpolation ranges between 20% and 25%. Windows with more required interpolation do not contain reliable results and are disregarded. The 1D method detects sand strips when the spectral peak, corresponding to the profile according to RMSE < 0.5, exceeds 10 $R^2 \cdot m$. For the 2D method, the spectral energy in the pre-proposed wavenumber range ($0.125 < k < 0.056$ m^{-1}) should exceed 1000 $(R^2 \cdot m)^2$. A quality assessment is examined on the method with two quantities (area-based and epoch-based) based on the percentage FP and FN, resulting in a percentage of area-based FN of 3.8% and area-based FP of 3.4%. The percentage epoch-based FN and FP are 3.6% and 3.9% respectively. These percentages are considered small enough, resulting in a method that works properly.

Is the derived method for the Noordwijk beach applicable on other sandy beaches?

The detection of sand strips depends on the spectral peak in the variance density spectrum and the corresponding wavenumber of the peak. Since the rapid surface drying seems important for the formation of sand strips, they will most likely not appear on every sandy beach around the world. Due to this limited area, it is likely that the bed properties of the beaches where sand strips could occur are comparable, probably resulting in wavelengths in the same order of magnitude. The wavenumber range that implies sand strip presence that is used can therefore most likely be applied to other sand strip situations as well. However, the used threshold for the peak depends on the calibration settings of the laser scanner and is dataset-dependent. For the used Riegl VZ-2000 at the Noordwijk beach this threshold is determined at 10 $R^2 \cdot m$ for the 1D Fourier transform and at 1000 $(R^2 \cdot m)^2$ for the 2D Fourier transform. The height determination can also be applied in other situations, if the accuracy in z-direction of the laser scanner is smaller than one centimetre due to the irregularities present on the beach. The method for the detection of the peak in the spectrum corresponding to the profile, and therefore the determination of the wavelength and orientation, can be applied as well for other situations, independent on the grid size and window length. It should however be noted that the accuracy of the determination of the wavelength and orientation depends on the window size.

What are the shape properties of the aeolian sand strips (e.g. wavelength, orientation)?

The shape properties considered are the wavelength, orientation and height. The wavelength of the sand strips varies between 8.9 *m* and 17.6 *m* with a mean of 13.2 *m* and a standard deviation of 1.5 *m*. The orientation of the sand strips varies between 29° and 142° relative to the beach-normal, where 90° corresponds to an alongshore orientation. The mean orientation is equal to 75°, and the IQR ranges from 55° to 90°. The overall orientation is therefore slightly alongshore-oblique. The height of the sand strips is in the order of a few centimetres, varying between 2.0 *cm* and 12.0 *cm* with a mean of 4.0 *cm*. The detected heights follow a positively skewed distribution where the IQR ranges from 3.2 *cm* to 4.6 *cm*.

How do the grain size and surface moisture vary over the aeolian sand strips?

In transverse direction of the sand strip some variation in grain size is observed. The crest of the sand strip consists of relatively the largest grain size, followed by the windward side of the sand strip. The leeward side consists of the smallest grain size of the sand strip, comparable with the grain size variation of aeolian sand ripples. This variation becomes more clear for smaller characteristic grain sizes. In longitudinal direction, there is no clear pattern observed. The moisture content differs significant between the sand strips and the surrounding beach. The mean moisture content of the sand strips is equal to 2.6%, while the mean moisture content on the surrounding beach is equal to 9.4%. Besides, the maximum measured moisture content on the sand strips was below 6.0%, while the surrounding beach had a moisture content of at least 6.0%. Therefore, there is a significant difference in moisture content between the sand strips and the surrounding beach.

What are the required environmental conditions for aeolian sand strips to develop?

The sand strips were mainly detected with alongshore winds of at least 8 *m/s*. The dominant wind direction ranged between 210° and 230° relative to North. This is considered alongshore since the orientation of the Noordwijk beach is equal to 30° relative to North. Although sand strips occurred at a wind velocity of at least 8 *m/s*, they formed at a minimum wind velocity of 10 *m/s*. However, the occurrence of sand strips does not solely depend on the wind conditions. Based on the reflectance values, the sand strips seem to “disappear” (i.e., not detected) during certain precipitation events and re-appear within one hour after the precipitation event stopped. However, due to the significant height difference between the sand strips and surrounding beach that is still present during some precipitation events, it is suggested that they remain present during these precipitation events. Furthermore, sand strips mostly formed during falling tide (58.8% of the times) and disappeared during rising tide (47.1% of the time).

What are the dynamic properties of the aeolian sand strips (e.g. migration rate, changes over time)?

Based on one life cycle of sand strips, the shape properties show dynamic behaviour since they changed over time while the weather conditions remained constant. The height of the sand strips increased, the wavelength of the sand strips decreased and the sand strip orientation became more inland. The more inland directed orientation over time corresponds to a varying migration rate over the width of the beach, decreasing towards the dunes. The lowest migration rate, equal to 0.3 *m/h*, is measured close to the dunes while the largest migration rate, 3.3 *m/h*, is measured close to the waterline.

8. Recommendations

This chapter provides recommendations for the improvement of sand strip related studies and is divided in two sections. First, improvements regarding the detection method are discussed (section 8.1), followed by suggestions for future studies (section 8.2).

8.1 Improvements of the detection method

For this study, the detection is based on solely the reflectance values. During precipitation events it is observed that sand strips were not all detected anymore due to the increasing moisture content that causes a smaller difference in reflectance between the sand strips and surrounding beach. This, eventually, prevents the total energy in the variance density spectrum to exceed the threshold for sand strip detection and therefore disregards these sand strips. In order to analyse them, they should be detected based on the height difference since the height difference between the sand strips and surrounding beach can be still significant during precipitation. Therefore, the detection of sand strips can be based on both the reflectance values as well as the height of the sand strips. A detection based on two characteristics will increase the computation time, and therefore possibly other simplifications might be applied (e.g., a larger grid size) to compensate this increase. For this extended detection method, it can be interesting to correlate the moisture content and the height, where the moisture content can be derived from the reflectance values (Di Biase et al., 2021).

Furthermore, the detection method is only applied when the beach width exceeds 40 *m*. Sometimes the beach width appeared to be smaller than 40 *m*, preventing the application of the detection method while sand strips can be present on these narrow beaches. Information regarding sand strip occurrence on these narrow beaches is missing, which can be obtained by applying a flexible window width. As in this study, the beach can be scanned with a fixed window width, and when approaching the dunes the window width can reduce, e.g., to 20 *m*, preventing the necessarily required width for the application of the detection method. It should however be noted that a smaller window width causes a less accurate determination of the wavelength and orientation due to the increase in the bandwidth (equation 5.1). Furthermore, due to this increasing bandwidth the energy in the spectrum can be distributed somewhat different over the spectrum, probably resulting in small variations in peak height.

8.2 Suggestions for future studies

For this study the average shape properties for each scan are analysed and therefore the variations in each scan are not considered. However, it can be imagined that some variation could appear over the location on the beach. The beach could be divided into multiple areas, each with their own characteristics (e.g., Figure 8.1) and sand strip behaviour and their corresponding shape properties can be analysed and compared for each sub-area. The area selection can be based on, e.g., (i) moisture content, due to the varying surface moisture over the width of the beach or; (ii) wind field, where the presence of the beach pavilion can cause a disturbance in streamlines. In Figure 8.1 the beach is divided in four sub-areas, with A and B both at the upper beach and C and D at the intertidal zone. Sand strip behaviour in sub-areas A and B can be compared to each other, where differences can be caused by the different wind field due to the presence of the beach pavilion. The surface moisture can be derived from the reflectance intensity according to Di Biase et al. (2021), hence the upper and lower beach can be compared to each other for the dependency on moisture content. Additionally, in section 5.4.2 it is observed that the migration rate decreases in duneward direction. This could be caused by topographic steering due to the presence of the dune (Bauer et al., 2012). Contrarily, the moisture content, which is larger near the waterline compared to close to the dunes, increases the threshold shear velocity (Hotta et al., 1984), implying an increase in transport potential in duneward direction. The variation in migration rate in cross-shore direction can therefore be studied as well in more depth.

Besides, in this study the sand strip orientation is compared to the wind direction, which mainly differed between 0° and 50°. The observed varying migration rate caused an increase in orientation, possibly preventing a proper alignment between the sand strip orientation and wind direction. The initial sand strip orientation could therefore be compared to the wind direction, excluding the increased orientation caused by the migration, which could give a more proper alignment and a more meaningful observation.

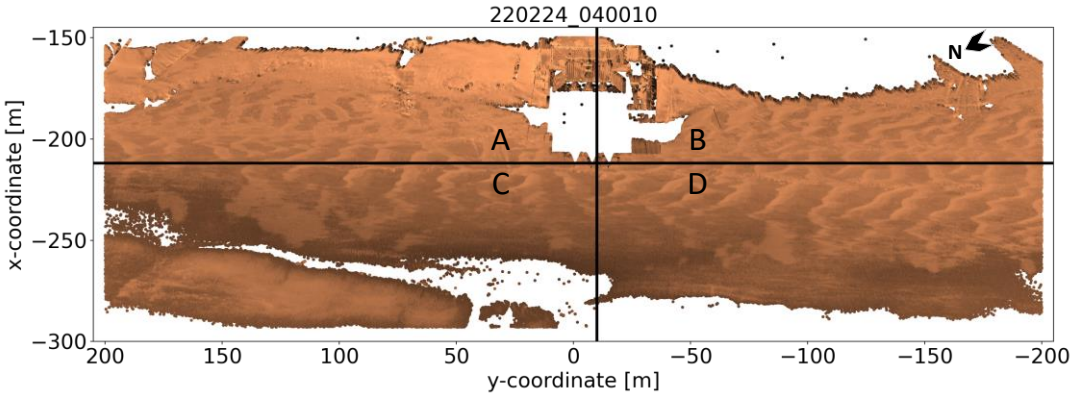

Figure 8.1. Division of the beach area in sub-areas with A and B the upper beach and C and D the intertidal zone; B located upwind from the beach pavilion and; A downwind.

Furthermore, the results obtained of the dynamic properties are only indicative due to the consideration of only one life cycle of the sand strips. A generic conclusion for the dynamic properties was therefore premature. Besides, for a better understanding of the role of moisture content in the migration of the sand strips, as discussed in section 6.3, it is desired to study more life cycles of sand strips. The time dimension can be included when extending the detection method to a 3D Fourier transform, obtaining the migration rates. In combination with the shape properties the amount of transported sand can be estimated, which subsequently also gives insight in dune growth and coastal resilience. The migration rate can be determined with the method developed by Matsuda et al. (2014). They studied atmospheric gravity waves with airglow intensity images and developed a method to obtain the power spectrum in the phase velocity domain, which is recognized and used by others (e.g., Tshuchiya et al. (2018) and (2019)). Although the spatial scale is much larger compared to sand strips, the method can be helpful. Matsuda et al. (2014) computed the 3D spectrum as a function of wavenumbers and frequency (the time interval between the images) using a 3D Fourier transform from a series of images. Subsequently, this 3D spectrum was converted to a phase velocity domain by integrating in the frequency domain. The velocity resolution depends on the frequency of interest and the size of the time window. Therefore it is important that the frequency is less than one hour due to migration rate of around 1 *m/h*. Besides, the sand strips should be present for a long enough time duration (the size of the time window).

References

Anders, K., Lindenbergh, R., Vos, S., Mara, H., de Vries, S., & Höfle, B. (2019). High-frequency 3D Geomorphic Observation Using Hourly Terrestrial Laser Scanning Data of a Sandy Beach. *ISPRS Annals of Photogrammetry, Remote Sensing and Spatial Information Sciences*, 317-324. doi:10.5194/isprs-annals-IV-2-W5-317-2019.

Angelopoulou, E., & Wright Jr., J. (1999). *Laser Scanner Technology.* University of Pennsylvania, Department of Computer & Information Science.

Baas, A. (2007). Complex systems in aeolian geomorphology. *Geomorphology, 91*(3-4), 311-331. doi:10.1016/j.geomorph.2007.04.012

Baas, A., & Sherman, D. (2005). Formation and behavior of aeolian streamers. *Journal of Geophysical Research, 110*, 1-15. doi:10.1029/2004JF000270

Baas, A., & Sherman, D. (2006). Spatiotemporal Variability of Aeolian Sand Transport in a Coastal Dune Environment. *Journal of Coastal Research, 22*(5), 1198-1205. doi:10.2112/06-0002.1

Baddock, M., Nield, J., & Wiggs, G. (2018). Early-stage aeolian protodunes: Bedform development and sand transport dynamics. *Earth Surf. Process. Landforms, 43*, pp. 339-346. doi:10.1002/esp.4242

Bagnold, R. (1935). The movement of Desert Sand. *The Geographical Journal, 85*(4), pp. 342-365. doi:10.2307/1785593

Bagnold, R. (1937). The transport of sand by wind. *The Geographical Journal, 89*(5), pp. 409-438. doi:10.2307/1786411

Bauer, B., & Davidson-Arnott, R. (2003). A general framework for modeling sediment supply to coastal dunes including wind angle, beach geometry, and fetch effects. *Geomorphology, 49*(1-2), 89-108. doi:10.1016/S0169-555X(02)00165-4

Bauer, B., Davidson-Arnott, R., Hesp, P., Namikas, S., Ollerhead, J., & Walker, I. (2009). Aeolian sediment transport on a beach: Surface moisture, wind fetch, and mean transport. *Geomorphology*(105), 106-116. doi:10.1016/j.geomorph.2008.02.016

Bauer, B., Davidson-Arnott, R., Walker, I., Heps, P., & Ollerhead, J. (2012). Wind direction and complex sediment transport responce across a beach-dune system. *Earth Surface Processes and Landforms, 37*, pp. 1661-1677. doi:10.1002/esp.3306

Benesty, J., Chen, J., Huang, Y., & Cohen, I. (2009). Pearson Correlation Coefficient. *Noise reduction in speech processing, 2*, pp. 1-4. doi:doi.org/10.1007/978-3-642-00296-0_5

Bosboom, J., & Stive, M. (2021). *Coastal Dynamics* (1269 ed.). Delft, The Netherlands: Delft University of Technology. doi:10.5074/T.2021.001

Brock, M. (2019). *Insight*. Retrieved from Data Visualization Using the Fourier Transform: https://insightincmiami.org/data-visualization-using-the-fourier-transform/

BS1377-2. (1990). Part 2: Classification tests. In *Methods of tests for soils for civil engineering purposes.* London: British Standard.

Charnock, H. (1955). Wind stress on a water surface. *Quarterly Journal of the Royal Meteorological Society, 81*, pp. 639-640. doi:10.1002/qj.49708135027

CoastScan. (2022a). *CoastScan Locations*. Retrieved from https://coastscan.citg.tudelft.nl/index.php/locations/

CoastScan. (2022b). *Important dates for the CoastScan project*. Opgehaald van CoastScan: https://coastscan.citg.tudelft.nl/index.php/important-dates-for-the-coastscan-project/

Cochram, W., Cooley, J., Favin, D., Helms, H., Kaenel, R., Lang, W., . . . Welch, P. (1967). What is the fast Fourier transform? *Proceedings of the IEEE, 55*(10), 1664-1674. doi:10.1109/PROC.1967.5957.

Cooley, J., & Tukey, J. (1965). An algorithm for the machine calculation of complex Fourier series. *Mathematics of computation, 19*(90), pp. 297-301. doi:10.2307/2003354

Cornelis, W., & Gabriels, D. (2003). The effect of surface moisture on the entrainment of dune sand by wind: an evaluation of selected models. *Sedimentology, 50*(4), pp. 771-790. doi:10.1046/j.1365-3091.2003.00577.x

Davidson-Arnott, R., & Bauer, B. (2009). Aeolian sediment transport on a beach: Thresholds, intermittency, and high frequency variability. *Geomorphology, 105*(1-2), 117-126. doi:10.1016/j.geomorph.2008.02.018

Davidson-Arnott, R., & Law, M. (1996). Measurement and Prediction of Long-Term Sediment Supply to Coastal Foredunes. *Journal of Coastal Research, 12*(3), 654-663.

Davidson-Arnott, R., Yang, Y., Ollerhead, J., Hesp, P., & Walker, I. (2008). The effects of surface moisture on aeolian sediment transport threshold and mass flux on a beach. *Earth Surface Processes and Landforms, 33*(1), pp. 55-74. doi:10.1002/esp.1527

de Vries, S., van Thiel de Vries, J., van Rijn, L., Arens, S., & Ranasinghe, R. (2014). Aeolian sediment transport in supply limited situations. *Aeolian Research, 12*, 75-85. doi:10.1016/j.aeolia.2013.11.005

Di Biase, V., Hanssen, R., & Vos, S. (2021). Sensitivity of near-infrared permanent laser scanning intensity for retrieving soil moisture on a coastal beach: calibration procedure using in situ data. *Remote Sensing, 13*(9), p. 1645. doi:10.3390/rs13091645

Di Biase, V., Kuschnerus, M., & Lindenbergh, R. (2022). Permanent laser scanner and synthetic aperture radar data: correlation characterisation at a sandy beach. *Sensors, 22*(6). doi:10.3390/s22062311

Duran, O., Claudin, P., & Andreotti, B. (2011). On aeolian transport: Grain-scale interactions, dynamic mechanisms and scaling laws. *Aeolian Research, 3*(3), pp. 243-270. doi:10.1016/j.aeolia.2011.07.006

Ewing, R., & Kocurek, G. (2010). Aeolian dune interactions and dune-field pattern formation: White Sands Dune Field, New Mexico. *Sedimentology, 57*(5), 1199-1219. doi:10.1111/j.1365-3091.2009.01143.x

Gray, J. (1978). Johann Heinrich Lambert, mathematician and scientist, 1728 - 1777. *Historia Mathematica, 5*(1), pp. 13-41. doi:10.1016/0315-0860(78)90133-7

Hage, P., Ruessink, B., & Donker, J. (2018b). Determining sand strip characteristics using Argus video monitoring. *Aeolian Research, 33*, 1-11. doi:10.1016/j.aeolia.2018.03.007

Hage, P., Ruessink, G., & Donker, J. (2018a). Using Argus video monitoring to determine limiting factors of aeolian sand transport on a narrow beach. *Journal of Marine Science and Engineering, 6*(4), 1-17. doi:10.3390/jmse6040138

Hage, P., Ruessink, G., van Aartrijk, Z., & Donker, J. (2020). Using Video Monitoring to Test a Fetch-Based Aeolian Sand Transport Model. *Journal of Marine Science and Engineering, 8*(2), 1-22. doi:10.3390/jmse8020110

Holthuijsen, L. (2007). *Waves in oceanic and coastal waters.* Cambridge University Press.

Hotta, S., Kubota, S., Katori, S., & Horikawa, K. (1984). Sand transport by wind on a wet sand surface. *Coastal Engineering*, pp. 1265-1281.

Jackson, N., & Nordstrom, K. (1998). Effects of Time-dependent Moisture Content of Surface Sediments on Aeolian Transport Rates Across a Beach, Wildwood, New Jersey, U.S.A. *Earth Surface Processes and Landforms*. doi:10.1002/(SICI)1096-9837(199707)22:7<611::AID-ESP715>3.0.CO;2-1

Joosse, X. (2021). *Assessing alongshore variability of intertidal channels at Noordwijk by means of LiDAR measurements.* Master Thesis, TU Delft. Retrieved from http://resolver.tudelft.nl/uuid:53ab4432-ece6-4eeb-a8b8-0ac0389a849c

Kirmse, A., & de Ferranti, J. (2017). Calculating the prominence and isolation of every mountain in the world. *Progress in Physiscal Geography, 41*(6), 788-802. doi:10.1177/0309133317738163

KNMI. (2001). Wind. In *Handboekwaarnemingen; meetstation algemeen* (pp. 91-112).

Kocurek, G., Ewing, R., & Mohrig, D. (2009). How do bedform patterns arise? New views on the role of bedform interactions within a set of boundary conditions. *Earth Surface Processes and Landforms, 35*, 51-63. doi:10.1002/esp.1913

Kocurek, G., Townsley, M., Yeh, E., Havholm, K., & Sweet, M. (1992). Dune and dune-field development on Padre Island, Texas, with implications for interdune deposition and water-table-controlled accumulation. *Journal of Sedimentary Research, 62*(4), 622-635. doi:10.1306/D4267974-2B26-11D7-8648000102C1865D

Lindenbergh, R., Soudarissanane, S., de Vries, S., Gorte, B., & de Schipper, M. (2011). Aeolian Beach Sand Transport Monitored by Terrestrial Laser Scanning. *The Photogrammetric Record, 26*(136), 384-399. doi:10.1111/j.1477-9730.2011.00659.x

Locci-Lopez, D., Zhang, R., Castagna, J., & Oyem, A. (2018). The multi-scale Fourier transform. *SEG International Exposition and 88th Annual Meeting*, (pp. 4176-4180). doi:10.1190/segam2018-2994723.1

Luijendijk, A., Hagenaars, G., Ranasinghe, R., Baart, F., Donchyts, G., & Aarninkhof, S. (2018). The State of the World's Beaches. *Scientific Reports, 8*(6641). doi:10.1038/s41598-018-24630-6

Markevich, N., & Gertner, I. (1989). Comparison among methods for calculating FWHM. *Nuclear instruments and methods in physics research, 283*(1), 72-77. doi:10.1016/0168-9002(89)91258-8

Matsuda, T., Nakamura, T., Ejiri, M., Tsutsumi, M., & Shiokawa, K. (2014). New statistical analysis of the horizontal phase velocity distribution of gravity waves observed by airglow imaging. *Journal of Geophysical Research: Atmospheres, 119*(6), pp. 9707-9718. doi:10.1002/2014JD021543

Medina, R., Losada, M., Losada, I., & Vidal, C. (1994). Temporal and spatial relationship between sediment grain size and beach profile. *Marine geology, 118*(3-4), 195-206. doi:10.1016/0025-3227(94)90083-3

Mitha, S., Tran, M., Werner, B., & Haff, P. (1986). The grain-bed impact process in aeolian saltation. *Acta Mechanica, 63*, pp. 267-278. doi:doi.org/10.1007/BF01182553

Nield, J. (2011). Surface moisture-induced feedback in aeolian environments. *Geology, 39*(10), 915-918. doi:10.1130/G32151.1

Nield, J., & Wiggs, G. (2011). The application of terrestrial laser scanning to aeolian saltation cloud measurement and its response to changing surface moisture. *Earth Surface Processes and Landforms, 36*, 273-278. doi:10.1002/esp.2102

Nield, J., Wiggs, G., & Squirrel, R. (2011). Aeolian sand strip mobility and protodune development on a drying beach: examining surface moisture and surface roughness patterns measured by terrestrial laser scanning. *Earth Surface Processes and Landforms, 36*, 513-522. doi:10.1002/esp.2071

Oliphant, T. (2006). *Guide to Numpy.*

Pye, K., & Tsoar, H. (2008). *Aeolian bed forms.* Berlin: Springer. doi:10.1007/978-3-540-85910-9

Quartel, S., Ruessink, B., & Kroon, A. (2007). Daily to seasonal cross-shore behaviour of quasi-persistent intertidal beach morphology. *Earth Surface Processes and Landforms, 32*(9), 1293-1307. doi:10.1002/esp.1477

Sherman, D., & Hotta, S. (1990). Aeolian sediment transport: theory and measurement. *Coastal Dunes: Form and Process*, 17-37.

Sherman, D., Zhang, P., Martin, R., Ellis, T., Kok, J., Farrell, E., & Li, B. (2019). Aeolian ripple migration and associated creep transport rates. *Geosciences, 9*(9). doi:10.3390/geosciences9090389

Small, C., & Nicholls, R. (2003). A Global Analysis of Human Settlement in Coastal Zones. *Journal of Coastal Research, 19*(3), 584-599.

Smit, Y., Ruessink, G., Brakenhoff, L., & Donker, J. (2018). Measuring spatial and temporal variation in surface moisture on a coastal beach with a near-infrared terrestrial laser scanner. *Aeolian Research, 31*, 19-27. doi:10.1016/j.aeolia.2017.07.004

Soudarissanane, S., Lindenbergh, R., Menenti, M., & Teunissen, P. (2011). Scanning geometry: Influencing factor on the quality of terrestrial laser scanning points. *ISPRS Journal of Photogrammetry and Remote Sensing, 66*(4), 389-399. doi:10.1016/j.isprsjprs.2011.01.005

Stive, M., de Schipper, M., Luijendijk, A., Aarninkhof, S., van Gelder-Maas, C., van Thiel de Vries, J., . . . Ranasinghe, R. (2013). A New Alternative to Saving Our Beaches from Sea-Level Rise: The Sand Engine. *Journal of Coastal Research, 29*(5), 1001-1008. doi:10.2112/JCOASTRES-D-13-00070.1

Swann, C., Lee, D., Trimble, S., & Key, C. (2021). Aeolian sand transport over a wet, sandy beach. *Aeolian Research, 51*. doi:10.1016/j.aeolia.2021.100712

Temmerman, S., Meire, P., Bouma, T., Herman, P., Ysebaert, T., & de Vriend, H. (2013). Ecosystem-based coastal defence in the face of global change. *Nature, 504*, 79-83. doi:10.1038/nature12859.

Tshuchiya, S., Shiokawa, K., Fujinami, H., Otsuka, Y., Nakamura, T., & Yamamoto, M. (2018). Statistical analysis of the phase velocity distribution of mesospheric and ionospheric waves observed in airglow images over a 16-year period: Comparison between Rikubetsu and

Shigaraki, Japan. *Journal of Geophysical Research: Space Physics, 123*(8), pp. 6930-6947. doi:10.1029/2018JA025585

Tsuchiya, S., Shiokawa, K., Fujinami, H., Otsuka, Y., Nakamura, T., Connors, M., . . . Poddelsky, I. (2019). Three-dimensional Fourier analysis of the phase velocity distributions of mesospheric and ionospheric waves based on airglow images collected over 10 years: comparison of Magadan, Russia, and Athabasca, Canada. *Journal of Geophysical Research: Space Physics, 124*(10), pp. 8110-8124. doi:10.1029/2019JA026783

Ungar, J., & Haff, P. (1987). Steady state saltation in air. *Sedimentology, 34*(2), pp. 289-299. doi:10.1111/j.1365-3091.1987.tb00778.x

Uphues, C., van IJzendoorn, C., Hallin, C., Pearson, S., van Prooijen, B., Moit da Silva, G., & de Vries, S. (2022). Coastal aeolian sediment transport in an active bed surface layer: Tracer study and conceptual model. *Earth Surface Processes and Landforms, 47*(13), pp. 3147-3162. doi:10.1002/esp.5449

van Tuyll, I. (2020). *Assessing and reconstructing the weather data from a temporary weather station: focus on a weather station in Noordwijk.* Bachelor Thesis, Delft University of Technology, Faculty of Civil Engineering and Geosciences, Delft.

van Westen, B. (2018). *Numerical modelling of aeolian coastal landform development.* Master Thesis, Delft University of Technology, Faculty of Civil Engineering and Geosciences. Retrieved from http://resolver.tudelft.nl/uuid:83344d5b-f232-4085-985c-d1ec38903254

Virtanen, P., Gommers, R., Oliphant, T., Haberland, M., Reddy, T., Cournapeau, D., . . . Scipy 1.0 contributors. (2020). SciPy 1.0: Fundamental algorithms for scientific computing in Python. *Nature Methods, 17*(3), pp. 261-272. doi:10.1038/s41592-019-0686-2

Vos, S., Anders, K., Kuschnerus, M., Lindenbergh, R., Höfle, B., Aarninkhof, S., & de Vries, S. (2022). A high-resolution 4D terrestrial laser scan dataset of the Kijkduin beach-dune system, The Netherlands. *Sci Data, 9*(191). doi:10.1038/s41597-022-01291-9

Vos, S., Kuschnerus, M., & Lindenbergh, R. (2020). Assessing the error budget for permanent laser scanning in coastal Areas. *Proceedings of the FIG Working Week*.

Vos, S., Lindenbergh, R., de Vries, S., Aagaard, T., Deigaard, R., & Fuhrman, D. (2017). Coastscan: Continuous monitoring of coastal change using terrestrial laser scanning. *Proceedings of Coastal Dynamics*, 1518-1528.

Walker, J. (1981). *An experimental study of wind ripples.* Master thesis, Massachusetts Institute of Technology, Department of Earth and Planetary Sciences.

Walstra, D., Reniers, A., Ranasinghe, R., Roelvink, J., & Ruessink, B. (2012). On bar growth and decay during interannual net offshore migration. *Coastal Engineering, 60*, 190-200. doi:10.1016/j.coastaleng.2011.10.002

Werner, B. (1995). Eolian dunes: computer simulations and attractor interpretation. *Geology, 23*(12), pp. 1107-1110. doi:10.1130/0091-7613(1995)023<1107:EDCSAA>2.3.CO;2

Werner, B., & Kocurek, G. (1997). Bed-form dynamics: Does the tail wag the dog? *Geology, 25*(9), 771-774. doi:10.1130/0091-7613(1997)025<0771:BFDDTT>2.3.CO;2

Wiggs, G., Baird, A., & Atherton, R. (2004). The dynamic effects of moisture on the entrainment and transport of sand by wind. *Geomorphology, 59*, pp. 13-30. doi:10.1016/j.geomorph.2003.09.002

Wijnberg, K., & Terwindt, J. (1995). Extracting decadal morphological behaviour from high-resolution, long-term bathymetric surveys along the Holland coast using eigenfunction analysis. *Marine Geology, 126*(1-4), 301-330. doi:10.1016/0025-3227(95)00084-C

Yang, Y., & Davidson-Arnott, R. (2005). Rapid measurement of surface moisture content on a beach. *Journal of Coastal Research, 3 (213)*, pp. 447-452. doi:10.2112/03-0111.1

Appendix A. Workflow of the research questions

In this appendix, a workflow of the research questions is given in Figure A.1. From this visualization the order of sub-questions can be found. For some sub-questions, answers on other sub-questions are needed in order to answer that specific sub-question. Therefore the figure visualizes which questions should be answered first in order to answer the next question.

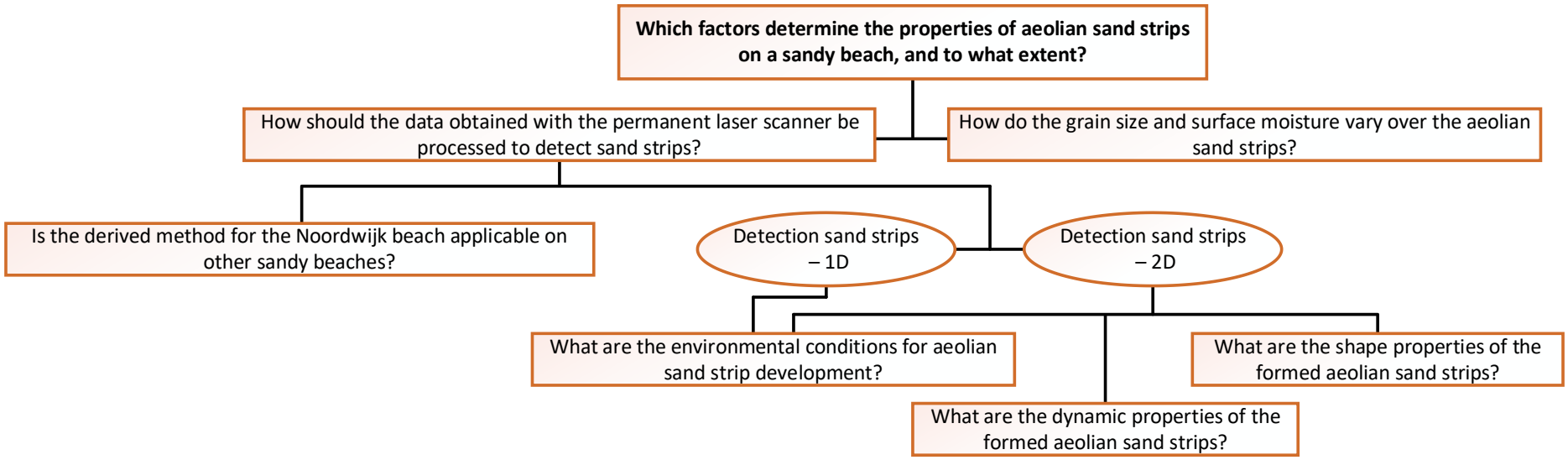

Figure A.1. Workflow of the research question with the corresponding sub-questions

Appendix B. Sample locations on each specific day

In this appendix, the sample locations are shown in more detail. In Figure 3.7 all the sample locations can be seen in one scan. However, these samples are taken on different days, resulting in different sand strips that were present. Therefore the sample locations are shown in more detail in this appendix for a better interpretation of the sand strips that are sampled. It should be noted that only the crests that are sampled are marked. The corresponding leeward side and windward side are not marked as well as the surrounding beach (except for February 17th).

February 17th

During the 17th of February, most samples are taken in the shadow zone of the dune (Figure B.1).

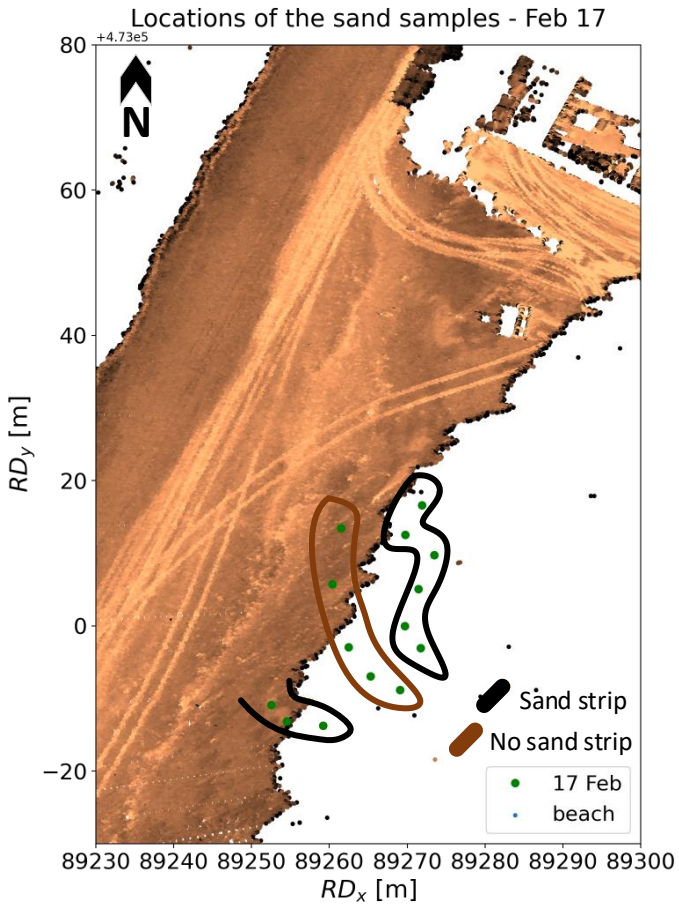

Figure B.1. Sample locations February 17th

February 18th

During February 18th, only the crests, wind- and leeward sides are sampled (Figure B.2).

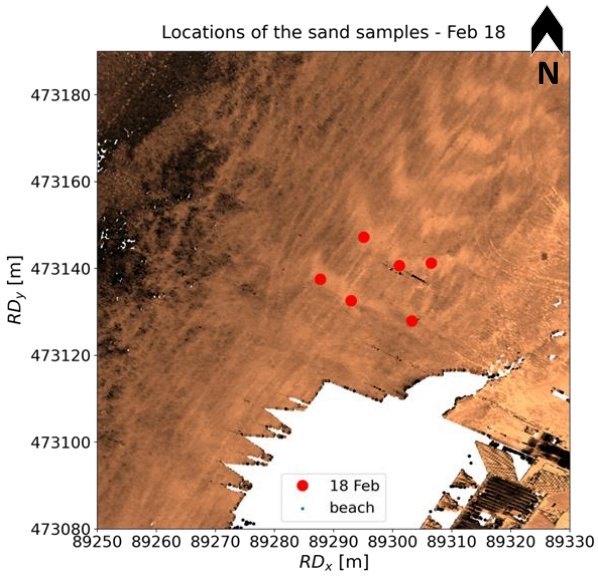

Figure B.2. Sample locations February 18th

April 6th

During April 6th, three sand strips were sampled with the similar method as February 17th and February 18th. At these sand strips the crest is sampled, both the wind- and leeward side and the surrounding beach. Furthermore, one sand strip is sampled (only the crest) in more detail in longitudinal direction (Figure B.3).

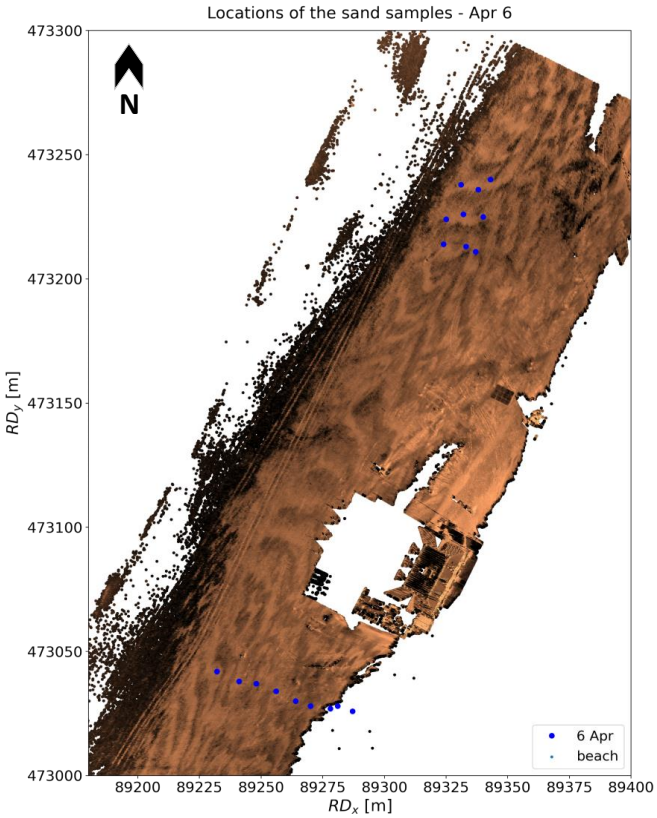

Figure B.3. Sample locations April 6th

Appendix C. The Fourier transform - information

A way to decompose a signal with different waveforms into components of different wave numbers is by applying a discrete Fourier transform (DFT) as visualized in Figure C.1. A DFT is often used to transform a time or space domain into a frequency domain and it is defined by equation C.1 (Cochram, et al., 1967).

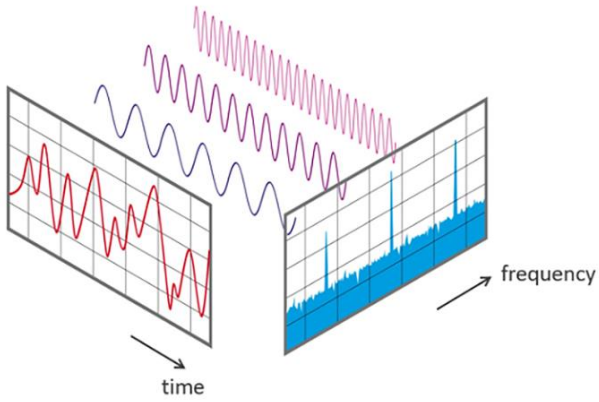

Figure C.1. Fourier transform, transformation of the time domain into a frequency domain (Brock, 2019)

$$A_r = \sum_k^{N-1} X_k \cdot \exp\left(\frac{-2\pi \cdot j \cdot r \cdot k}{N}\right),\ r = 0, \dots, N-1 \quad \text{(C.1)}$$

It should be noted that the definition of the DFT is not uniform in literature, sometimes the DFT coefficient is referred to as $\frac{A_r}{N}$, or $\frac{A_r}{\sqrt{N}}$ (Cochram, et al., 1967).

In equation C.1, A_r is the r-th coefficient of the DFT and X_k denotes the k-th sample of the space domain of which consists of N samples and $j = \sqrt{-1}$, making A_r almost always complex. The X_k's are often values of a function at discrete time points, and the index r is sometimes called the "frequency" of the DFT (Cochram, et al., 1967).

The DFT has a computation time of $O(N^2)$, which becomes really large for a large dataset with a lot of points or samples. A fast Fourier transform (FFT) is a method for efficiently computing the DFT. The FFT calculates the coefficients of the DFT iteratively, and this results in a more efficient computation. The computation time of a FFT is given by $O(N \cdot \log_2 N)$, which is much smaller than $O(N^2)$ for large N. The FFT not only reduces the computation time, it also reduces rounding errors associated with the computations with the same factor (Cochram, et al., 1967).

Appendix D. Determination of the percentage area-based false positives and false negatives

In this appendix, an example is given for computing the area-based false positives (*A-FP*) as well as the area-based false negatives (*A-FN*). The scan of February 23, 2022 at 22:20*h* is used as example and visualized in Figure D.1, with the detected sand strips surrounded by the blue boxes. Not all sand strips are detected and one detected area contains partly no sand strips, resulting in both *A-FN* and *A-FP* bigger than zero. The total beach area of this scan is estimated to be equal to 22.800 m^2. The total area where sand strips are present is estimated around 15.650 m^2, while the detected sand strips have an area of 12.600 m^2 (the area within the blue boxes). The beach area without sand strips is equal to the difference between the total beach area and the area where the beach surface is covered with sand strips and is therefore equal to 7.150 m^2.

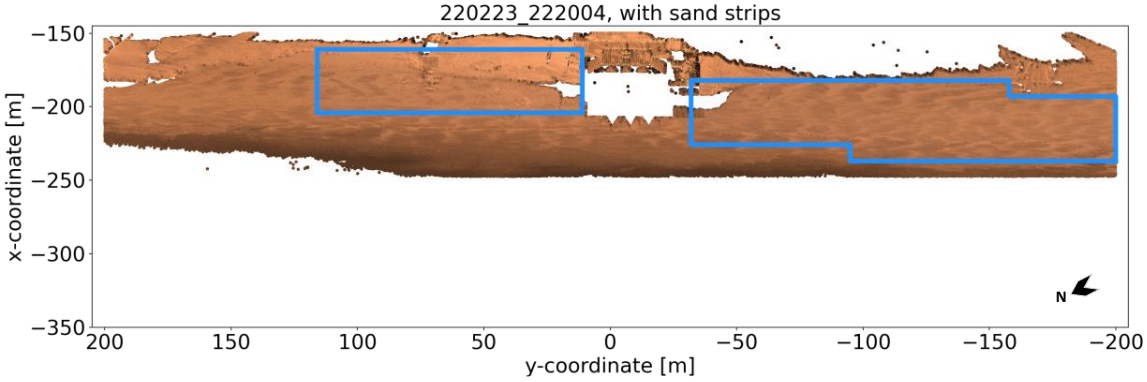

Figure D.1. Scan of the beach of Feb 23rd, 22:00h with sand strips. The detected sand strips are framed in blue, not all the sand strips are detected

With the estimated areas, the percentage of *A-FN* and *A-FP* can be determined according to equations 5.4 and 5.5 respectively. The numerator of equation 5.4 for computing the *A-FN* is equal to the yellow area in Figure D.2, and the numerator of equation 5.5 for computing the *A-FP* is equal to the red area in Figure D.2. The percentages *A-FN* and *A-FP* are therefore 19.5% and 14.0% respectively:

$$A\text{-}FN = \frac{(A_{sand\ strips} - A_{detected})}{A_{sand\ strips}} \cdot 100\% = \frac{(15.650 - 12.600)}{15.650} \cdot 100\% = 19.49\%$$

$$A\text{-}FP = \frac{(A_{false\ detected})}{A_{no\ sand\ strips}} \cdot 100\% = \frac{100 \cdot 10}{7.150} \cdot 100\% = 13.99\%$$

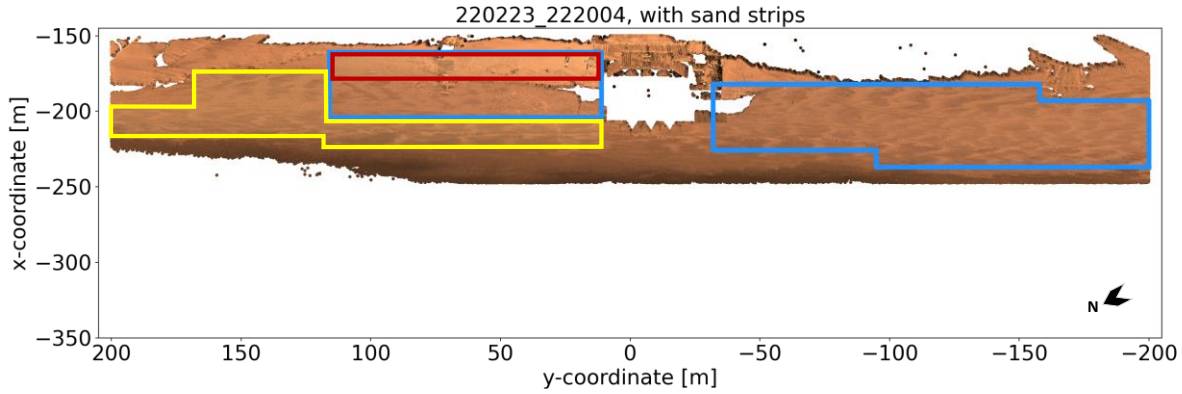

Figure D.2. Scan of the beach of Feb 23rd, 22:00h with sand strips. The detected sand strips are framed in blue, not all the sand strips are detected. The yellow area corresponds to false negatives, the red area to false positives

Appendix E. Overview of the environmental conditions

In this appendix an overview of the occurred environmental conditions that are considered is given (Figure E.1). This overview eases a comparison between certain periods regarding the occurrence of sand strips. In Figure E.1-A a black dashed line is visualized, corresponding to the orientation of the Noordwijk beach. Furthermore, two black lines are drawn in Figure E.1-B, corresponding to wind velocities of 8 *m/s* and 10 *m/s*.

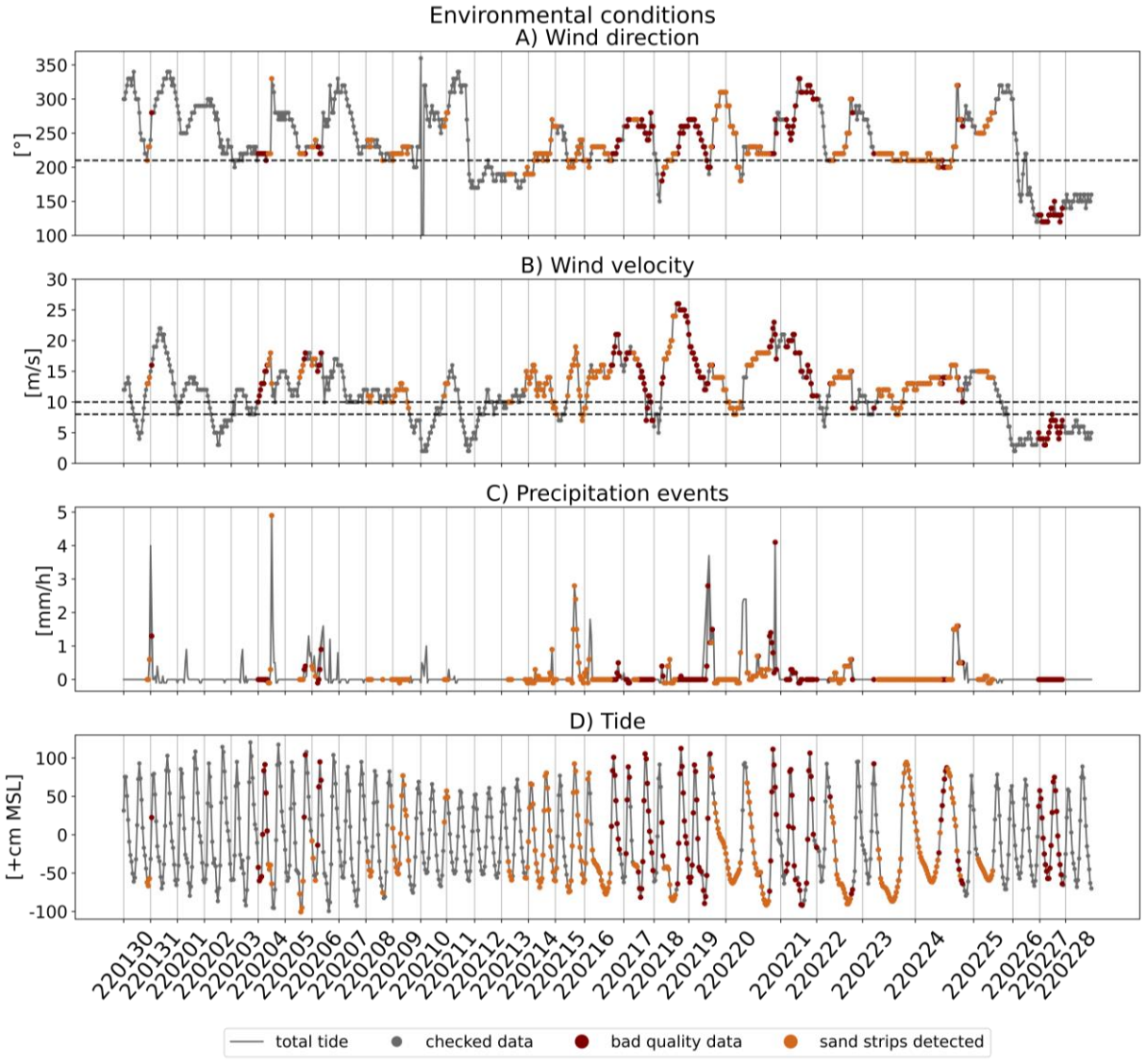

Figure E.1. Environmental conditions that are considered for the studied time period

Appendix F. Precipitation event February 16th

On February 16th a precipitation event occurred (Figure F.1), affecting the detection of sand strips, despite the detection of sand strips during a longer precipitation event with a larger intensity on February 15th. The precipitation event occurred on the 16th of February, starting between 04:00*h* and 05:00*h* with an intensity of 6 *mm/h* and ending between 07:00*h* to 08:00*h*. The peak intensity occurred between 05:00*h* and 06:00*h* with an intensity equal to 18 *mm/h*. Between 07:00*h* and 08:00*h* the intensity was equal to 13 *mm/h*. The corresponding scans of the beach, based on the reflectance values, are visualized in Figure F.2, ranging from February 16th 04:59*h* to 07:59*h*.

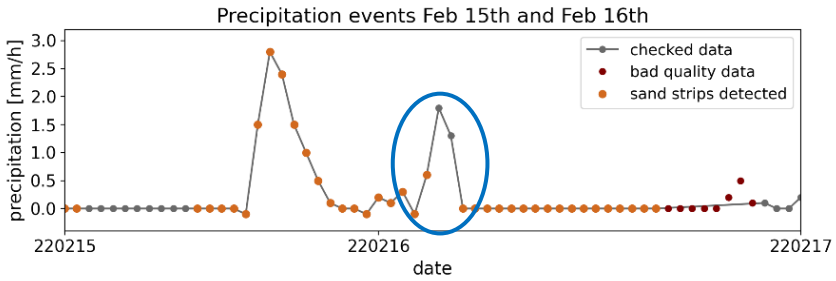

Figure F.1. Precipitation events from February 15th and February 16th. The analysed precipitation event (Feb 16th) is framed with a blue circle

The reflectance values suggest the disappearance of the sand strips during the precipitation event (Figure F.2). However, during the precipitation event there is still a significant height detectable between the sand strips and the surrounding beach (Figure F.3 to Figure F.6). Multiple windows for each scan are analysed, while only one profile in one window is shown in Figure F.3 to Figure F.6 for illustrational purposes. The detected height of the sand strips according to these lines are summarized in Table F.1.

Table F.1. Detected sand strip height for the precipitation event

Hours	**Precipitation [*mm/h*]**	**Detected based on reflectance?**	**Height [*cm*]**
05:00	6	Yes	6.0
06:00	18	No	5.1
07:00	13	No	4.9
08:00	0	Yes	5.6

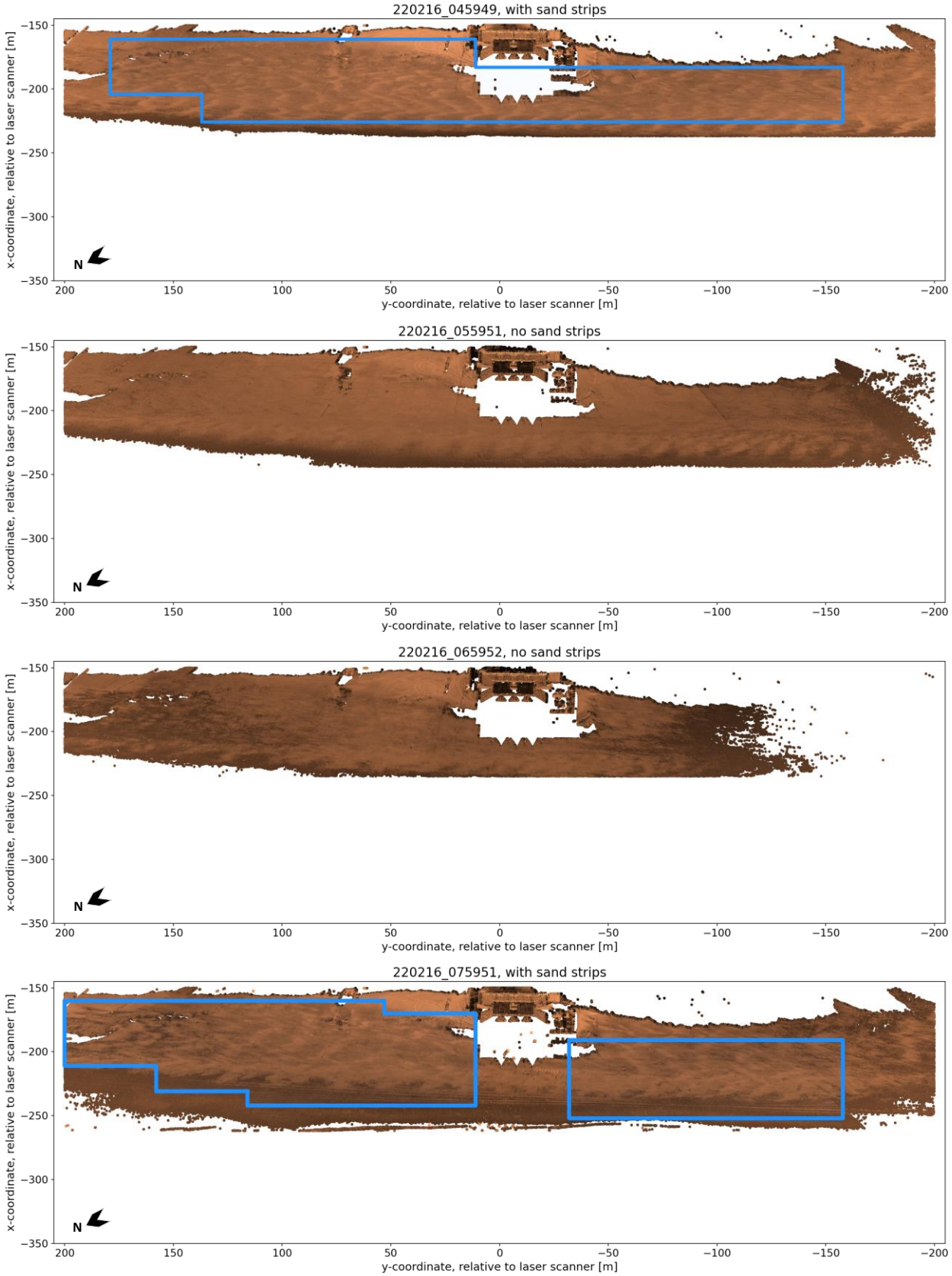

Figure F.2. Scans of the beach, based on the reflectance values, during the precipitation event

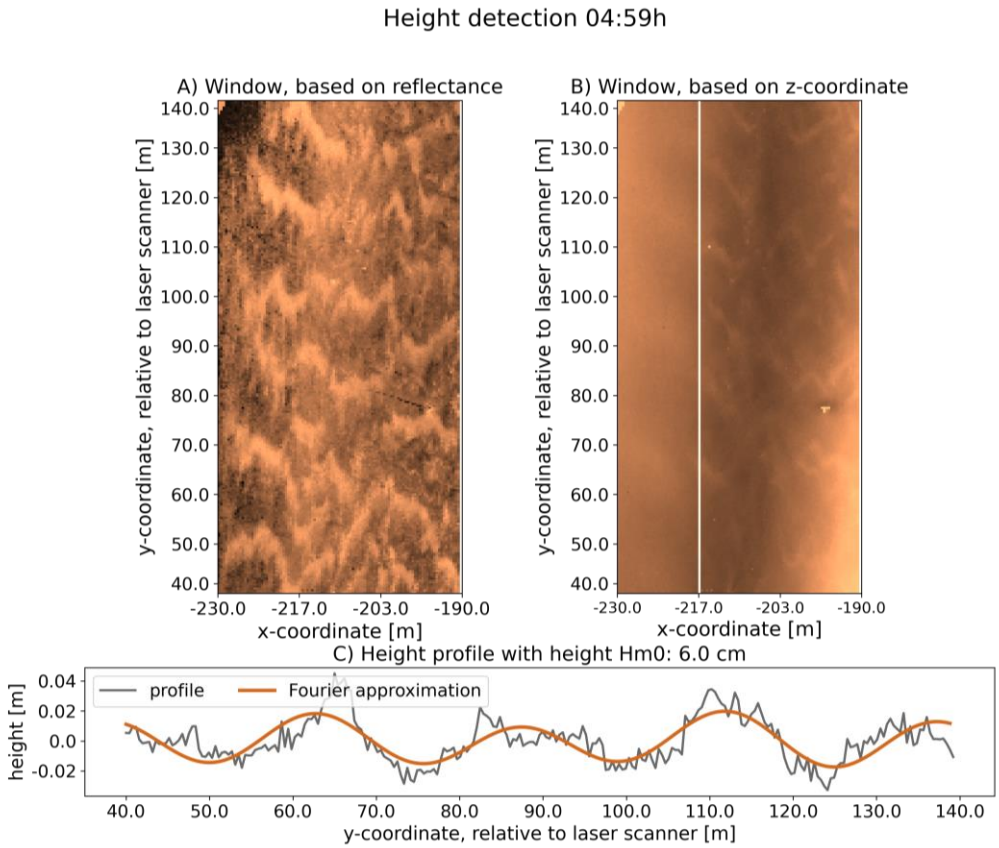

Figure F.3. Sand strips present in a window at 04:59h. They are detected on both the reflectance values and the height

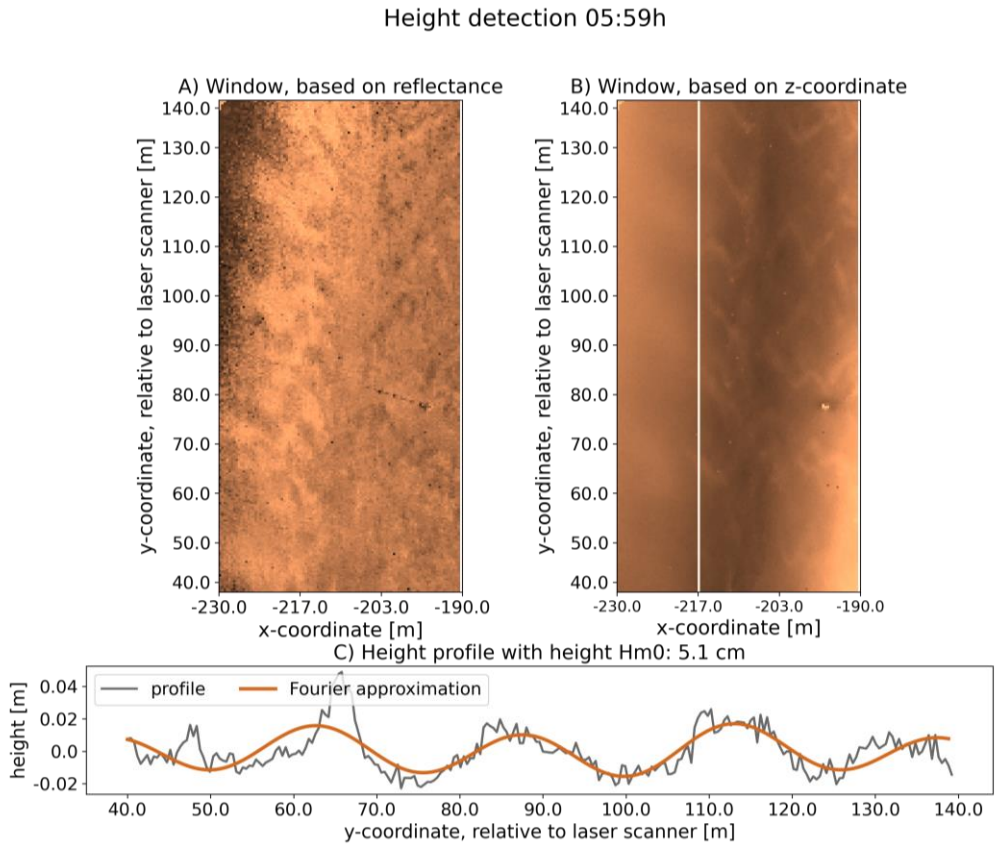

Figure F.4. Sand strips present in a window at 05:59h. They are not detected based on the reflectance values, but they are detected based on the height

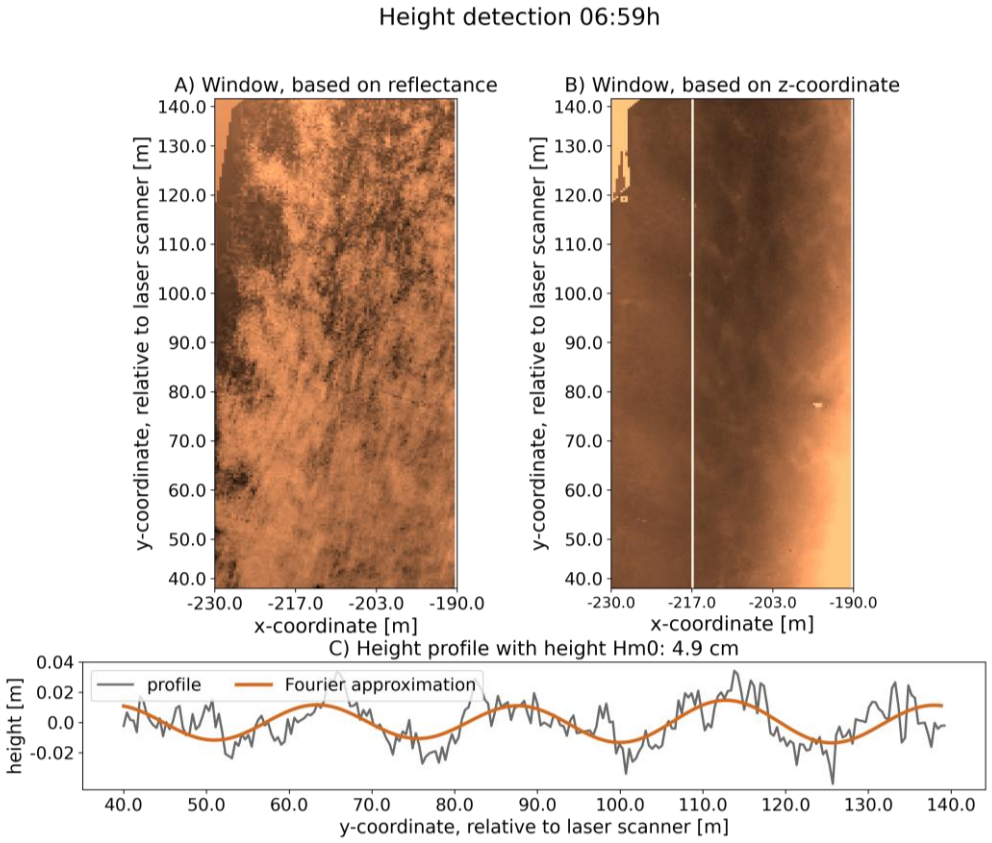

Figure F.5. Sand strips present in a window at 06:59h. They are detected on both the reflectance values and the height

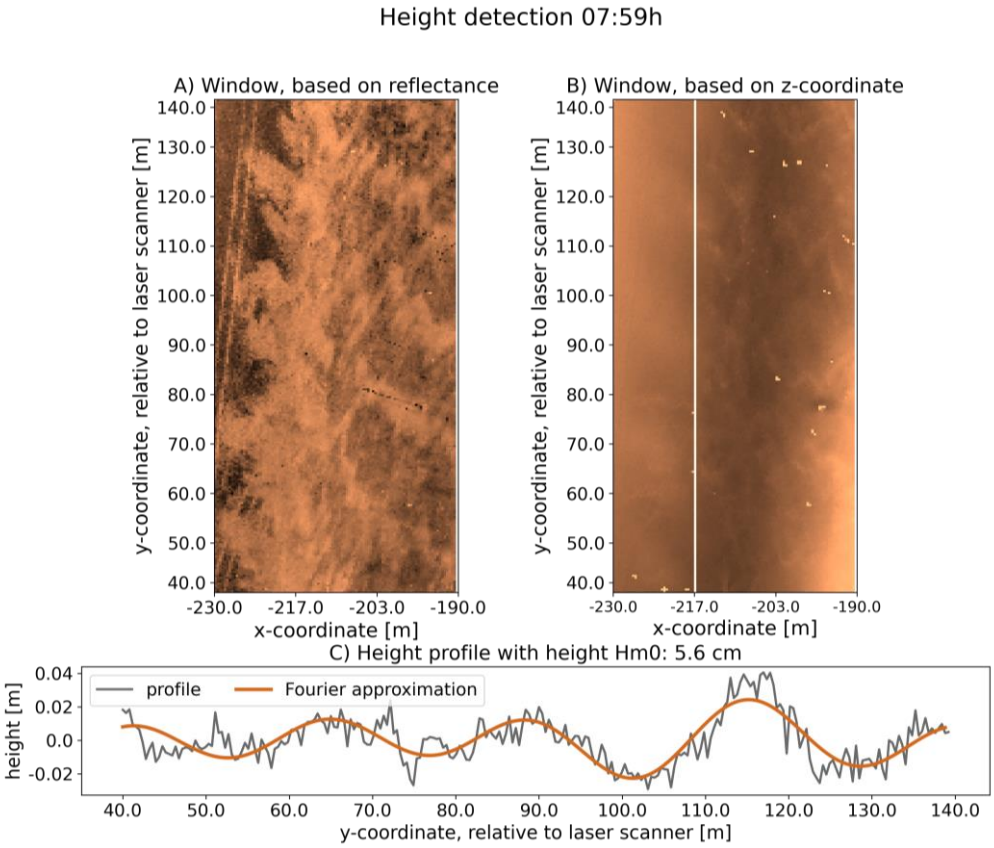

Figure F.6. Sand strips present in a window at 07:59h. They are not detected based on the reflectance values, but they are detected based on the height

The height-profile results in a wavelength equal to the wavelength obtained with the reflectance profile. In the upper figure of Figure F.7, the point cloud of 04:59*h* is shown again with the window surrounded in grey. In this window, a horizontal line is drawn and both the reflectance and height profile are visualized in the bottom figure. It can be seen that the wavelength according to the reflectance profile is equal to the height profile. Furthermore, one hour later (at 05:59*h*; Figure F.8) the sand strips are not detected anymore based on the reflectance values. However, according to the height-profile, the wavelength is equal to the wavelength of 04:59*h*. Besides, the determined significant height are also comparable.

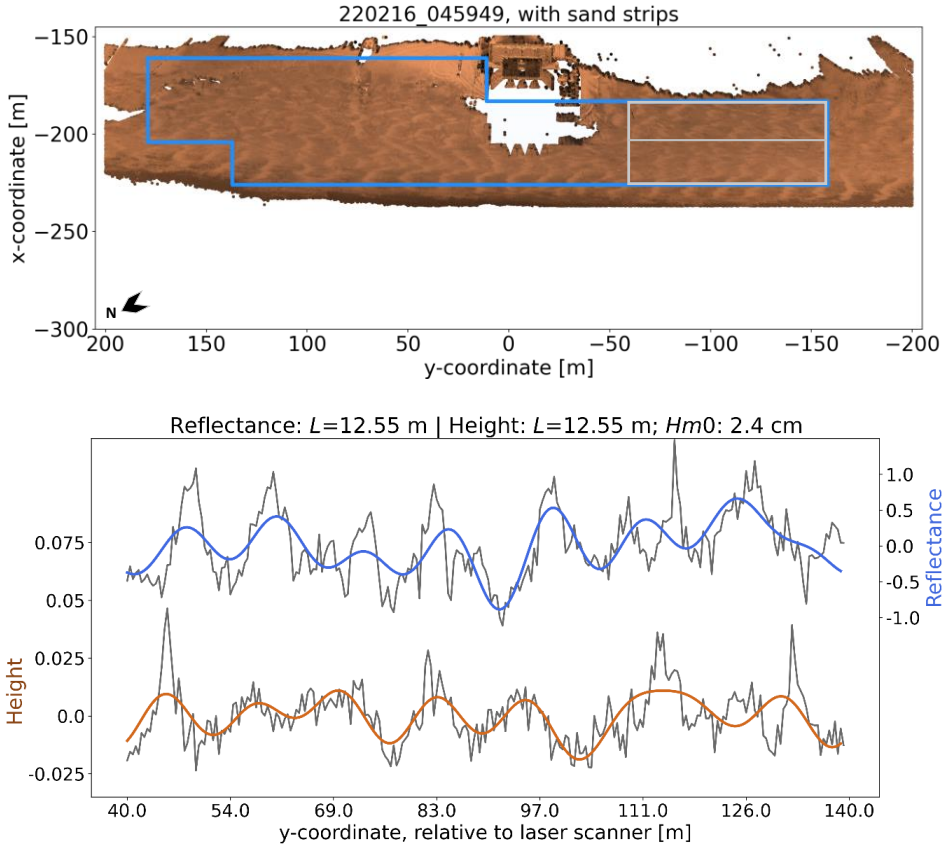

Figure F.7. Reflectance profile and height profile for 04:59h

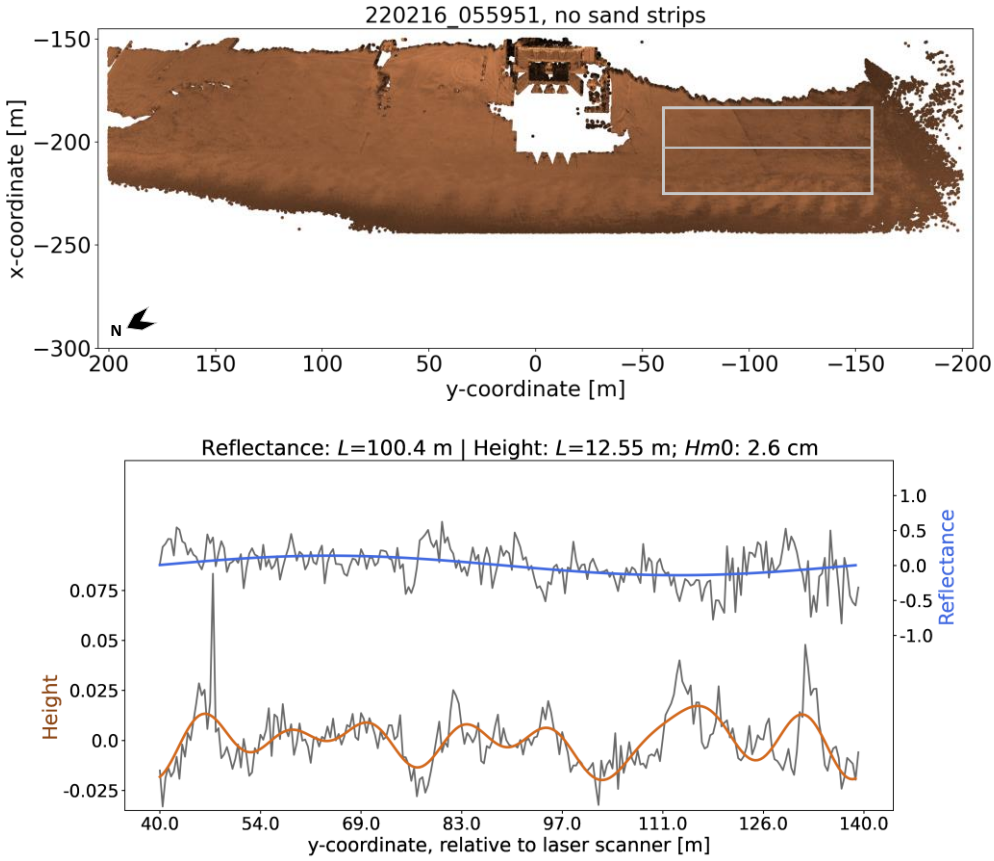

Figure F.8. Reflectance profile and height profile for 05:59h

Appendix G. Equations for the (threshold) shear velocity

In this appendix, the equations for the calculations of the shear velocity and the threshold shear velocity are presented.

Shear velocity

The shear velocity (u_*) is computed according to the Law of the Wall (equation G.1) in combination with Charnock's (1955) relation as given in equation G.2 (Sherman, et al., 2019).

$$u_* = \kappa \cdot u_z / ln\left(\frac{z}{z'_0}\right) \tag{G.1}$$

With:

- u_*: shear velocity [*m/s*]
- κ: von Karman constant (= 0.4)
- u_z: wind speed at elevation z above surface [*m/s*]
- z: elevation height at which wind speed is measured [*m*]
- z'_0: saltation-induces roughness length [*m*]

$$z'_0 = \frac{C \cdot {u_*}^2}{g} \tag{G.2}$$

With:

- C: Charnock constant (= 0.085 for general field applications)
- g: gravity constant (= 9.81 m/s^2)

The regional wind data measured at IJmuiden that is used in the analysis (u_z) is measured at a height of 10 *m* above ground level (Hage, Ruessink, & Donker, 2018b), and therefore z = 10 *m*. All other variables are known, resulting in a shear velocity for every measured wind velocity (the orange line in Figure 6.4).

Threshold shear velocity

The threshold shear velocity (u_{*t}) is the critical wind velocity where some grains start to move, and can be computed according to Bagnold's (1935) model (equation G.3). However, moisture content is considered an important feature of sand strips, which is not included in Bagnold's (1935) model. There are several models for the computation of the threshold shear velocity on wet surfaces (Cornelis & Gabriels, 2003). The comparison of Cornelis & Gabriels (2003) showed that the model of Hotta et al., (1984) (equation G.4) was most applicable for this study.

$$u_{*t} = A \cdot \sqrt{g \cdot d \cdot \left(\frac{\rho_s - \rho}{\rho}\right)} \tag{G.3}$$

$$u_{*tw} = A \cdot \sqrt{g \cdot d \cdot \left(\frac{\rho_s - \rho}{\rho}\right)} + 7.5 \cdot w \tag{G.4}$$

With:

- A: empirical constant (= 0.1 for fluid threshold)
- ρ: fluid density (1.22 kg/m^3)
- d: sand grain size [*m*]
- ρ_s: sediment density [kg/m^3]
- w: moisture content [*mass/mass*]